UNIVERSIDAD AUTÓNOMA DE SAN LUIS POTOSÍ
FACULTAD DE CIENCIAS
INSTITUTO DE INVESTIGACIÓN EN COMUNICACIÓN ÓPTICA

EEG CHARACTERIZATION USING ACOUSTIC STIMULI FROM CHAOTIC SYSTEM CIRCUITS

A dissertation presented to the Posgrado en Ciencias Aplicadas

in partial fulfillment of the requirements for the degree of

Master of Science

Author
GERARDO ACOSTA MARTÍNEZ, EE

Supervisor
LUIS JAVIER ONTAÑÓN GARCÍA PIMENTEL, PhD

Co-Supervisor
EDGAR TRISTÁN HERNÁNDEZ, PhD

San Luis Potosí, S.L.P.
August, 2019

UNIVERSIDAD AUTÓNOMA DE SAN LUIS POTOSÍ
FACULTAD DE CIENCIAS
INSTITUTO DE INVESTIGACIÓN EN COMUNICACIÓN ÓPTICA

EEG CHARACTERIZATION USING ACOUSTIC STIMULI FROM CHAOTIC SYSTEM CIRCUITS

GERARDO ACOSTA MARTÍNEZ

Synodal Committee

LUIS JAVIER ONTAÑÓN GARCÍA PIMENTEL, PhD

MARCELA MEJÍA CARLOS, PhD

EDGAR GUEVARA CODINA, PhD

ELEAZAR SAMUEL KOLOSOVAS MACHUCA, PhD

San Luis Potosí, S.L.P.
August 15, 2019

To Fer

Don't think about why you question, simply don't stop questioning. Don't worry about what you can't answer, and don't try to explain what you can't know. Curiosity is its own reason. Aren't you in awe when you contemplate the mysteries of eternity, of life, of the marvelous structure behind reality? And this is the miracle of the human mind—to use its constructions, concepts, and formulas as tools to explain what man sees, feels and touches. Try to comprehend a little more each day. Have holy curiosity.

—ALBERT EINSTEIN

Abstract

Dynamical systems theory has given way to the development of theoretical models, mathematical tools and experimental techniques in current neuroscience research. As such, neuroscience has come to strongly rely on the use of these nonlinear dynamics to better understand the characteristics of these processes, specially through the properties from its most notorious feature of which is chaos.

A very interesting feature of chaos is that it basically involves variations over time, and it does so in a very specific way that is unpredictable, aperiodic, but deterministic. As such, these variations create oscillations that lead to the formation of waves with defined amplitude and frequency.

Taking into the account this fact, the main objective of this investigation was to record acoustic signals derived from the voltage of chaotic systems implemented using electronic circuits and utilize them as auditory stimuli to analyze brain effects using perception evaluations and power spectral features on EEG signals.

In this investigation we acquired acoustic signals from one aleatory and four deterministic processes. Among this, three of them constituted signals derived from strange attractors and one from a limit cycle behavior. The aim was to study the different effects that these random and deterministic processes could provoke in the human brain, specially those derived from chaotic dynamics.

The present work confirmed that the three auditory stimulation processes derived from chaotic systems presented stronger relative and statistical differences from basal state compared to the aleatory and periodic stimulations. Specifically, up to negative (30 and 40) % relative differences in delta and theta power were found in specific EEG locations, mainly frontal regions of the brain, using these chaotic stimulations.

List of Figures

List of Tables

Contents

Chapter 1

INTRODUCTION

Dynamical systems theory has given way to the development of theoretical models, mathematical tools and experimental techniques in current neuroscience research [1]. Here, the premise is that the rhythm and periodicity of biological processes are central to life [2, 3], alluding to cycles such as breathing, heart pulse, sleep and neural activity, to name a few. To understand the motion, behaviour, evolution and relation over time of a given process or phenomena, is the main essence of analysis in dynamical systems. Thereby, neuroscience has come to strongly rely on the use of these nonlinear dynamics to better understand the characteristics of these processes, specially through the properties from its most notorious feature of which is chaos.

Chaos is a class of dynamical behavior in nonlinear systems [4]. One of the pioneers in its discovery was Henri Poincaré, who in 1881, created a mathematical method that focused on a geometric qualitative approach in the study and analysis of what is now known as dynamical systems [5]. Later, in 1963, Edward Lorenz published a nonlinear model of the atmosphere, defining for the first time a mathematical model that displayed chaotic behaviour in what is now known as strange attractor [6]. Since then, chaos has been modeled and utilized in different behaviors such as turbulence, thermodynamics, chemical reactions, analog circuits and electric brain activity [7–11].

To understand what "chaos" means, there is no single-universally accepted definition of the term, but rather a description of characteristics that chaotic dynamics present [1]. First, the long-term behaviour is aperiodic. Second, the dynamics can change dramatically depending on the initial conditions of the system, leading to unpredictability. And third, the behaviour is deterministic, which means that it obeys certain "laws" that defines its movement, much unlike random or aleatory processes. Robert L. Devaney [4] summarizes these characteristics as, ". . . a chaotic map possesses three ingredients: unpredictability, indecomposability, and an element of regularity."

In the electric brain activity, analyzed using electroencephalography (EEG), different patterns in the variation of voltage can be seen (in μV), which oscillate in specific frequencies creating waves with unique characteristics and functions [12]. Here, the implication of chaotic properties in these neural signals would bring new insight in its control parameters and understanding through nonlinear EEG methods and techniques of characterization [13,14]. Therefore, there is a wide range of reported research around this field [15–17], where neural models have been implemented using nonlin-

ear dynamical systems, described by differential equations in terms of states and parameters of voltage and time.

Another very interesting feature of chaos is that it basically involves variations over time (and it does so in a very specific way that is unpredictable, aperiodic, but deterministic). As such, these variations create oscillations that lead to the formation of waves with defined amplitude and frequency. If it happens that these waves oscillate in a human-audible frequency range, then the result would be that sound would be created from these chaotic processes. This fact laid the groundwork for this present thesis investigation, where we started with the question of how would an acoustic wave derived from chaotic behaviour be perceived? How would it sound? And moreover, how would it relate with the presumably glimpsed presence of chaos in the human mind?

It is known that the acoustic waves captured by the human ear have notable effects in the neural activity of the brain [18]. This electrical signals basically cause a cascade of events that have psychological and physiological implications, which constitute the brain activity in response of these acoustic waves. Even so, the influence of sound in the human mind can not be determinedly understood, paraphrasing György Buzsáki in [3]: "If the brain were simple enough for us to understand it, we would be too simple to understand it". Still, this investigation hopes to contribute with new insight from a different kind of acoustic rhythm and its influence on brain features and sound perception.

Former studies have proved that using oscillatory acoustic signals, brain features denominated waves or rhythms (alpha, delta, beta, theta and gamma) can be enhanced or inhibited [19]. This can lead to an infinite possibility of amplitude combinations that basically determine the cognitive processes of the mind [20–22]. Although some specific activities are related to each one of the brain waves, Başar *et al.* [20] suggest that it is not the isolated behaviour of the waves but rather the interaction between them what forms the solid groundwork for neural communication processes.

Despite the wide range of research on sound transduction of the brain, studies that involve sound directly generated from chaotic processes and its influence over neurological behaviour, have proven scarce and hard to find. Probably, the closest to chaos type of reported acoustic stimulation could be that performed under the binaural beats (BB) theory [23]. Here, the basic concept is the sound exposition of two tones with a differing frequency, one tone to each ear. This results in an irregular, but controlled, overall stimulation that causes the brain to "make up" for this aperiodic rhythm by enhancing or inhibit its own frequency waves.

Gálvez *et al.* [24], for instance, found significant decreases in theta wave over several EEG localizations using BB's stimulation in patients with Parkinson's disease. According to this study and its referenced literature, patients suffering from Parkinson's disease exhibit an increase in the power of theta waves compared to healthy subjects. The aim, then, was to decrease these irregularly high theta amplitudes using an arrhythmic auditory stimulus. The possible similarities here between BB and chaotic dynamics is only that both result in controlled aperiodic stimulations. However, as we will further show in this investigation, chaos is a much more complex process that has many other properties and characteristic besides aperiodicity.

Taking into account the exposed context, we studied acoustic design from chaotic behaviour and analyze the response of the human brain using EEG characterization

methods and comparisons with effects from other non-deterministic processes.

1.1 Hypothesis

The hypothesis of this study is that the human brain will show stronger effects by the auditory stimulation from the acoustic signals generated from chaotic systems, caused by the aperiodic nature of the signals and resonance provoked in the neural activity. Moreover, we hypothesize that the dynamical properties of the system sound will be related to power features of the brain but not on the subjective perception from the sounds.

1.2 Justification

EEG analysis is considered one of the best-suited methods for brain activity studies in neuroscience. Currently, EEG systems with advantages as wireless transmission, dry electrodes and designs that minimize the preparation for measurement and analysis have been developed, improving even more the accountability of this method (as we will aboard in depth during the following chapters of this investigation). The study of effects on the neuronal behavior in presence of acoustic waves from chaotic models will complement the actual research of how the mind interprets and process acoustic waves.

1.3 Objectives

The present thesis has the following objectives:

General Objective

Generate and record acoustic signals derived from the voltage of chaotic systems implemented using electronic circuits and utilize them as auditory stimuli to compare models of chaos, periodicity and randomness using brain effects on perception evaluations and power spectral features on EEG signals.

Specific Objectives

1. Numeric modeling of chaotic systems with parameters of bifurcation

2. Analog design and electronic implementation

3. Digital voltage acquisition of the electric signals derived from state variables

4. Sound design for acoustic stimuli generation from the signals

5. Auditory perception analysis of sounds

6. Experimental protocol design for EEG study using acoustic stimulation

7. Segmentation into basal and stimulated classes

8. Extraction of delta, theta, alpha, beta and gamma power bands from EEG signals

9. Statistical tests of differences between stimulus classes

1.4 Structure

The rest of this thesis is organized as follows. Chapter 2 describes the principles of electrophysiology, from the basic structure of the Central Nervous System to its underlying working mechanism. It also contains a brief overview of the most common techniques for monitoring brain activity, the classical cerebral attributes of studies and its auditory processes influence.

A review of linear and non-linear dynamical system fundamentals is presented in Chapter 3. It defines a group of chaotic systems that were designated as the acoustic stimuli for this study according to their properties and complexity.

Shifting now to the experimental context, Chapter 4 contains the methodology and materials used for the experiment performed to asses the main objectives of this study. It also describes the analysis and signal processing used after data acquisition. Finally, the results and conclusion obtained from the aforementioned experimental protocol are presented in Chapters 5 & 6.

Chapter 2

ELECTROPHYSIOLOGY AND AUDITORY STIMULATION

To have a better understanding of the brain signals required for the analysis of acoustic stimulation performed in this study, it is necessary to define essential concepts related to the source and generation of these signals, as well as the different methods for the recording of brain activity and its processing, which are of great importance in the assessment of provoked effects.

In this chapter are presented the basic concepts of the Central Nervous System and its fundamental processes underlying the mechanism for neural activity, specifically for auditory processes in the brain.

2.1 Central Nervous System

The Nervous System is formed by the Central Nervous System (CNS) and the Peripheral Nervous System (PNS). Together, they coordinate the functions and activity of the body by transmitting signals around the muscles and other human systems.

The CNS is conformed by the brain and spiral cord. Functions like thinking, feeling and remembering are carried out by the brain along with the processing complex sensory information. It is protected by layers of skin, bone, cerebrospinal fluid and the meninges: dura mater, arachnoid and pia mater.

The brain has three main parts: brainstem, cerebellum and the cerebrum. They are connected to the spinal cord that acts as the conduit through which the brain transmits and receives signals from the rest of the body [25].

2.1.1 Cerebrum

The cerebrum is the largest region of the brain and it performs functions like voluntary movement, learning and regulating emotions, among others. A longitudinal fissure in the middle separates it into two lateralized hemispheres that are communicated through nerve fibers called the corpus callosum [26].

Each cerebral hemisphere also has smaller fissures that divide them into 4 lobes, the frontal lobe, parietal lobe, occipital lobe, and temporal lobe. Each one is responsible
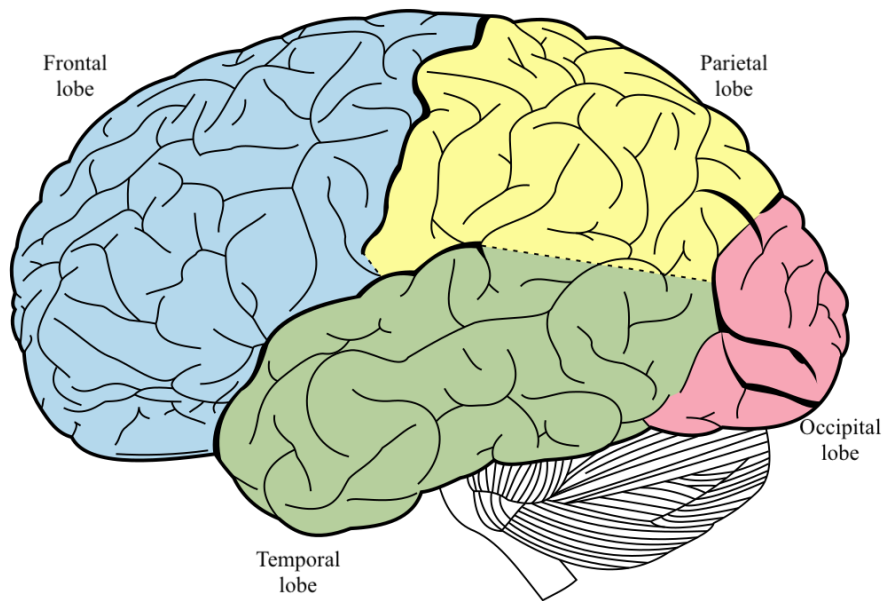
Figure 2.1: Cerebral lobes localization [27]

for a series of given specific functions, as described in Table 2.1, which shows some related processes of the lobes. Figure 2.1 illustrates the 4 areas in the cerebrum and its localization, where the blue region corresponds to frontal lobe, green to the temporal lobe, yellow to the parietal lobe and red region to the occipital lobe.

The cerebrum has an external layer of gray matter called the cerebral cortex and the inner layer is made up of white matter. The cerebral cortex is of great interest in this study because of the electrochemical phenomena that takes place in that layer.

2.1.2 Action Potential

The CNS is made up of nervous tissue formed mainly by cells: the glial cells (neuroglia) and the nerve cells. These last are also called neurons and they are capable of responding to stimulus and transmit electrochemical signals [28].

There are different types of neurons: bipolar (interneuron), unipolar (sensory neuron), multipolar (motor neuron), among others; but all of them have the same basic components, consisting of the cell body, dendrites and axon. The dendrites receive information from other neurons, and the axon is responsible for the transmission of that

Table 2.1: Lobes of the cerebrum

Lobe	Processes involved
Frontal	Cognitive functions, planning, motor skills, muscle movement
Parietal	Pain, pressure, touch, coordination, perception
Occipital	Visual information processing
Temporal	Language, memory, auditory functions
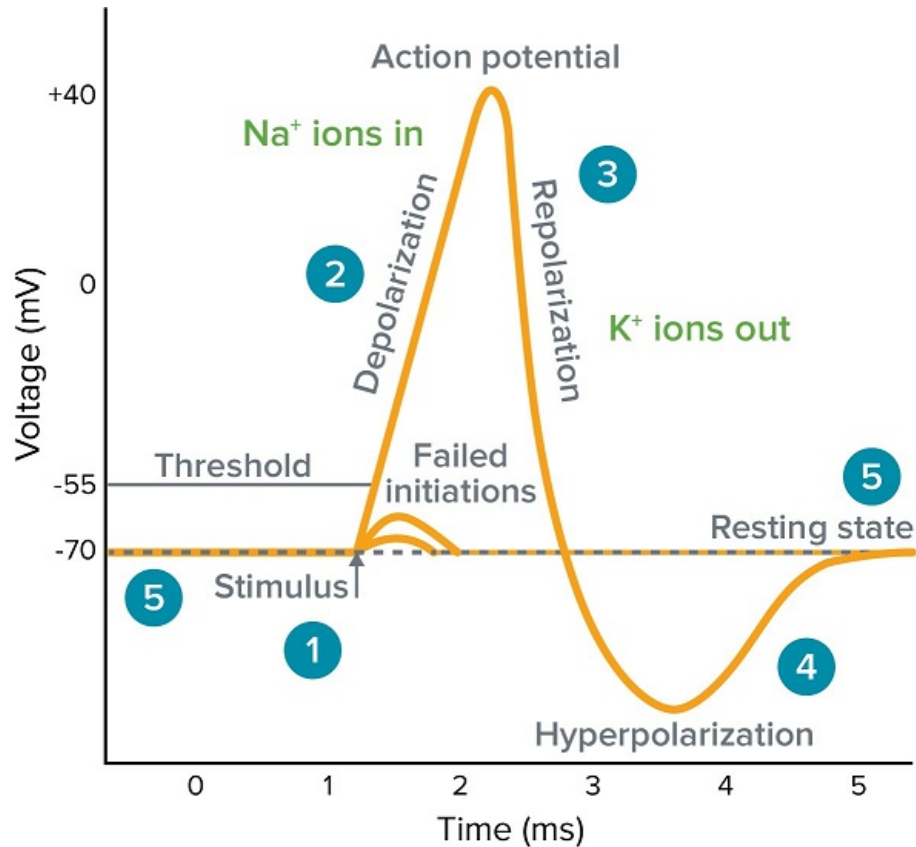
Figure 2.2: Action potential phases [33]

information to other neurons.

When a neuron is stimulated by sensory input or neighboring neurons, it fires an electrical impulse that travels along its axon, this is called action potential [29]. Neurons have a difference in voltage between the inside and outside of the membrane, a resting neuron is more negative on the inside, relative to the space outside it. This neuron voltage goes around -70 mV and is defined as the resting membrane potential.

The electrical charges of the neuron are mainly generated by sodium (Na^+) ions outside the cell and potassium (K^+) ions inside of the cell [30, 31]. When a neuron is inactive, a protein called the Sodium-Potassium Pump creates an electrochemical gradient by moving 3 sodium ions to the outside per every 2 potassium ions it moves inside of the cell, leading to the overall negative potential. In this state, the neuron is said to be polarized.

In addition to the pumps, ions can also pass across the membrane through other proteins when their respective gates open up, these are called ion channels. There are several different types of ion channels, and each one only provides passage to specific ions under certain conditions depending on their structure and purpose [31].

Figure 2.2 shows the voltage fluctuations over time for the neural phenomenon of the action potential. It can be described into 5 main phases, which are indicated by the blue numbers depicted in the figure and will be noted below.

The sodium channels of the neuron are voltage-gated channels, which means that their gate opening is triggered by voltage. Some others are mechanically-gated chan-

nels and they open in response to mechanical vibration or pressure, such as sound or touch stimuli. For the Na^+ channels, this potential is around -55 mV and it is known as the threshold for action potential [32] (see phase 1, marked as the circle labeled 1 in Figure 2.2).

The action potential is an all-or-nothing phenomenon defined by the threshold level. In other words, when a neuron is stimulated and its potential becomes more positive, it has to reach the threshold level for the Na^+ channels to open and fire the action potential. When this happens, the interior of the membrane becomes positive and reaches around +40 mV [34], this is called depolarization (phase 2).
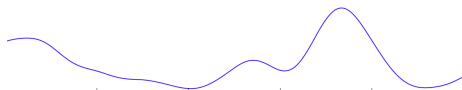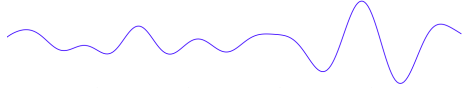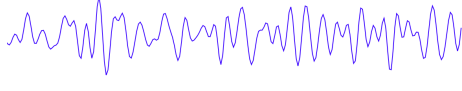
Shortly after, the process of repolarization (phase 3) would start and now the voltage gated potassium channels would open. This provides passage to K^+ ions outside of the membrane, making the interior more negative. A brief transitory state of hyperpolarization (phase 4) takes place, dropping around -75 mV. Then, the sodium-potassium pump would bring the neuron back to its negative resting state (phase 5).

The action potential of the neuron sends the electrical signal through the axon, which can travel like a wave along the nerves, muscles and it may also trigger other neighbor cells. This transmission of information is one of the most important mechanism of communication of the CNS [35].

When the neuron has been stimulated and is in the middle of an action potential, it can not respond to another stimulus, no matter how strong it may be. This is due to a process defined as the refractory period—the time that it takes for the cell to be ready for another stimulus.

It is worth noting that the voltages for every phase of the action potential are always the same, even though they can vary depending on factors like the type of cell. However, the voltage does not depend on the type or strength of stimulus. The potential levels are always the same but what does change is the conduction velocity and frequency of the potentials, as will be considered on the following section.

Table 2.2: Brain rhythms

Rhythm	Band (Hz)	Processes associated	Form in one second window
Delta (δ)	1 to 4	Sleep	
Theta (θ)	5 to 7	Awareness	
Alpha (α)	8 to 13	Eyes closed	
Beta (β)	14 to 31	Default mode	
Gamma (γ)	Above 32	Mindfulness	

2.2　Brain Waves

One of the main focus on brain signals is their spectral features, called brain waves or brain rhythms [3]. The five main waves are delta, theta, alpha, beta, and gamma. They are classified in terms of their frequency (impulse velocity) and amplitude (sum of activated potentials), as shown in Table 2.2, as well as by their associated functions and processes of the brain.

Studies often analyze the amplitude and band-variability of the waves related to events or types of stimulus applied. Experimental results have shown that brain waves are not independent of each other, and that they not only act in isolated processes but also exist in parallel functions creating blocks for the complete functioning of the brain. In addition, other parameters such as amplitude, blocking time, delay or duration of the wave are strongly related to neuronal communication and play an essential role in cognitive processes [20].

2.3　Methods for Registration of Brain Activity

The electric currents and activity generated by populations of neurons underlie the fundamentals of certain brain functions and processes studies, these can be monitored and analyzed by different time-varying techniques.

Among the more commonly used methods are non-invasive techniques like functional Magnetic Resonance Imaging and invasive ones like Electrocorticography. Below follows a brief description of the main techniques, putting emphasis on the modality employed in this investigation: Electroencephalography.

2.3.1　Electrocorticography (ECoG)

ECoG was developed in 1940 by Wilder Graves Penfield and Herbert Jasper [37]. It consists of the direct recording of electric potentials generated by the populations of neurons from the cerebral cortex. ECoG has been widely used in epilepsy surgery to identify cortical areas and help delineate epileptogenic regions for the determination of surgical areas considered for resection.

ECoG invasive nature of recording during surgery provides good quality and low noise signals useful to study fundamental processes at high spatial and temporal resolution. However, the anesthetic agents and surgical stress of the patient can affect the normal brain functions. Operations during ECoG may be performed under local anesthesia to preserve normal activity on the regions.

2.3.2　Functional Magnetic Resonance Imaging (fMRI)

The electric potential of neurons and cerebral blood flow are coupled, the blood flow of a region increases when that area of the brain is active. The fMRI measures brain activity indirectly by the detection of changes in blood flow due the use of energy of brain cells.
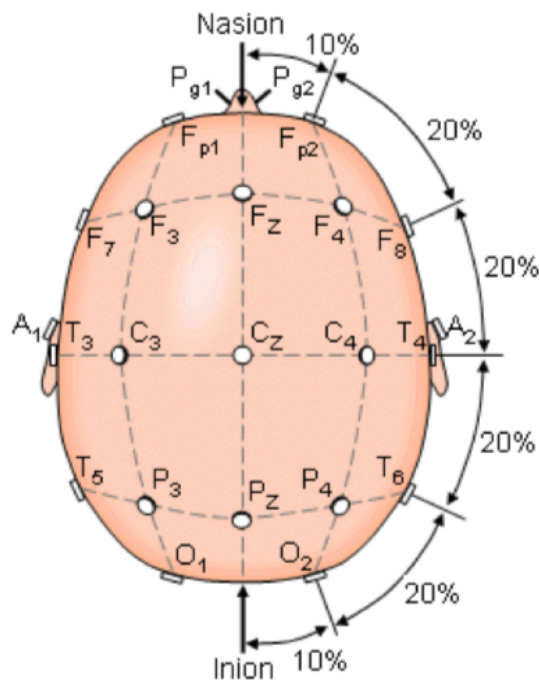
Figure 2.3: Electrode positions according to the 10-20 system [42]

Japanese researcher Seiji Ogawa discovered Blood Oxygen Level Dependent (BOLD) contrast [38], which is the technique underlying fMRI. It works by mapping the changes of magnetic resonance imaging properties of the brain caused by increases in blood oxygen levels under mental processes. It basically reflects which areas of the brain respond to specific cognitive functions.

It's been widely used on neuroscience mapping research due to advantages like its non-invasive, radiation-free nature and fine spatial resolution. However, some disadvantages would be its relatively high cost of use and low temporal resolution. It is also not possible to perform in patients with metallic implants or monitoring devices.

2.3.3   Electroencephalography (EEG)

The invention of EEG is attributed to Hans Berger with his first experiments on electric potentials in the human brain and paper published in 1929 [39]. Since then, it has been widely used to study brain functions, neurological disorders and brain-computer interfaces (the communication through mental activity to control devices) [40].

EEG is a technique that monitors time-varying voltage fluctuations of the cerebral cortex through multiple electrodes positioned along the scalp [41]. As is also the case of ECoG, the acquired signals come from small electrical currents (in the order of μV) generated from populations of neurons in the brain.

The placement of EEG electrodes is commonly arranged according to the 10-20 international system [43]. This method describes the localization of electrodes on the scalp in order to standardize analyzed regions in EEG studies. The system is named after the distance between electrodes set to 10% and 20% of the length from nasion to ion, as shown in Figure 2.3. Higher resolution systems have also been used, such as
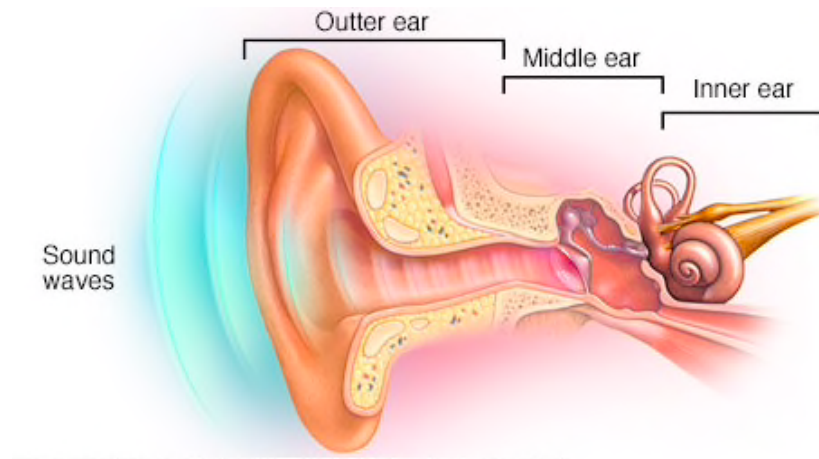
Figure 2.4: Parts of the human ear [46]

the 10-10 and 10-5 systems.

The positions of electrodes are labeled by initial and number according to the brain region where they are localized—central (C), frontal (F), pre-frontal (Fp), parietal (P), occipital (O) and temporal (T). There's also the z-points, placed on the midline sagittal plane of the skull, even numbers are placed to the right and odd to the left of this reference middle plane.

The EEG electrodes can make contact with the scalp through saline-based gel or paste, this aids in the electrical conduction of the skin. Dry-electrode systems are commonly used as well, and compared to the wet sensors, they are more comfortable [44] and their set up process is minimum or faster.

Studies based on EEG mainly focus either on the Power Spectral Density (PSD) of the EEG signals or on Event-Related Potentials (ERP). The ERP focuses mainly on time-locked properties of response to specific auditory, sensory, motor or cognitive event. The PSD investigates frequency content of the voltage oscillations generated by neural communication involved in cerebral cognition and functioning [20].

2.4   Sound Transduction

The auditory system is responsible for the conversion of acoustic waves into neural impulses required for sound interpretation [45]. These impulses can be sound sources such as ambient noise, music, speech or many other sources. This is achieved through the mechanoelectrical transduction that the human ear is responsible for. The ear is one of the main sensory organs of the system, it is divided into three sections: the outer, middle and inner ear (see Figure 2.4).

The outer ear catches acoustic waves and passes them through the auditory canal onto the tympanic membrane or eardrum, it amplifies certain frequencies around the range from (3 to 12) kHz. When the eardrum vibrates due acoustic pressure, it passes these vibrations to the three tiny bones that conform the middle ear: the malleus, incus, and stapes; also known as hammer, anvil and stirrup. The middle ear is also called tympanic cavity, and it focuses the pressure of sound waves onto the inner ear through
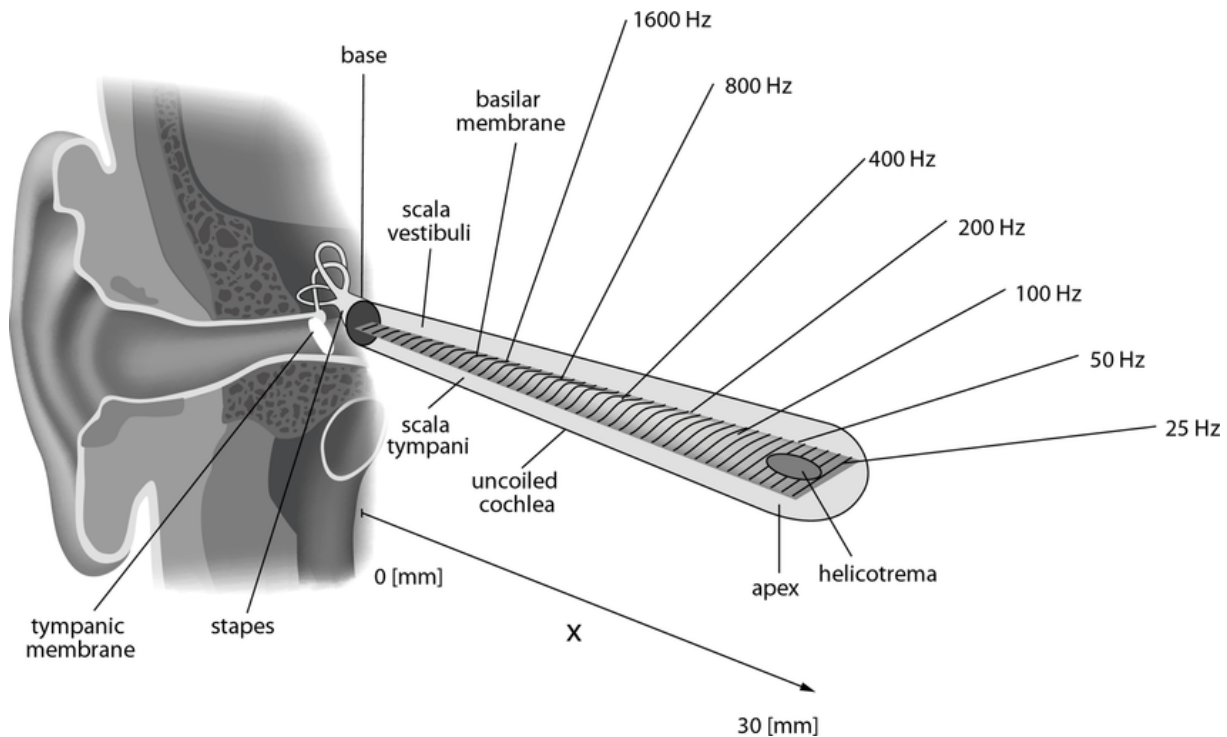
Figure 2.5: Uncoiled cochlea and basilar membrane [47]

the superior oval window.

In the inner ear, the sound pressure is now transmitted through special fluid instead of air. In turn, a coiled structure called the cochlea converts these physical vibrations into electrical signals for the brain. It accomplishes this through the basilar membrane and the organ of Corti. The basilar membrane is a band of fibers that resonate at different locations depending on the wave frequency transmitted by the cochlear fluid. Figure 2.5 shows that fibers near the base of basilar membrane are shorter and vibrate in response to high-frequency oscillations, whereas fibers closer to the end are longer and resonate with low-frequency pressure. These vibrations in the basilar membrane stretch tiny sensory cells of the organ of Corti, also called hair cells [48]. When they are triggered, they open up mechanically gated Na^+ channels that generate action potentials in the cochlear nerve, the so-called auditory nerve [48].

The action potentials are propagated from the cochlear nerve thought the auditory pathway and up to the cerebral cortex. In the temporal lobe of the cerebrum is located the auditory cortex, which is responsible for the perception and interpretation of the electric potentials generated by sound [49]. Neurons in the auditory cortex can detect the pitch of sound based on the location of hairs cells triggered in the organ of Corti. Greater sound pressure produces more hair cell vibrations, which in turn generates more frequent action potentials. These electric frequencies, among other acoustic parameters from auditory signals, are attributes associated with the perception and cognition evoked by received sound.

Chapter 3

DYNAMICAL SYSTEMS THEORY

In this chapter is presented an introduction to central concepts and fundamentals necessary for the understanding of nonlinear systems and chaos. In order to accomplish this, we start with a definition for a wider subject known as dynamics. The aim is to make a clear distinction of what it means for a dynamic behaviour to be periodic or chaotic. For this, we introduce basic terminology from dynamical systems theory such as state space, strange attractors, Poincaré maps and bifurcations.

Moreover, the final section of this chapter will introduce a set of chaotic systems which are the base for the forthcoming experiments to be reported in the present investigation. This group of systems was utilized as the chaotic means of experimentation in this study. It was determined taking into account the state waveform frequencies of the systems, as well as the simplicity of their mathematical model equations used to describe and implement them.

3.1 Dynamical Systems

One of the main objectives of physics in science has been the study of motion, to understand the underlying laws that describe and govern movement. This can be traced back to the essential discoveries of Issac Newton [50], such as his laws of motion in classical mechanics and the law of universal gravitation. Once these laws were known, the possibility to predict movement and future events became the groundwork for latter findings on diverse fields of investigation.

Around 1880, the studies of Poincaré [5] on the so-called three-body problem contributed with a geometric approach on how to observe the behaviour over time of systems—in this case, the solar system. He found that the movement of three celestial bodies was much more complex given the now known nonlinear influence from the inverse law of gravitational attraction. He described the concept of nonlinearity where small differences on initial conditions produce great ones on the final behaviour, becoming impossible to make long-term predictions. Therefore, his geometric point of view focused on qualitative rather than quantitative properties of the long-term behaviour. This laid the essential foundation for a field now called dynamical systems theory [51], where one of the main objectives is to characterize the dynamics of linear and nonlinear systems.

Dynamics describe the evolution and variation over time of systems [1]. These systems can be defined in terms of differential equations or iterated maps [4]. The evolution from systems of linear and nonlinear differential equations is described in continuous time, whereas the one from iterated maps correspond to discretized time. To our purposes, in this investigation we will refer only to the former type of systems.

A general homogeneous system of differential equations can be described as

$$\dot{\mathbf{x}} = \mathbf{A}\mathbf{x} \tag{3.1}$$

such that

$$
\begin{bmatrix} \dot{x}_1 \\ \dot{x}_2 \\ \vdots \\ \dot{x}_m \end{bmatrix} =
\begin{bmatrix}
a_{1,1} & a_{1,2} & \cdots & a_{1,n} \\
a_{2,1} & a_{2,2} & \cdots & a_{2,n} \\
\vdots & \vdots & \ddots & \vdots \\
a_{m,1} & a_{m,2} & \cdots & a_{m,n}
\end{bmatrix}
\begin{bmatrix} x_1 \\ x_2 \\ \vdots \\ x_m \end{bmatrix} \tag{3.2}
$$

where overdots denote differentiation with respect to t. Hence $\dot{x}_m \equiv \mathrm{d}x_m/\mathrm{d}t$. Here $\mathbf{x} = [x_1, \ x_2, \ \cdots, x_m]^T \in \mathbb{R}^m$ is known as the state vector of the system, in physical applications the states may represent variables such as position, velocity, temperature, to name a few. Coefficients $a_{m,n}$ with $(m, n) = [1, 2, \cdots]$ in matrix $\mathbf{A}$ correspond to parameters of the corresponding state, they might be stationary or varying depending on the problem at hand.

The system of differential equations described in Equation 3.1 is said to be linear given that all the states in vector $\mathbf{x}$ are elevated only to the first power, and all the coefficients in matrix $\mathbf{A}$ are defined such that $[a_{m,n}] \in \mathbb{R}^{m \times n}$. On the contrary, if the matrix $\mathbf{A}$ involves other algebraic or exponential terms, the system is now called nonlinear, as so it is the case when any of the states in $\mathbf{x}$ are elevated to second power or more. Consequently, a nonlinear system is more convenient to represent using the following notation

$$
\begin{aligned}
\dot{x}_1 &= f_1(x_1, \ x_2, \ \cdots, x_m, \ t) \\
\dot{x}_2 &= f_2(x_1, \ x_2, \ \cdots, x_m, \ t) \\
&\vdots \\
\dot{x}_m &= f_m(x_1, \ x_2, \ \cdots, x_m, \ t)
\end{aligned}
\tag{3.3}
$$

where $f_1, \ f_2, \ \cdots, f_m$ are arbitrary functions defined in terms of states $x_1, \ x_2, \ \cdots, x_m$ from the system, and the independent variable of time t.

This presented notation (3.3) will be utilized when defining nonlinear systems in forthcoming sections. It can also be written in a compacted vector notation as

$$\dot{\mathbf{x}} = \mathbf{f}(\mathbf{x}) \tag{3.4}$$

where $\mathbf{x} = (x_1, \ x_2, \ \cdots, x_m)$ and $\mathbf{f}(\mathbf{x}) = (f_1(\mathbf{x}), f_2(\mathbf{x}), \ \cdots, f_m(\mathbf{x}))$. Here, this set of functions $\mathbf{f}(\mathbf{x})$ can involve nonlinear terms such as state products $(x_1 x_2)$, powers (x_m^2), or other complex functions (such as $\sin(x_2)$ or e^{x_1}). These nonlinear terms might represent physical variables like viscosity of a fluid, forces of inertia, or inverse gravitation attraction (as encountered by Poincaré), to name a few.

Plotting the numerical solutions of the differential equations from a given initial position over variations in time is commonly the first step to characterize the dynamics
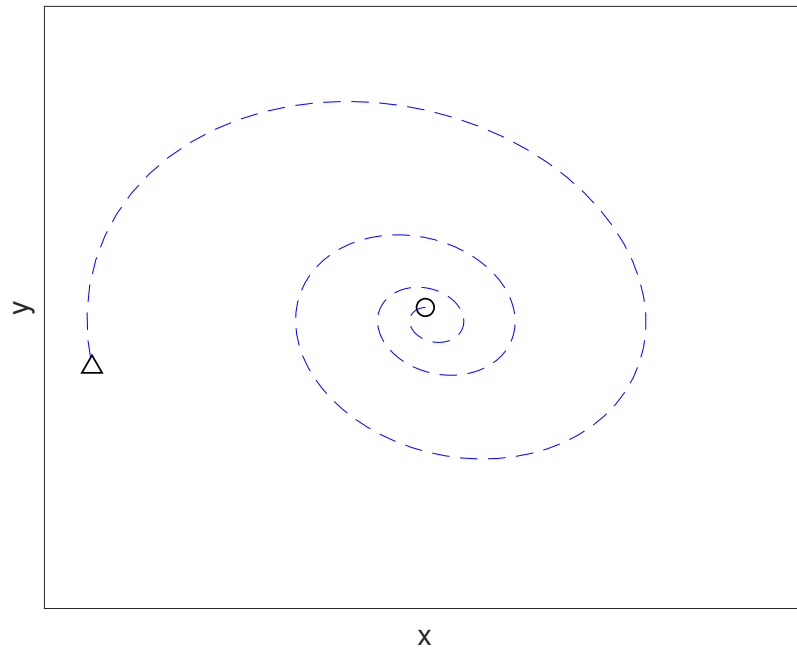
Figure 3.1: Fixed point attractor

of a system. This is possible by constructing an orthogonal vector field where each of the coordinate directions represent a variable from the dynamical system, this is known as state space (also called phase space or phase portrait). The paths traced in it by the instantaneous state evolution of a system are called trajectories, and they represent the behaviour of dynamics from the system at study.

The state space allows to determine qualitative behaviour from the evolution of a system instead of focusing on the analytic solutions from the differential equations, which can often be very complex and hard to interpret [1]. Phase space then makes easy to represent very complex numerical behaviour in a geometric and more visual form. Through the dynamics displayed in the phase space of the systems, it is possible to characterize them into a wide variety classes. For our purposes, in this study we are going to focus on three general kinds of dynamical behaviour known as attractors.

3.2 Attractors

The term attractor is used to describe a geometrical configuration in the state phase to which initial conditions or nearby trajectories are attracted by and tend to converge over time. Steven Strogatz [50] defines it in a simple manner as ". . . a set to which all neighboring trajectories converge. Stable fixed points and stable limit cycles being examples".

Figure 3.1 shows an example of the simplest attractor, known as stable fixed point. Here the triangle indicates a set of coordinates from a given initial condition in the phase space, which corresponds to (x, y) plane. The circle mark shown in the center
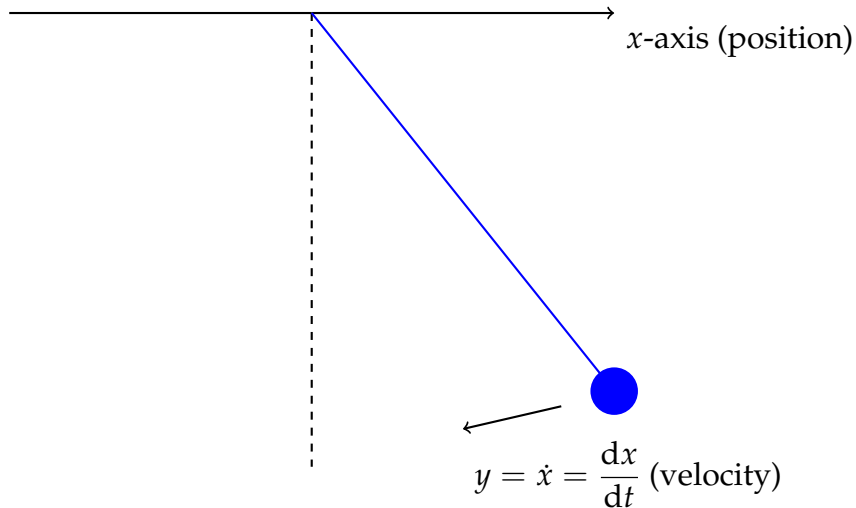
Figure 3.2: Swinging pendulum

of space corresponds to the attractor, a fixed point to which close trajectories converge to rest state. The path traced by the dashed blue line shows the trajectory for how the states approach the fixed point after a few oscillations.

The path traced to settle into the fixed point depends on the given system at hand, in Figure 3.1 it is in form of orbits. This attractor is often explained in a simple manner using the example of a swinging pendulum, where state x would correspond to position and y to velocity of the pendulum over time (see Figure 3.2). Here, the swings of the pendulum would decay after every oscillation due to friction in the air. This would be seen in the space phase in the form of spirals from the oscillations of both position and velocity, eventually settling into rest.

Another class of dynamics is formed when we consider that now the swinging pendulum has an external constant force that helps maintain the same swing potency. In this case, when the pendulum starts swinging from a given initial condition, its highest position x after every swing does not change but repeats itself once the external force leads to periodicity. Consequently, the same happens to the velocity y given that they depend on one another, they both keep repeating themselves after every swing.

This kind of motion represents periodic behaviour and its corresponding trajectory is known as limit cycle. In Figure 3.3 is shown a limit cycle attractor, which is represented by the continuous blue curve depicted in the plot. Here, the triangle represents a given initial condition that follows the trajectory traced by the dashed line, until it eventually merges into the attractor at the point marked with a black circle.

This occurs given that limit cycles are isolated closed trajectories with a defined period, waveform and amplitude, determined by the structure of the system itself. Consequently, any nearby trajectory will be attracted and spiral towards the limit cycle. It's worth noting that this class of attractor can not occur in linear systems of the type $\dot{x} = \mathbf{Ax}$. Limit cycles are a kind of dynamics particular to nonlinear systems, as it is also the case with the third attractor that we will introduce in this investigation.

Steady states and periodic behaviour were the only predictable forms of stability until, in 1963, the computational experiments of Edward Lorenz led him to the discovery of a different kind of dynamic behaviour [6]. Lorenz was studying weather
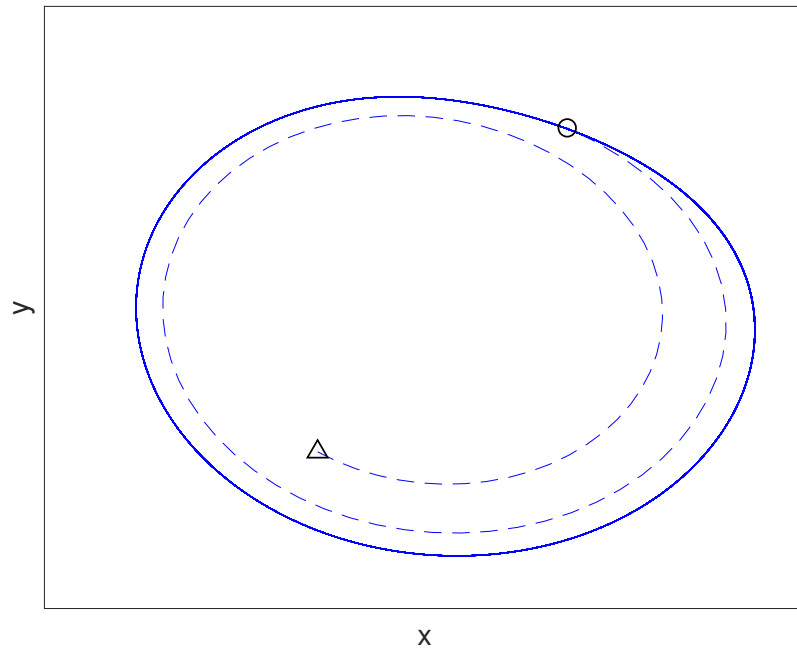
Figure 3.3: Limit cycle attractor

forecasting. For this, he developed a simplified mathematical model that described interrelations of convection rolls and temperature in the atmosphere. His differential model equations are the following:

$$\dot{x} = \sigma(y - x)$$
$$\dot{y} = x(\rho - z) - y \qquad (3.5)$$
$$\dot{z} = xy - \beta z$$

where x relates to fluid's flow, y to the temperature of a convection roll, and z to the nonlinearity in temperature difference along the roll. Values of σ, ρ, and β are parameters that characterize fluid, thermal and geometric configuration of the system. This model corresponds to a nonlinear system of the type $\dot{\mathbf{x}} = \mathbf{f}(\mathbf{x})$ according to the description provided in (3.4), given the state product terms.

By looking at the time series from the numerical solutions of the system, Lorenz found that they didn't behave in any periodic sequence neither settled into steady state. Instead, they seemed to continue oscillating in what it looked like a random pattern. Additionally, these numerical solutions seemed to vary drastically if he made small variations on the initial conditions of the simulation. At first, he attributed this to malfunctions of the computer, but then, he plotted the phase space of the system. He noticed that the solutions led to a butterfly-shaped form of dynamics, leading to the discovery of what is now known as a "strange attractor" (term coined latter by Ruelle & Takens on turbulence behaviour [52, 53]). This kind of attractor was defined by the main property of exhibit sensitive dependence on initial conditions [50].
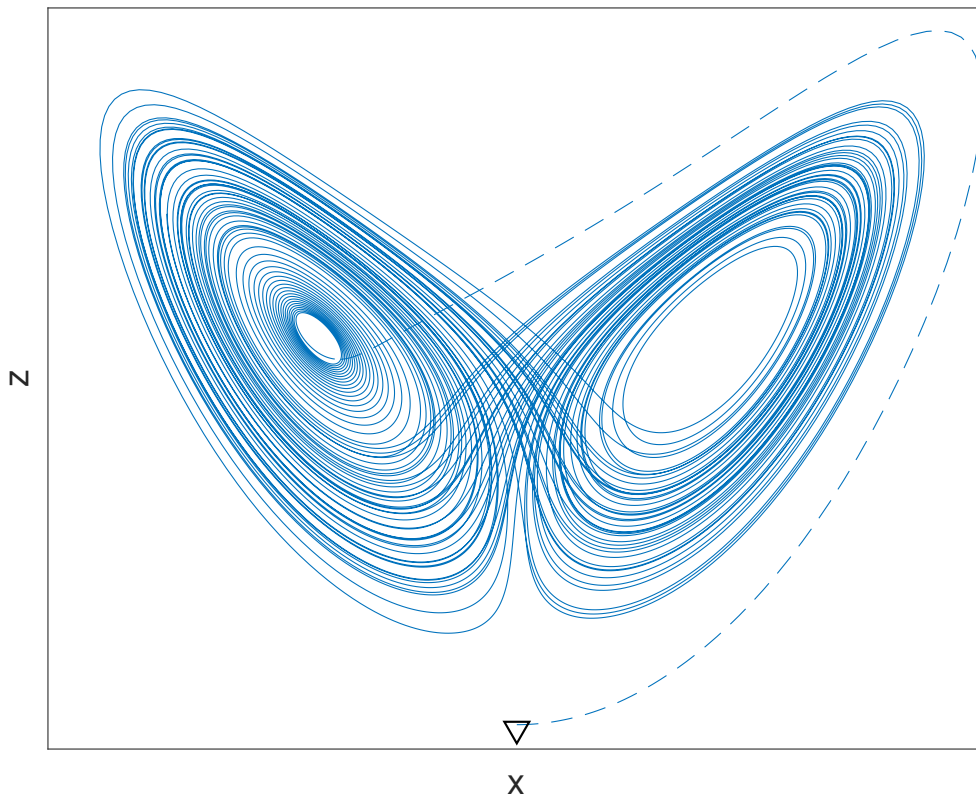
Figure 3.4: Strange attractor from Lorenz system projected on (x, z) plane

In Figure 3.4 we show the attractor formed by the system from Equation 3.5 with parameter values of $\sigma = 10$, $\rho = 28$, and $\beta = 8/3$. This attractor could be presented in its three-dimensional space (x, y, z), but we choose to show a projection of the plane (x, z) in order to make emphasis on the geometric differences with the two dimensional examples shown for fixed point and limit cycle attractors.

The attractor in Figure 3.4 corresponds to the geometric pattern formed by the trajectory represented with the continuous blue line in the space. This is the popular Lorenz's strange attractor for which the theory of "butterfly effect" is known for. The dashed line here shows the trajectory for how a given initial condition (here marked with a triangle) would spiral into the attractor, although the exact point where the trajectory merges with the strange attractor is not clear to note here. This is due to the dense orbits that the attractor is made of.

Unlike the limit cycle, the strange attractor from the model of Lorenz equations does not have a closed trajectory with defined period and amplitude, neither is a fixed point where systems settle. Instead, this attractor is considered a fractal, and it illustrates the main features for a new class of aperiodic behaviour in nonlinear systems known as chaos [50].

Chaotic behaviour can display stable and unstable properties in the dynamics, but leading to an overall stability of the system. What we mean by this is that in different

sections the nonlinear terms of the system can cause exponential growth in some directions, while in another section the attractor could have nonlinear decay. This is caused by a combination of stable and unstable eigenvalues of the system, which basically determine if equilibrium points of the attractor are repulsive or attracting. Consequently, nearby trajectories separate from each other into infinite surfaces but without loosing its deterministic geometric pattern [1].

Although there is no single universally accepted definition of chaos, it is generally attributed three essential characteristics: unpredictability, indecomposability, and an element of regularity [4]. Steven Strogatz [50] gives an elegant definition where he summarizes and explains these properties as:

> "**Chaos** is *aperiodic long-term behavior* in a *deterministic* system that exhibits *sensitive dependence on initial conditions*."

1. "Aperiodic long-term behaviour" alludes to the formation of strange attractors as $t \to \infty$ from a given initial condition

2. "Deterministic" means that the system does not have random inputs or parameters

3. "Sensitive dependence on initial conditions" means rapid separation of nearby trajectories, leading to dense orbits

Numerous nonlinear systems with chaotic behaviour and different dimensionality have been studied since Lorenz's publication of his model. In this investigation we are going to study three mathematical models of chaotic systems in $\mathbb{R}^3$.

3.3   Chaotic Systems

In this section we define a set of chaotic systems that will be utilized in the forthcoming experimental section of this investigation. The definition of the mathematical model of differential equations and dynamics of the system is presented, where it is possible to observe the chaotic behaviour for each one of them. These presented attractors are plotted using the standard parameter-values that are reported to generate chaotic behaviour in the systems. It's important to note that the numeric solutions from the nonlinear systems was carried out using an implementation of the numeric integrator method of Runge Kutta.

The group of chaotic system is conformed by the following models:

- Chen system

- Rössler system

- Unstable Dissipative (UD) system

One of the many fields where chaotic behaviour has been observed and studied is electronic circuits design. Nonlinear systems design is possible given that differential equations of the models can be also expressed as integrals instead of differentiations with respect of time. Opportunely, integration processes with electronic circuits

are relatively easy to implement with operational amps using the analog computation method proposed by Orponen *et al.* in [54]. We then took advantage of this property from the systems to be able to obtain chaotic signals for our auditory stimulation.

As will be fully described in the following chapter of this investigation, the set of chaotic systems were implemented analogically to extract the sound generated from the voltage of their state variables. In order to achieve this, the methodology of electronic design reported by Salas (2018) [55] was followed respecting to Chen and Rössler systems. As for the electronic implementation of the UD system, it was carried out using the exact same method described by Ontañón *et al.* in [10].

3.3.1 Chen System

The Chen system was published in 1999 by Guanrong Chen [56] in his pursuit for anticontrol of chaos. The model was basically derived from the same equations of the Lorenz system, having the exact same functions corresponding to f_1 and f_3, following the nonlinear system notation described in Equation 3.3. It is conformed by the following set of equations:
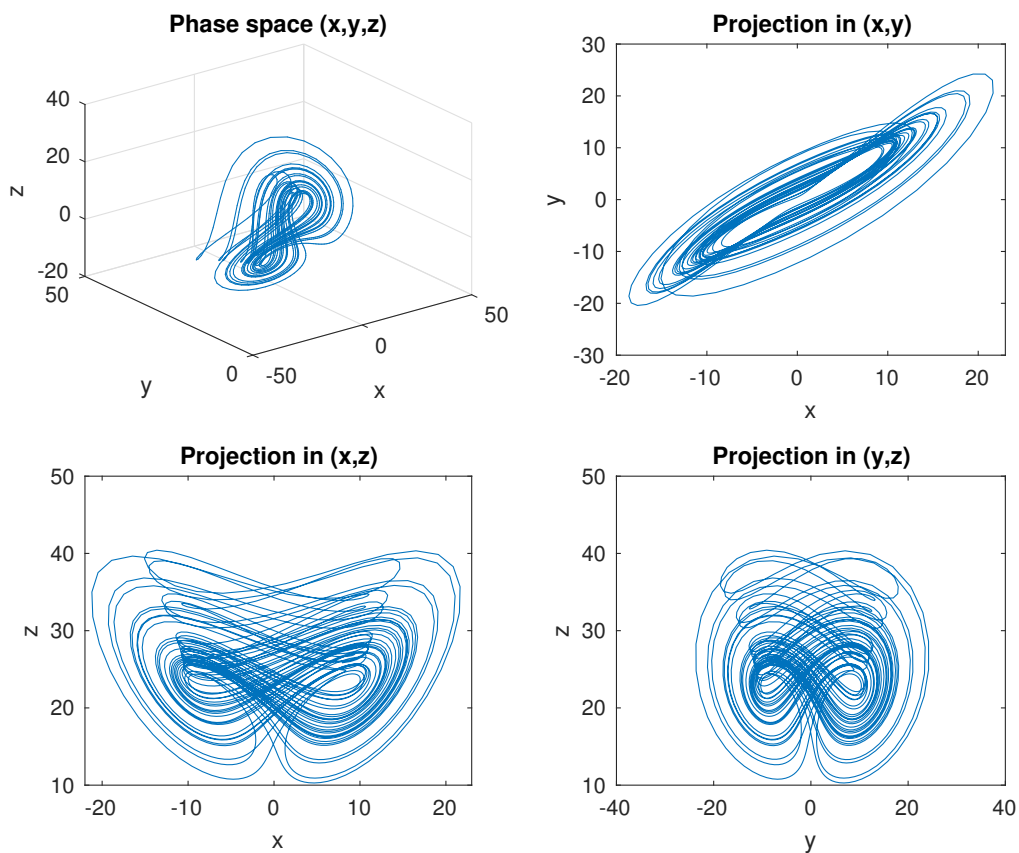
Figure 3.5: Strange attractor from Chen system

$$\dot{x} = a(y - x)$$
$$\dot{y} = (c - a)x - xz + cy. \tag{3.6}$$
$$\dot{z} = xy - bz$$

This system presents three states $(x, y, z) \in R^3$ as well as three parameters $(a, b, c) \in R^3$. The reported values for which the model generates chaotic properties are the following: $a = 35$, $b = 3$, and $c = 28$.

Figure 3.5 presents the attractor formed by this system with the parameters just described above. Here we show the form of the attractor on its three dimensional phase space, along with projections over different two-dimension planes. By looking at the (x, z) plane of the attractor, its familiar features from Lorenz system become evident. This attractor also has the butterfly-shaped form of Lorenz system, but with an additional kind of tornado rising from the middle of the wings.

3.3.2 Rössler System

This system was published by Otto Rössler in 1976 [58]. This model is also commonly compared to Lorenz system, given that the intention for it was to create an attractor
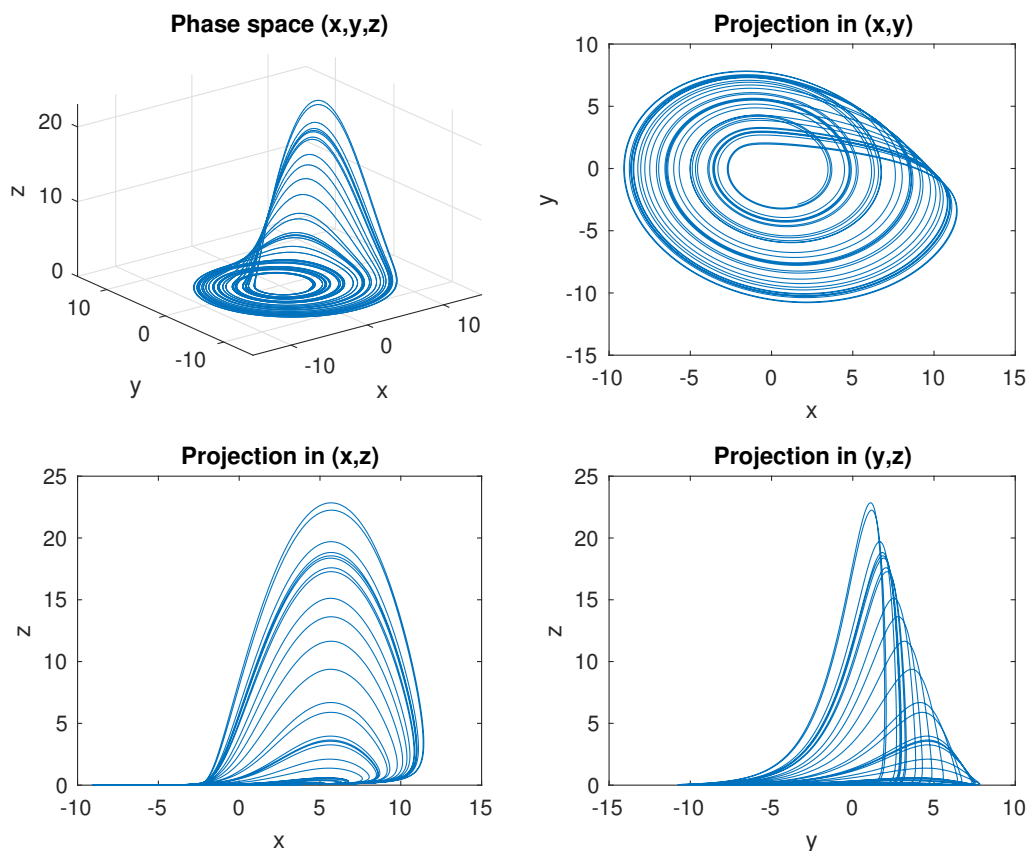
Figure 3.6: Strange attractor from Rössler system
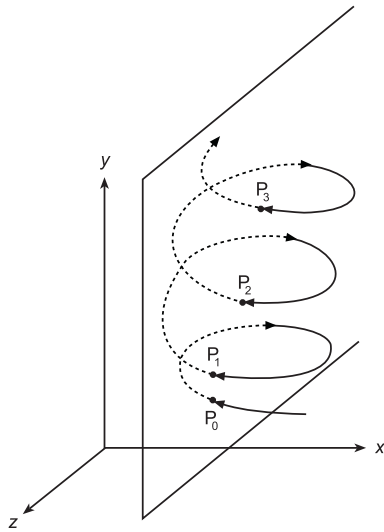
Figure 3.7: Poincaré section placed in the (y, z) plane with crossing points P_0, P_1, P_2 and P_3 [59]

with similar behaviour but using simpler equations. The system is described as fol-
lows:

$$\dot{x} = -y - z$$
$$\dot{y} = x + ay \qquad\qquad (3.7)$$
$$\dot{z} = b + z(x - c)$$

where $(x, y, z) \in R^3$ are the states, and $(a, b, c) \in R^3$ the parameters of the system. Originally, the model was published using the following values of $a = 0.2$, $b = 0.2$, and $c = 5.7$, for which the model generates chaotic behaviour and lead to the attractor presented in Figure 3.6. As described for Chen system, the attractor is shown in its three dimensional space along with projections over the planes.

By looking at the equations on (3.7), we can note that Rössler system only presents one nonlinearity (given by the zx product), unlike Lorenz and Chen systems which both present two nonlinear terms. This results in a one-scroll attractor with only two equilibrium points [59], instead of three. Given this, we choose this system to use a very important feature of nonlinear systems that are capable of display chaotic behaviour. One of the major advantages of chaos is that it can be switched from one kind of dynamic to another with very small alterations on its parameters. In other words, the systems can show rapid transitions between various dynamics using very weak control signals to force what is known as bifurcation.

Bifurcation in dynamical systems refer to changes of behaviour. It can be defined as "a division in two, a splitting apart, a change" [50]. Here, the aim is to study what is known as bifurcation points, which are often studied through a reduction of the phase space dimension using a Poincaré section (or Poincaré map). This method is depicted in Figure 3.7, where a return map is used to intersect a given trajectory to simplify and analyze the dynamics without altering its properties. Here, the plane placed in the (y, z) corresponds to the Poincaré section, and a sampling for every time the trajectory passes through the map is represented by the points P_0, P_1, P_2 and P_3.
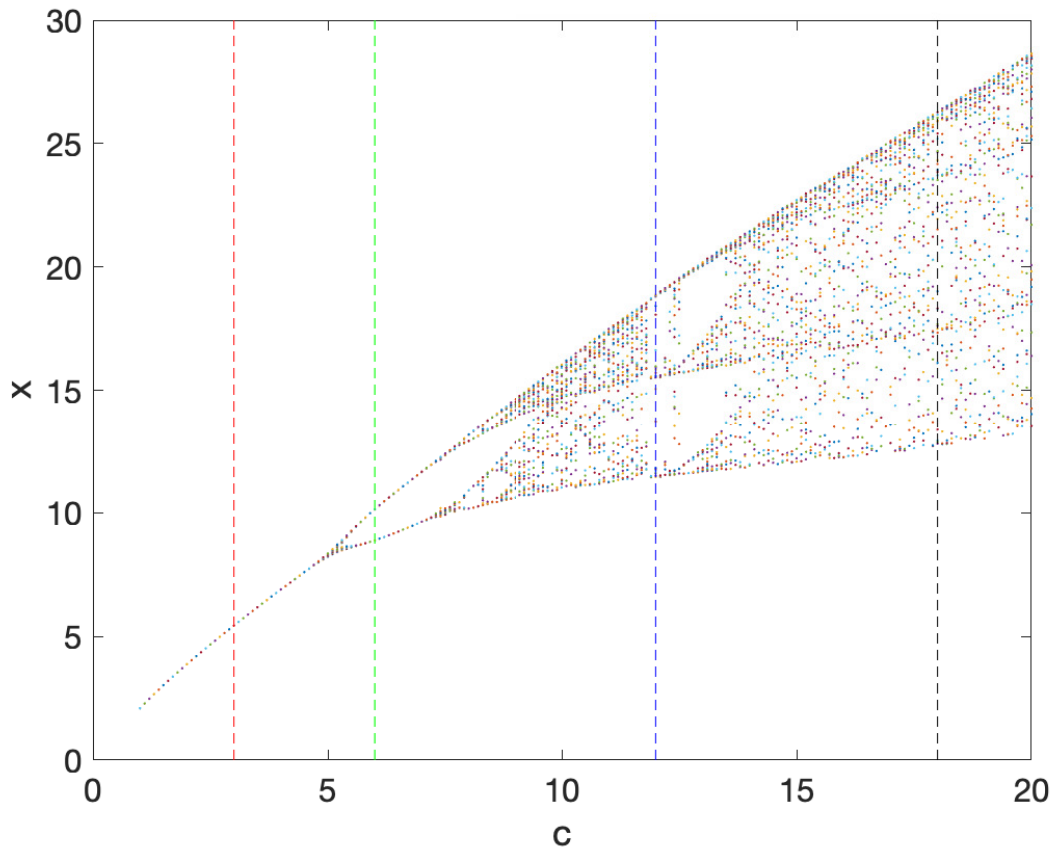
Figure 3.8: Bifurcation diagram for $c = [1 : 0.1 : 20]$ with $a = b = 0.1$

The object of bifurcation analysis is to study the changes of these intersection points from the maps as parameters change. This can be described graphically using a bifurcation diagram, which plots the number of intersection points in the map versus the sweeping values of a bifurcation parameter all awhile setting the remaining parameters constant.

Figure 3.8 shows a bifurcation diagram for Rössler system varying the parameter c. This was derived by the positioning of a Poincaré section in the plane (y, z), which results in a plot for the x coordinates where the map is intersected by the trajectory over sweeping values of parameter c. Here, the parameters a and b were both set to 0.1, which are also studied values for the analysis of Rössler system. Vertical dashed lines are plotted in c values of 3, 6, 12, and 18, where the number of times that a vertical line crosses a point in the diagram relate to the orbit period of the system.

In Figure 3.8 we can see a single line of points in the diagram from around (1 to 5) values of c. This means that for all these c-values, the trajectory only intersects the map in one point, which means that the trajectory is a limit cycle of period 1. Then at around $c = 6$ the line of points is divided in two, this is the essential meaning of a bifurcation. It indicates that now the trajectory hits the plane in two points, leading to periodic dynamic of two closed orbits.

Figure 3.9 shows projections of the system from the bifurcation points marked by
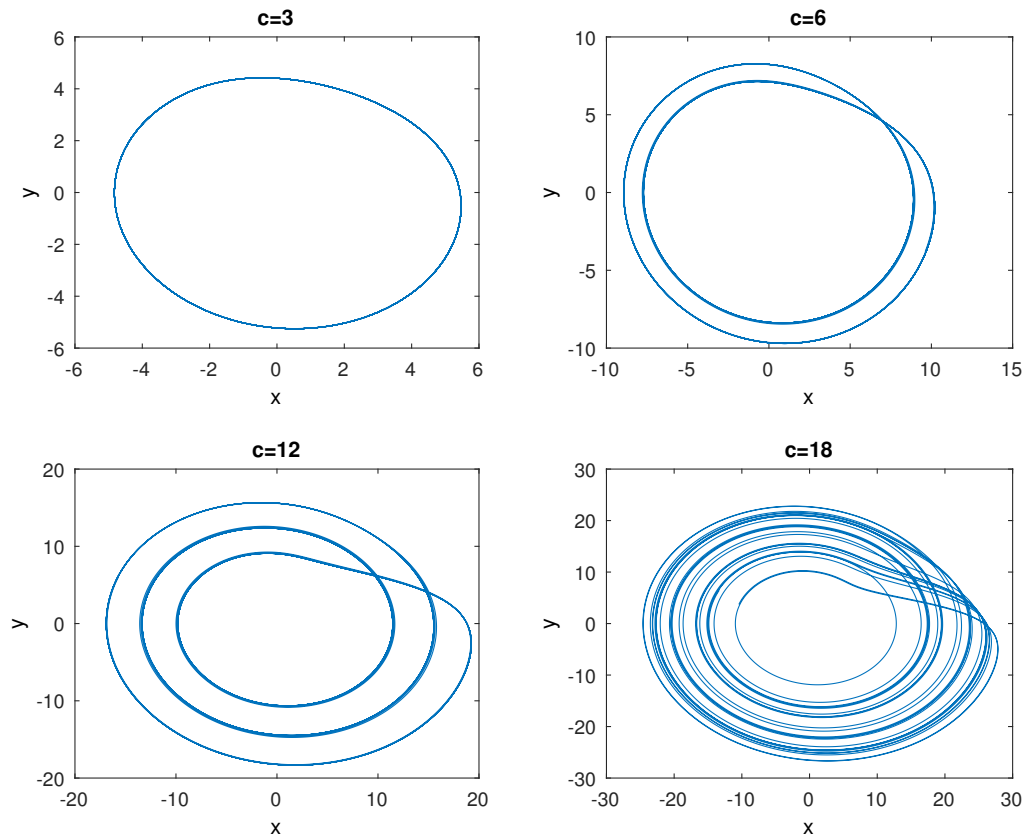
Figure 3.9: Projection (x, y) of Rössler system with periodic and chaotic dynamics setting $a = b = 0.1$

the dashed lines in Figure 3.8. Note how for $c = 12$ the dynamic has period 3, which implies that the system can present chaotic behaviour [60]. For $c = 18$ the system is now chaotic (aperiodic), according to the "infinite" (depending on numerical resolution [50]) points that resulted from the bifurcation diagram. Others values of c would also lead to chaos (for instance c=9, according to the bifurcation diagram), differences between these chaotic dynamics is generally compared using other methods for chaos quantification [1].

We will use this bifurcation property of the Rössler system in forthcoming sections of this investigation to generate periodic and chaotic dynamics from the system for auditory stimulation.

3.3.3 Unstable Dissipative System

The UD system [57] comes from a base of linear differential equations. It is a three dimensional system as defined by Equation 3.1, only that it is not homogeneous, which involves a vector $\mathbf{B} = [b_1, b_2, b_3]^T \in \mathbb{R}^3$. The system is then written as

$$\dot{\mathbf{x}} = \mathbf{A}\mathbf{x} + \mathbf{B}. \tag{3.8}$$

This system is based on piecewise linear (PWL) systems which consist of dynamical systems with solutions that results in an attractor presenting two or more scrolls along
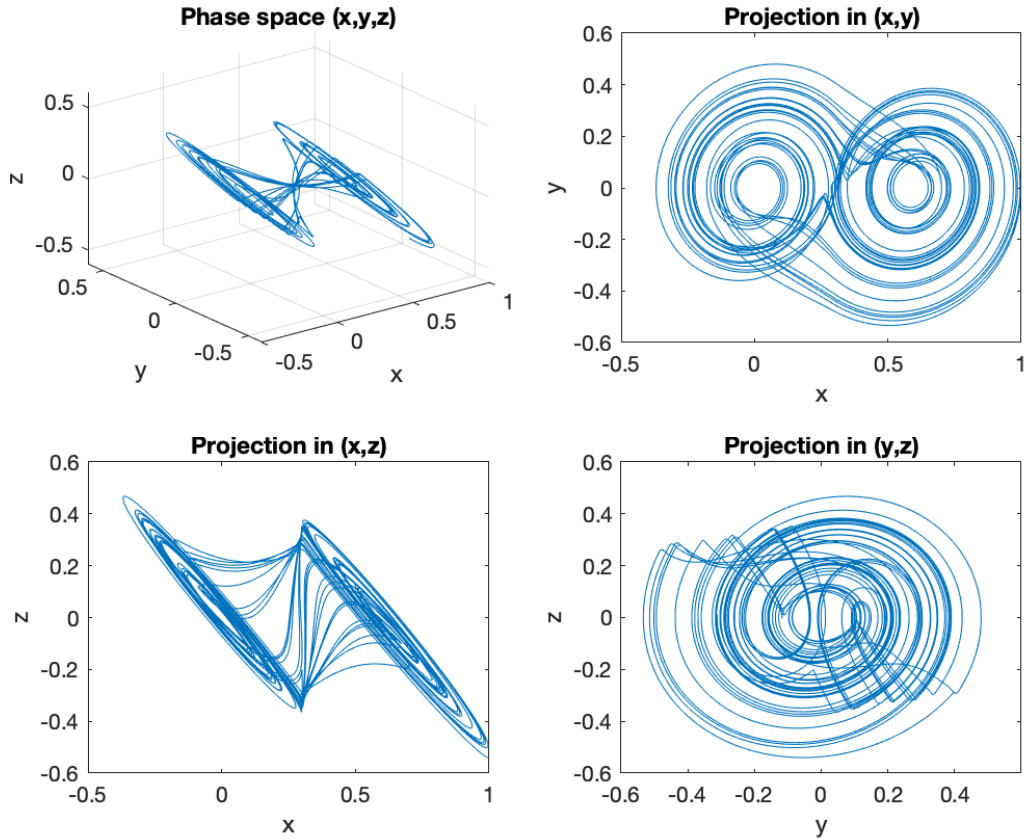
Figure 3.10: Strange attractor from UD system

time, depending on the values of the vector B (see [10] for a more detailed specification). For our particular case of study, the vector **B** is defined in function of the x position to switch the equilibrium point of the dissipative system, and thus maintaining the stability while generating chaotic dynamic. Since we will work with a two-scroll UD system, this is denoted as:

$$\dot{\mathbf{x}} = \mathbf{A}\mathbf{x} + \mathbf{B}(\mathbf{x}) \tag{3.9}$$

with

$$\mathbf{A} = \begin{bmatrix} 0 & 1 & 0 \\ 0 & 0 & 1 \\ -3/2 & -1 & -1 \end{bmatrix} \tag{3.10}$$

and

$$\mathbf{B}(\mathbf{x}) = \begin{cases} \mathbf{B_2} = [0,0,0.9]^T & \text{if } x \geq 0.3; \\ \mathbf{B_1} = [0,0,0]^T & \text{otherwise} \end{cases} \tag{3.11}$$

These conditions give form to the two-scroll attractor showed on Figure 3.10. As presented for the other systems, the attractor is shown on its three dimension space and plane projections, where $\mathbf{x} = [x, y, z]^T$.

Now that we have defined the chaotic systems that will be implemented in this investigation, in the following chapter we describe the methodology utilized to acquire the sound generated from these attractors in order to perform auditory stimulation.

Chapter 4

MATERIALS AND METHODS

As mentioned in Chapter 1, the main objective of this investigation is to record acoustic signals derived from the voltage of chaotic systems implemented using electronic circuits and utilize them as auditory stimuli to analyze brain effects using perception evaluations and power spectral features on EEG signals. In this chapter are presented the procedure and methodology utilized to implement the experimental design to test our hypothesis.

The chapter is divided into 4 sections. In the first one, we describe the procedure required for the acquisition of our acoustic stimuli to perform the experiments. Then, Section 4.2 contains the general structure and materials from the experimental design that was carried out. And finally, the last two sections describe the two phases in which the complete experiment was divided into. The first phase was defined "Perception Experiment", this was the first part of the experimental design and consisted on the subjective annoyance evaluation of the sounds generated from the chaotic systems through standardized questionnaires. The second part of the experiment was denominated "EEG Experiment", here is where we analyzed the electrophysiology influence of our chaotic signals through auditory stimulation.

Figure 4.1 shows a flow chart of the experimental protocol designed for this investigation. The first necessary step to achieve the main objective was the selection of chaotic systems from which we would generate acoustic signals. For this, the electronic design and implementation of a chaotic systems group was carried out using the analog computation methods described by Orponen *et al*. in [54]. After this, the analog responses of the systems was recorded by capturing the voltage states using an audio interface that converts analog signals into digital vectors that we later processed to create the auditory stimuli.

We then performed a series of preliminary experiments in order to subjectively determine the general effects provoked by the sound exposure of these signals and how it varied from one system to another. These experiments consisted on the subjective analysis of a total of 6 systems, from which we selected the two that proved more interesting effects (described in the following section) according to the results of perception questionnaires. The summarized data from these preliminary experiments can be found in Appendix A.

We then proceeded with the creation and implementation of the experimental design described in Section 4.2 to analyze the auditory effects of these chaotic signals.
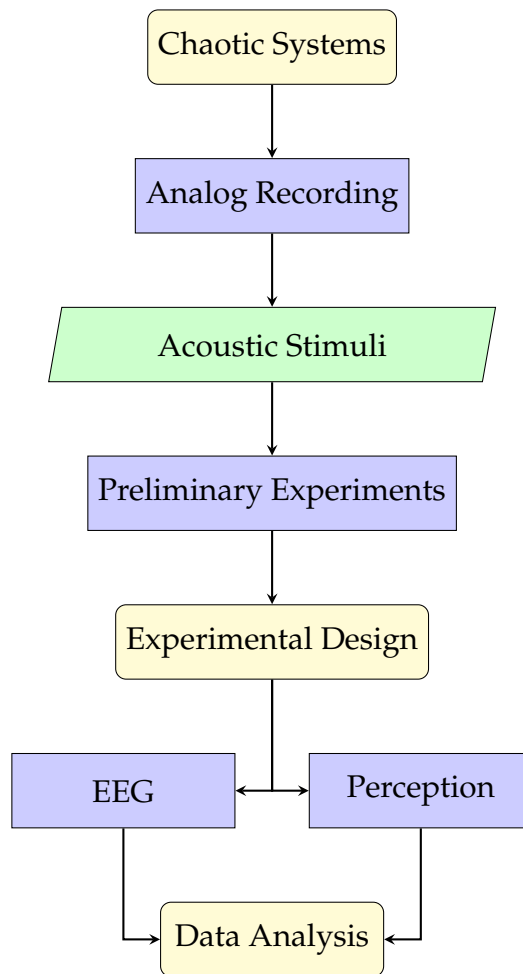
Figure 4.1: Experimental flow chart

4.1 Acoustic Stimuli

The chaotic systems studied for this experiments were:

- Chen system [56]

- Unstable dissipative (UD) system [57]

- Rössler system [58] parameters $a = b = 0.2$

  - Chaotic attractor, using $c = 5.7$
  - Limit cycle (denoted as Rössler*) setting $c = 3.7$

The state dynamics of these systems will be addressed in dept below. As described in Chapter 3, the first step to capture the signals derived from the systems was to implement them on electronic circuits. Then, the acoustic signals stimuli could be derived
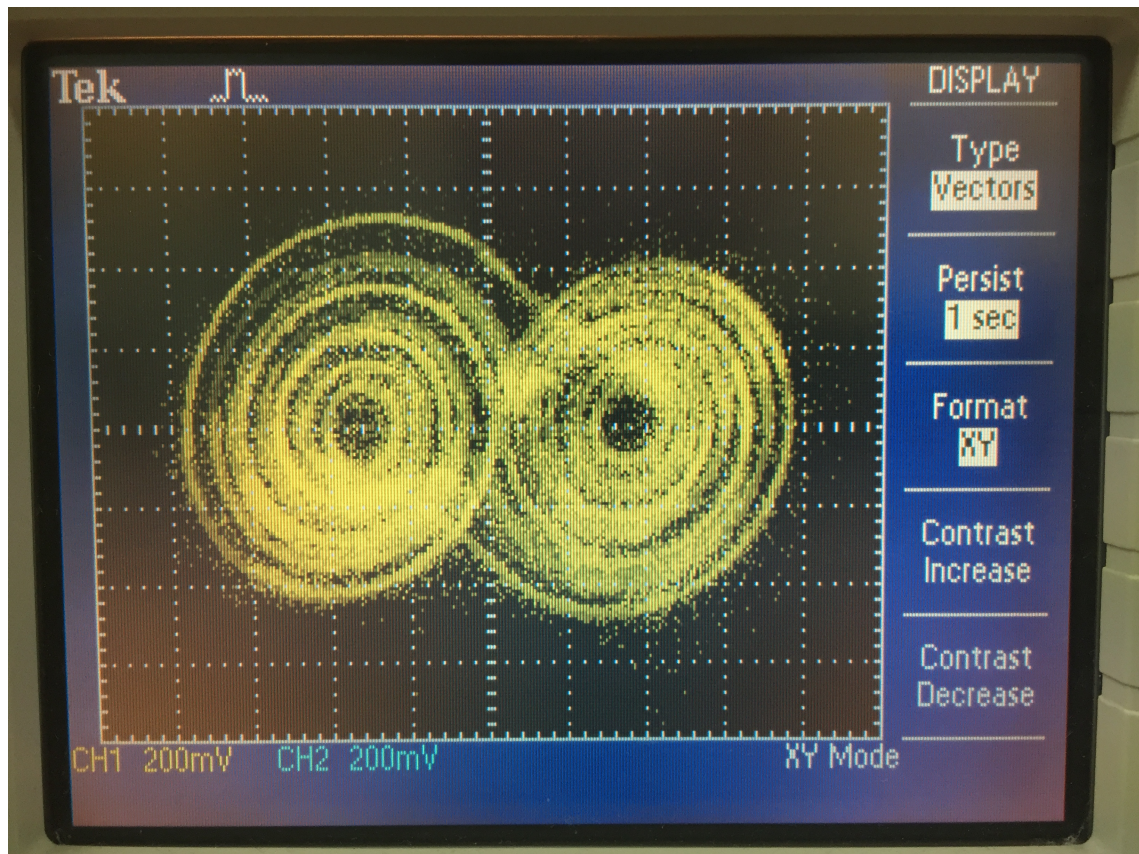
Figure 4.2: Phase space of analog signals from UD system

from the voltages of each state variable of the system. Figure 4.2 illustrates a phase space of the signals derived from one of the electronic circuits described in Chapter 3, signals are displayed in a Tektronix® TDS2000C digital oscilloscope on XY mode.

In order to be able to use this as acoustic stimuli, the analog signals of the circuits were recorded with an audio interface, converting them into uncompressed stereo digital signals in Waveform Audio File (WAV) format (16-bit resolution at 44 100 Hz sample rate). The recordings were edited to 30 second long and normalized using Logic Pro X. For both experimental sessions described below, the sound stimulation was presented through the use of wide-spectrum headphones Sennheiser® CX 300-II Precision Earbuds.

It's worth mentioning that, since audio systems basically consist of two channels—left and right—it was opted to work with only two from the three variables (x, y) from each system. This was achieved by panning the final audio from each system to reproduce x on the right channel and y on the left. This resulted in a stereo sound with the channels slightly out of phase to each other, given the nature of chaotic systems, since their states are always different between them and never repeat themselves.

Once having the digital signals of the sound, they were controlled and reproduced using MATLAB® software. This made the proper system recording possible to confirm by plotting their dynamics. Figure 4.3 shows the state phase of 0.5 s from each of the sounds used for the experiment, along with pink noise, which is commonly presented as a "neutral" sound and was used as a control stimulus. Figure 4.4 shows a 0.1
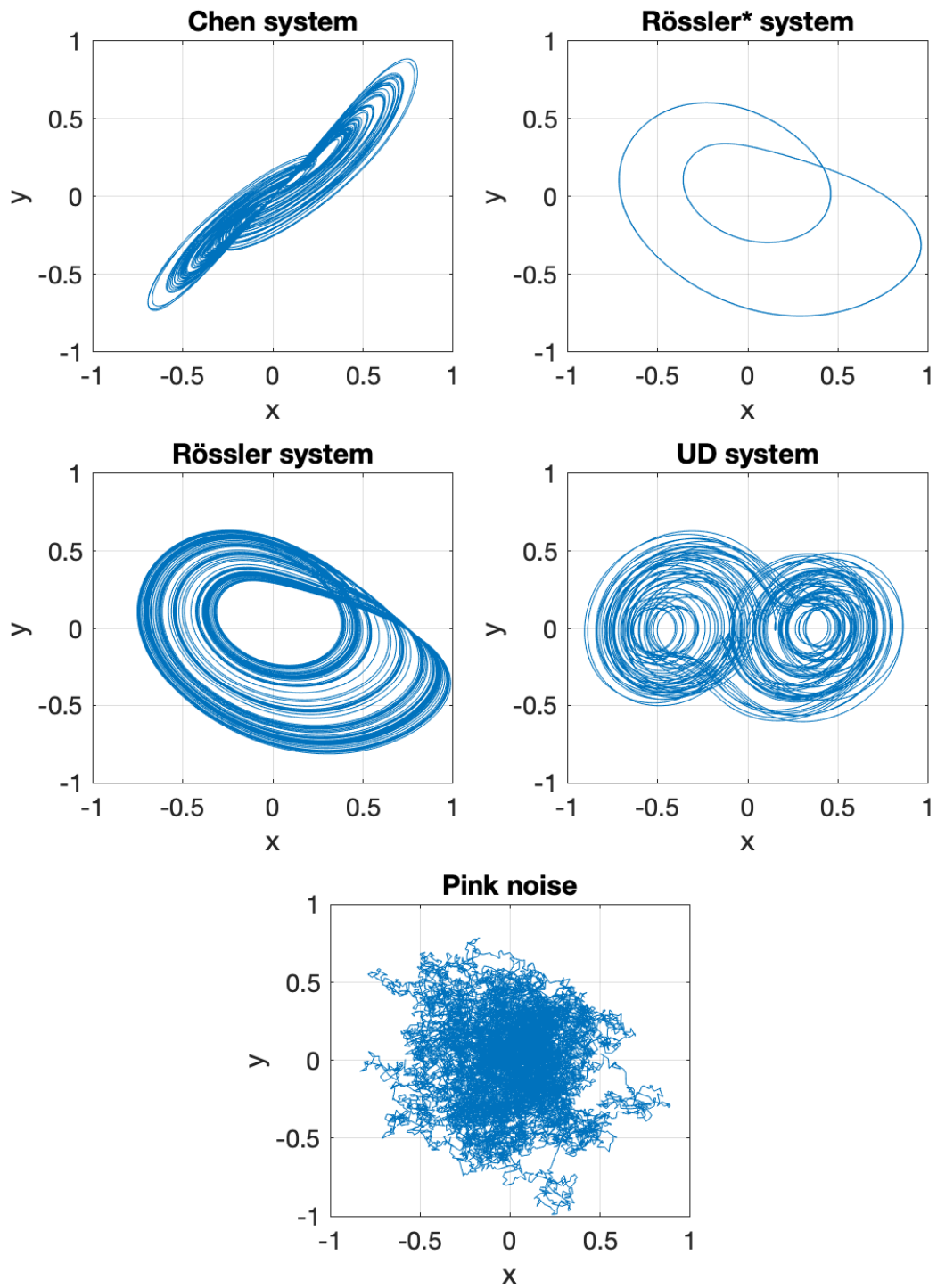
Figure 4.3: State space of the five acoustic stimuli utilized
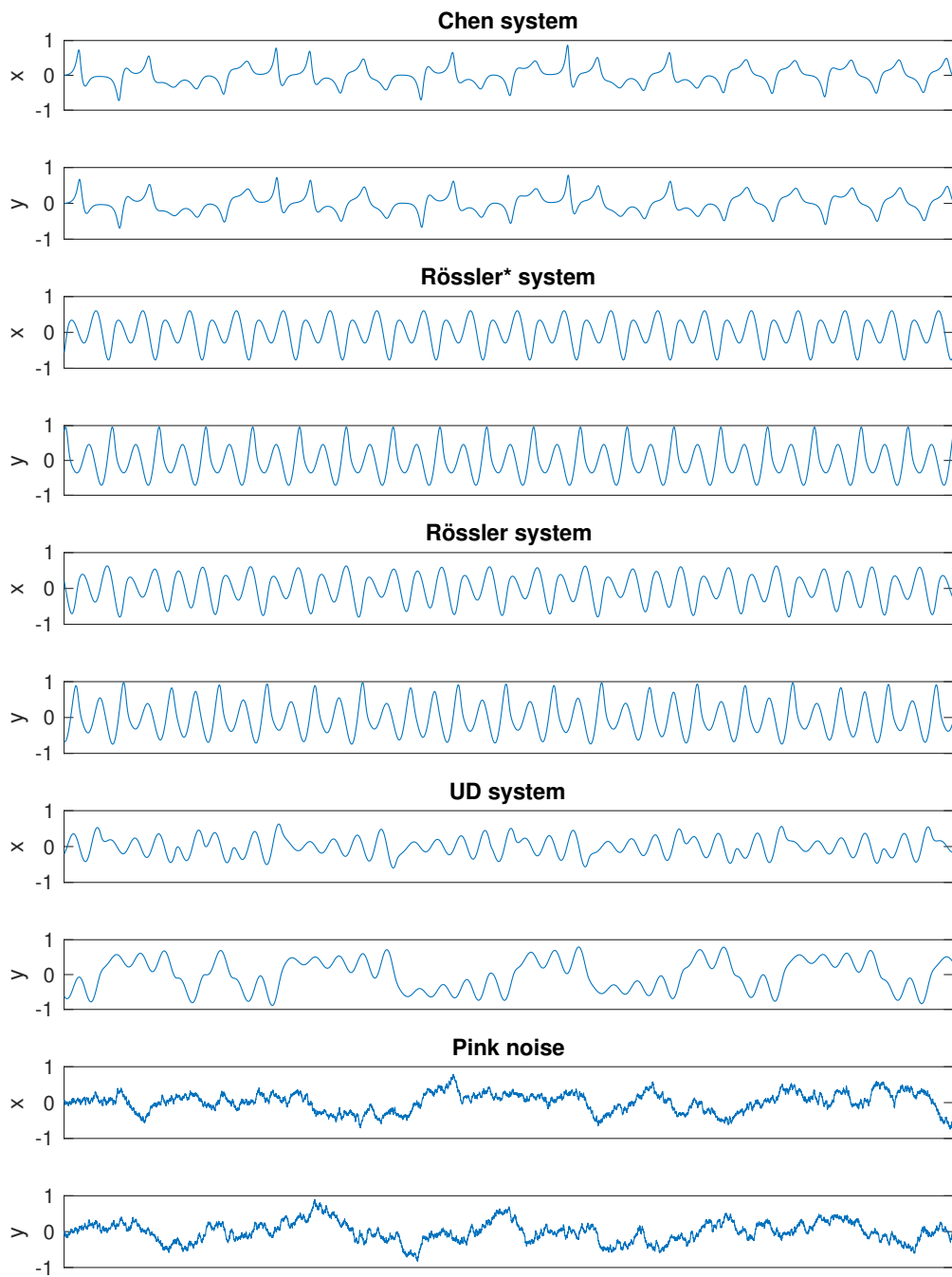
Figure 4.4: Acoustic stimuli signals over time in a 0.1 s window
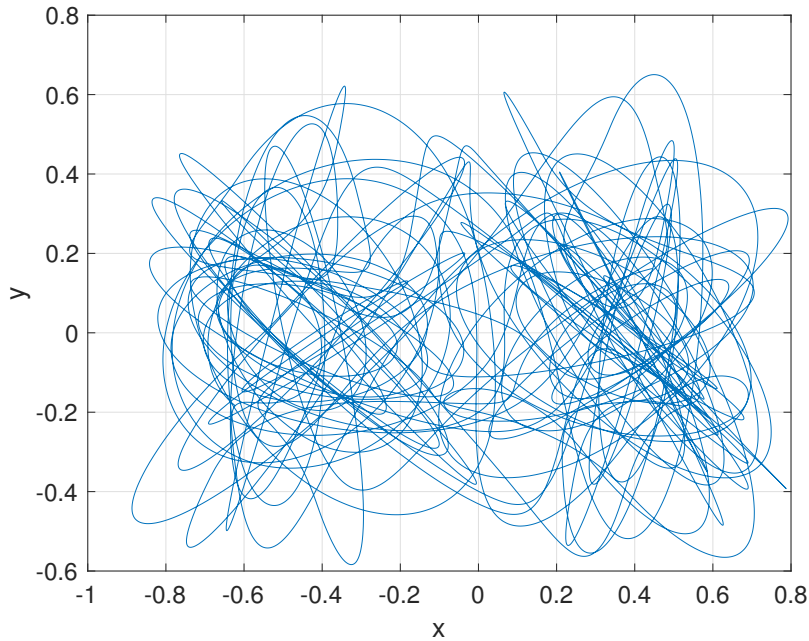
Figure 4.5: Desynchronized UD system

s window of the acoustic stimuli. Chen, Rössler and UD systems shown in Figure 4.3 represent the chaotic-derived stimulus, whereas Rössler* system and Pink Noise are periodic and aleatory processes, respectively.

It's important to note that time synchronization of the recordings proved essential to maintain the state dynamics of the systems. By recording the channels independently over different times, we found that the chaotic property of never repeating the same states would be neglected and the attractor form got lost, as depicted in Figure 4.5. Summing the signals into one single mono channel neither showed convenient, as the dynamics would also be lost and the result of mixing chaotic signals seemed unclear.

4.2 Experimental Design

For the experiments carried out in this study, we had the opportunity to establish a collaboration with Dr. Diogo Coutinho Soriano from the Federal University of ABC. There, we could perform the experiments as well as the required analysis and processing of the EEG acquired data from volunteer students of the university. Next follows a detailed description of the experimental design.

The experiments took place at the Laboratory of Computational Methods for Bio-Engineering of the Federal University of ABC, located in São Bernardo do Campo, São Paulo, Brazil. The whole procedure and requirements for the experiments were approved by the local ethics committee of the university (CAAE: 96052418.4.0000.5594) and performed under the supervision of Dr. Soriano.

Internal noise levels under 40 dB(A) were measured inside the laboratory using a *NIOSH Sound Level Meter* mobile application running on an Apple® iOS 12.3 device.

The app has been tested and verified at the National Institute for Occupational Safety and Health (NIOSH) Acoustic Laboratory [61].

In order to participate on the experiment, participants required to read and sign an informed consent letter with instructions and a manifest that they:

- Agreed to participate in the study, understanding that they may withdraw at any time

- Haven't drunk any stimulating nor intoxicating substance or beverage before the session

- Have slept at least eight hours the night before

- Have no medical history of migraine, anxiety disorders or neurodegenerative diseases

The original consent letter (written in Portuguese) signed by the participants is included in Appendix B.

One of the most important requirements for the participants was healthy good hearing levels, therefore, an evaluation of potential hearing loss was carried out before the session. We used the Mimi Hearing Test to perform an app-based audiometry using the pre-calibrated Apple® Earpods. Appendix C shows an example of the audiograms that the test provides as results, where the frequency range analyzed with the test goes from 250 Hz to 8 kHz octave bands. For our purposes, participants that presented or exceeded 20 dB hearing loss in any band were excluded from the study.

A total of $N = 31$ healthy students, with characteristics shown in Table 4.1, met the presented inclusion criteria and participated following the protocol of sound exposure described below. Volunteers were aged 23.6 $\pm$ 4.77 (mean $\pm$ standard deviation), 18 males and 13 females. Information referring to laterality and musical skills was also asked to the participants, however, this information was collected regarding possible future analysis and we did not make any kind of discrimination between them.

4.3 Perception Experiment

In order to determine the level of perceived annoyance from the implemented sounds, volunteers were asked to respond a questionnaire in the first session of the experiment. Participants sit comfortably and focused on 10 seconds of a given acoustic stimuli and

Table 4.1: Baseline characteristics of the participants

Gender (M|F)	Age (yrs)	Laterality (R|L)	Musicality (N|B|I)	Education (B|M|D)
18|13	23.6 $\pm$ 4.77	31|0	13|15|3	20|9|2

Note: Age reported as the mean $\pm$ standard deviation; Laterality: handedness, R (right), L (left); Musicality: musical skills according to practiced time and instruments, N (none), B (basic), I (intermediate); Education: degree level, B (bachelor), M (master), D (doctorate).

then respond two questions based on their perception of the sound. This process was repeated for each of the sounds described above.

The applied questionnaire consisted of the standardized general-purpose noise reaction questions for community noise surveys [62] by the International Commission on Biological Effects of Noise (ICBEN). This survey contains one verbal five-scale (QV) and one numeric eleven-scale questions (QN).

The phrase and answers for the first question go as follows:

QV

"Thinking about the last 10 seconds, how much does noise from the recording bother, disturb, or annoy you; Extremely, Very, Moderately, Slightly or Not at all?"

a) Not at all
b) Slightly
c) Moderately
d) Very
e) Extremely

As for the numerical scale, the applied question and answers were the following:

QN

"Next is a zero to ten opinion scale for how much this noise bothers, disturbs or annoys you. If you are not at all annoyed choose zero, if you are extremely annoyed choose ten, if you are somewhere in between choose a number between zero and ten."

Not at all | 0 | 1 | 2 | 3 | 4 | 5 | 6 | 7 | 8 | 9 | 10 | *Extremely*

It's important to note that one of the main reasons it was opted to used this questionnaire to asses annoyance was to obtain homogenize criteria of perception. Currently, ICBEN is the only commission that provides standardization of nuisance levels.

As mentioned before, the study was conducted in a Brazilian university, therefore, it was opted to use a translated version of these questions and answers [63, 64]. The exact survey used for the experiment was written in Portuguese and can be found in Appendix B.

Table 4.2: Numerical assignation for verbal scale

Verbal scale	Numerical assignation
a) Not at all	0
b) Slightly	21.93
c) Moderately	47.34
d) Very	73.39
e) Extremely	97.72

To compare the answers given to both questions, Table 4.2 shows a numerical assignation provided by ICBEN to each verbal scale [62]. This allows to analyze the results using statistical methods.

First, a One-sample Kolmogorov Smirnov test [65] was used to determine normality in order to analyze the data. Results showed that data failed to pass the test with a significance value placed at $p = 0.05$. Therefore, the data from the two questions was analyzed using the Wilcoxon signed-rank test, which is a nonparametric version of a classical t-test, it assumes that the samples come from populations with the same continuous distribution. For this particular case, the MATLAB function *ranksum* from the Statistics toolbox was implemented. The significance was placed at $p = 0.05$ according to standard values [67]. The results of this test are reported using the median and quartiles as $median(Q1$ to $Q3)$ values, as will be stated in Chapter 5, Section 5.1.

Finally, to provide a general result for the perception of sounds, mean values for both question is averaged and ranked according to the numerical scales shown in Table 4.3. Results are reported in Chapter 5.1.

4.4 EEG Experiment

For this session of the experiment, participants were asked to wear an EEG system to record their brain waves under phases of silence and sound stimulation. This was achieved by synchronization of audio reproduction and EEG acquisition using MATLAB. The function for audio stimulation was programed using *Psychophysics 3* [68] toolbox for MATLAB. The function for EEG recording synchronization was developed on the work context of Rodrigues (2018) [69].

Electroencephalograms were recorded using g-Tec Medical Engineering® hardware: g.USBamp Biosignal Amplifier with 16 channels and Sahara-Dry® electrodes positioned according to the 10-20 EEG configuration. Figure 4.6 shows the specific brain positions for the 16 electrodes, sensors viewed from above of the head according to what was mentioned in Chapter 2.3.3; nose corresponds to the top. Ground and reference signals of the amplifier were positioned in the mastoid process. Sampling frequency for EEG acquisition of the equipment was adjusted to 256 Hz, which prevented aliasing according to Nyquist theorem.

Before the experiment began, the electrodes needed to be calibrated so that their impedance was between (0.3 and 5.0) kΩ, this also ensured that the dry electrodes were in full contact with the head scalp of the participant. An electrostatic grounded

Table 4.3: Relation between verbal and numerical scales

Verbal scale	Numerical scale
a) Not at all	0.0 to 3.6
b) Slightly	3.60 to 23.5
c) Moderately	23.5 to 58.6
d) Very	58.6 to 89.8
e) Extremely	89.8 to 100

Fpz

F7 F3 Fz F4 F8

T7 C3 Cz C4 T8

P7 P3 Pz P4 P8
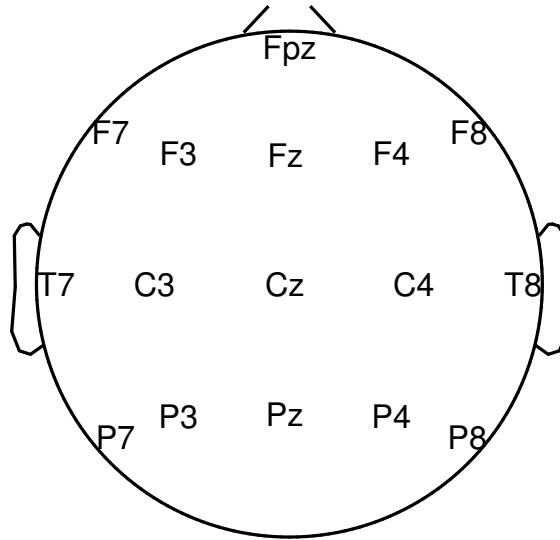
Figure 4.6: EEG electrode configuration for the experiment

wristband system was used in order to any possible electric shock and improve safety of volunteers and the equipment.

Table 4.4 shows the session of the complete experiment, where EEG recordings phases were adjusted to trials of 1 minute long for each of the stimuli described on the previous section. In order to analyze changes from basal to stimulus, every trial consisted of 30 seconds of rest state (silent condition) and 30 seconds of sound stimulation using the systems described in Section 4.1. As mentioned in last row of Table 4.4, the stimuli were presented using an aleatory pattern for the sound exposure sequence of the systems. Between each trial, a 10 second-minimum pause was given to the participant in order to avoid drowsiness or loss of attention.

Once all the equipment was set up, participants sit comfortably in front of a computer monitor. In it, a cross fixation point and instructions were synchronized with the EEG recording to give participants indications about the current phase (pause or EEG recording) of the experiment. They were instructed to focus sight on the monitor and avoid any kind of muscle contraction during EEG recording, and then do as they needed to relax on the pause phases. Figure 4.7 illustrates a participant during data acquisition with the head cap configuration described in Figure 4.6.

Table 4.4: Timeline of the session

EEG recording		Pause	EEG recording		Pause	EEG recording		Pause	EEG recording		Pause	EEG recording	
Rest	**Rössler**	Pause	**Rest**	**Chen**	Pause	**Rest**	**UD**	Pause	**Rest**	**Rössler***	Pause	**Rest**	**Pink**
30 s	30 s	10 s	30 s	30 s	10 s	30 s	30 s	10 s	30 s	30 s	10 s	30 s	30 s
					4.6 min block performed in an aleatory sequence								
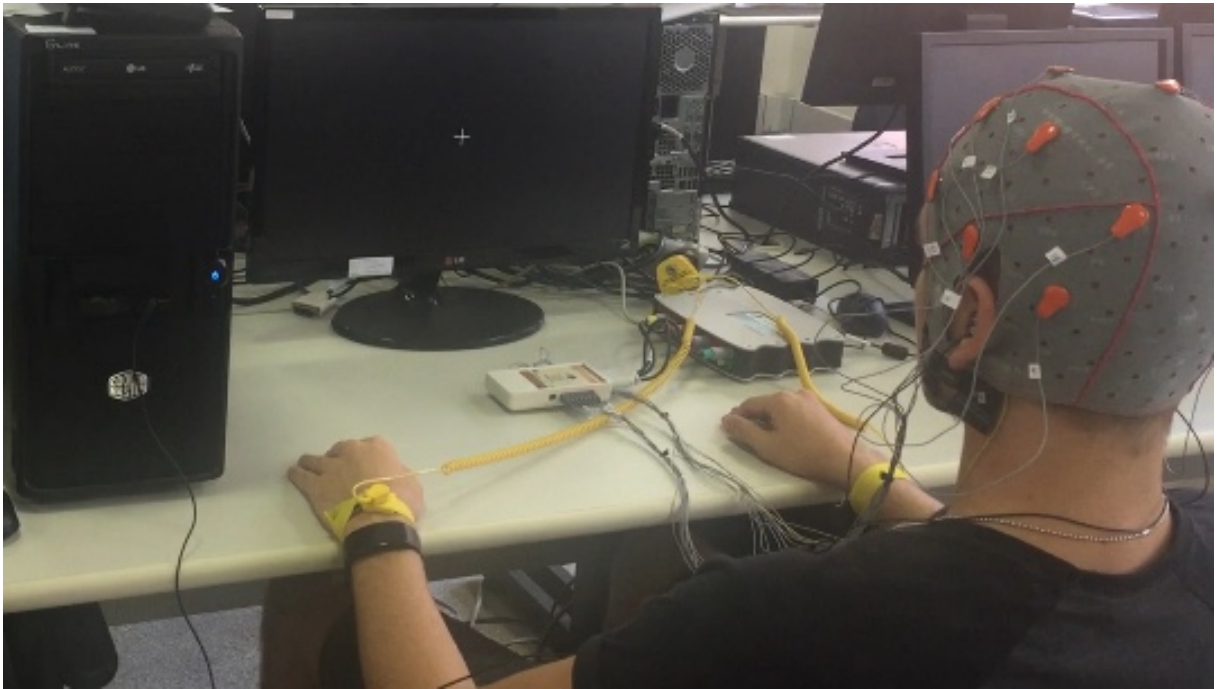
Figure 4.7: Equipment and volunteer during EEG recording

4.4.1 Time Series Analysis

Now, regarding the analysis of acquired data, the obtained EEG signals of each corresponding electrode (located in the headset as Figure 4.6 depicts) were acquired for one minute straight. This voltage signals were measured at a sampling frequency of $f_s = 256$ Hz and will be defined as $raw_\varphi[n] \in \mathbf{R}^n$, where φ correspond to each of the 16 electrodes presented in Figure 2.3 (*i.e.* Pz, F4, Cz, T8, ..., *etc.*), n correspond to the discrete sampling time in a way that $t = n/f_s$, and the length of each signal is determined by $n = 1, \ldots, N$ ($N = (60 \text{ s}) \times (f_s) = 15360$).

The acquired signal $raw_\varphi[n]$, already comes filtered by a fourth order Butterworth-Notch filter from 58 to 62 Hz to cut electrical interference, and an eighth order Band Pass filter between 0.5 up to 60 Hz. These values were considered according to the range of bands which we are interested in, as depicted in Table 1.2. Both filters are built-in analogically inside the g.Tec biosignal amplifier in the EEG with configurable cutting frequencies.

After the measurement of the raw signals, specific processing was considered for the analysis methodology of the data. This was carried out with some software functions and some mathematical procedures as will be described next. Figure 4.8 shows the summary of all the processes from following analysis.

Normalization and Segmentation

First, in order to prevent high inter-participant deviation, after the measurement of the signal, the raw data is normalized and centralized by means of the *zscore* MATLAB function which essentially results as:
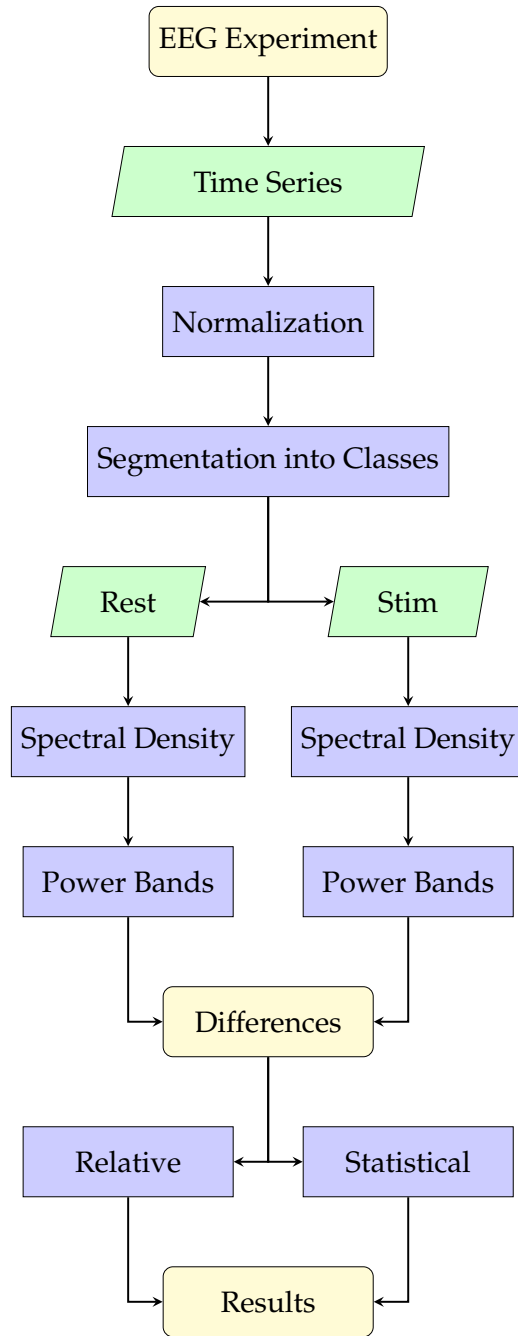
Figure 4.8: Data analysis for EEG experiment

$$z_\varphi[n] = \frac{raw_\varphi[n] - \overline{raw}}{S} \tag{4.1}$$

where the operation $\overline{\{\cdot\}}$ corresponds from now and on to the mean in a way that:

$$\overline{x} = \frac{1}{N} \sum_{i=1}^{N} x[i], \tag{4.2}$$

and S stands for the standard deviation:

$$S = \sqrt{\frac{(\sum_{i=1}^{N} x[i] - \mu)^2}{N}} \qquad (4.3)$$

with μ as the mean of the vector.

As mentioned before, every trial of acoustic stimulation was segmented into pairs of 30 second windows of Rest and Stimulus classes. Basically $z_\varphi[n]^{Rest}|n = 1, \ldots, L$ and $z_\varphi[n]^{Stim}|n = L+1, \ldots, N$, with $L = N/2$.

Spectral Density Estimation

In order to analyze the frequency content from all the time series of each participant and stimuli, the Power Spectral Density (PSD) was implemented to the acquired Rest and Stimulus classes. This function returns PDS estimate of the time series, which describes the distribution of power into the frequency content of the series and presents a reduction in the number of computations and in required core storage [70].

The PSD has units of watts per hertz (W/Hz) and it's based on the periodogram calculation through the Discrete Fourier Transform (DFT) from segmented windows of time series. The idea of this method is to take the available data, split it into segments and compute the periodograms for each segments and average the results, in order to reduce the variance associated with the periodogram estimate.

This function was implemented with the *pwelch* function of MATLAB, which consider the following input parameters, $nfft = 1024$ as the DFT length of the data segment, a sampling frequency of $fs = 256$ Hz and a frequency interval for the segment division of $f_0 = 0.25$ Hz. For further details on the calculations of the PSD see [70].

The results of this calculations can be appreciated in Figure 4.9, where an example of a spectrum obtained from one minute trial is depicted. The PSD_{Pz}^{Rest} estimate from the first 30 seconds of the trial are plotted with the blue line, and the PSD_{Pz}^{Stim} of the subsequent 30 seconds of stimulus class correspond to the red line. Both results on the Figure 4.9 were measured from the Pz electrode from (0 to 65) Hz. The cutting effect of the Butterworth-Notch filter described above is visible for both classes around 60 Hz, therefore, it was opted to work with a total bandwidth from (1 to 50) Hz for all the analyses described below.

The black dashed lines in Figure 4.9 correspond to the frequency limits of the brain waves presented in Table 2.2. Here the region from a to b lines corresponds to the frequency band for delta wave, b to c for theta wave, c to d for alpha wave, d to e for beta wave, and e to f for gamma wave (this also corresponds to our highest frequency limit, as we mentioned above) .

Power Bands

The main goal is to analyze power differences between both classes, visually, some peak fluctuations could be detected in the regions of delta and alpha waves for the given PSD shown in Figure 4.9. However, in order to numerically and statistically address these differences, the Power Band Area (PBA) was estimated, which corresponds to the area from each band of frequency for each measured signal. Its calculations are considered as follows:
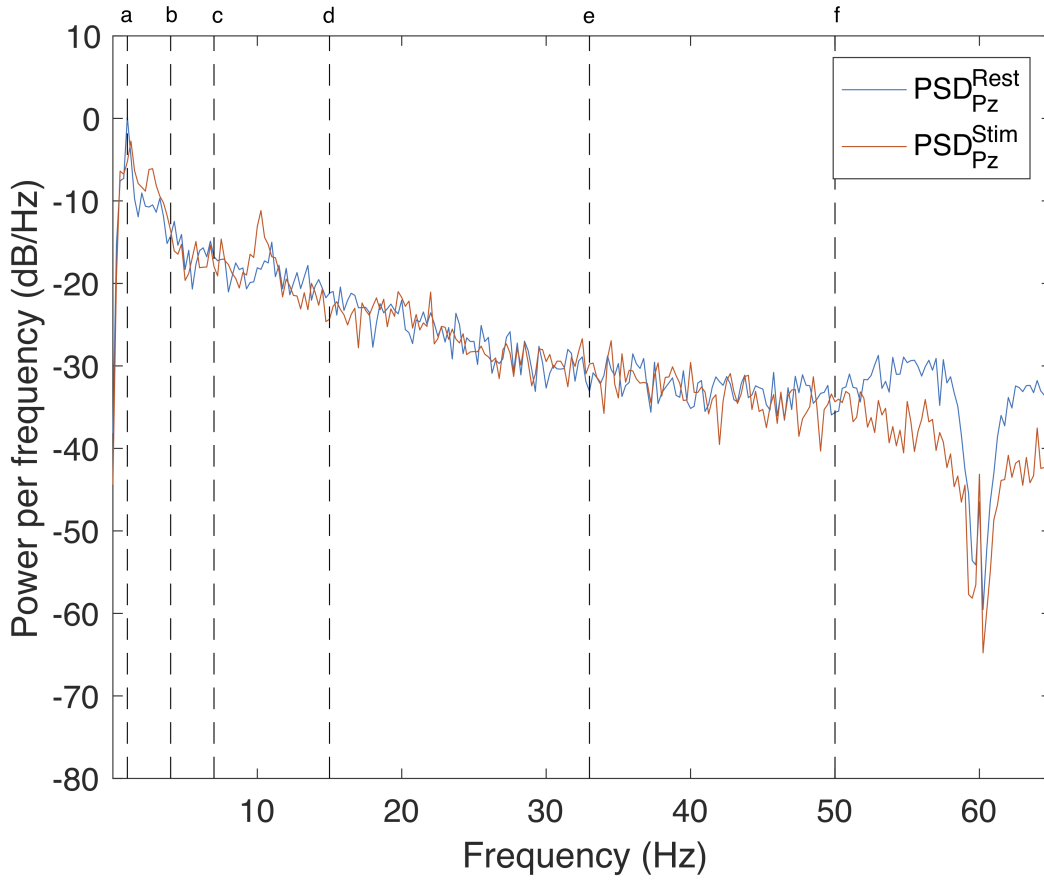
Figure 4.9: Welch PSD estimate

$$PBA^{\varepsilon}\varphi = \sum_{i=f_{min}}^{f_{max}} PSD^{\varepsilon}\varphi[i] \cdot f_0 \tag{4.4}$$

where $PSD^{\varepsilon}\varphi[i]$ is the spectral power on an arbitrary point in the i-th subinterval for the φ electrode and the $\varepsilon = Rest, Stim$ signal, f_0 is the step frequency of the Welch estimate function as described above and it will be considered here as a frequency mesh size, f_{min} corresponds to the lowest frequency of the bandwidth and f_{max} to the highest. It is important to mention that (4.4) represents a Riemann sum for the given function $PSD^{\varepsilon}\varphi[i]$ in a closed frequency interval [71], resulting in the area under the region of a curve defined by the PSD in a given frequency interval $[f_{min}, f_{max}]$.

If the PSD has units of W/Hz, and f_0 is the measure of frequency that determines the length of the horizontal axis (as shown in Figure 4.9), then for the equation to be dimensionally congruent, the following relation must hold:

$$PBA = f \cdot PSD$$

$$1\,\text{W} = (1\,\text{Hz})(1\,\text{W/Hz})$$

showing that PBA has units of watts (W).

Alpha, delta, beta, theta and gamma power bands were then determined by Equation 4.4 using the frequency intervals $[f_{min}, f_{max}]$ described in Chapter 2.2, page 9 for each brain wave. Results for all band power features are easy to analyze throughout their mean values in multiples of 10^3 (mW), determined by the following equation:

$$\overline{PBA^{\varepsilon}\varphi} = \frac{1}{P}\sum_{i=1}^{P} PBA^{\varepsilon}\varphi[i] \tag{4.5}$$

where P stands for the total number of participants (for this experiment there were 31 participants, as noted in Table 4.1), $PBA^{\varepsilon}\varphi[i]$ corresponds to the value measured of each power band (α, δ, θ, β, and γ according to the frequency intervals described in Section 2.2) of the i-th participant, and φ represents the specific location of the channels as illustrated in Figure 4.6.

Determination of Differences

Results are reported with the open source EEGLAB [72] toolbox for MATLAB$^{\circledR}$. This toolbox allows us to plot the Relative Difference (RD) and Significant Difference (SD) comparisons for each EEG location to determine changes of Stimulus power class relative to the mean Rest power class. Relative Difference is expressed as a ratio from (0 to ± 1), it is a positive unit-less number for values greater than the reference, and negative for decrements relative to the reference. It was determined as follows:

$$RD\varphi = \frac{\overline{PBA^{Stim}\varphi} - \overline{PBA^{Rest}\varphi}}{\overline{PBA^{Rest}\varphi}}. \tag{4.6}$$

The Significant Difference was obtained from the null hypothesis for equal means of statistical tests used to compare the classes. First, data was tested for normal distribution using the One-sample Kolmogorov-Smirnov test with *kstest* MATLAB function. A one-sample and paired-sample *t*-test was carried out to asses mean changes for all the participants intra-electrode using the *ttest* function by MATLAB.

Finally, means from inter-electrode 16 channels for both classes were analyzed using a one-way Analysis of Variance (ANOVA) with function *anova1* by MATLAB, results are expressed as mean and standard deviation. Significance for all the tests was placed at $p < 0.05$.

Chapter 5 shows the results from both experimental methods described above. Starting with the perception experiment, followed by a subsection of results from the EEG experimental protocol.

Chapter 5

RESULTS

In this chapter are presented the results obtained from both experimental designs described in Chapter 4. The chapter is divided in two sections, the first is devoted to the perception experiment and the second shows results from the EEG experimental recordings.

5.1 Perception Experiment

5.1.1 Verbal QV Analysis

For this question, 5-scale verbal answers a) Not at all, b) Slightly, c) Moderately, d) Very, and e) Extremely were analyzed for each of the sounds generated from Chen, Rössler with periodic dynamic (Rössler*), Rössler and UD systems.

All percentage results from the answers given to this question are shown in Table 5.1 and represented graphically in Figure 5.1. According to the maximum percentage values obtained from the results, almost half of participants (46.8 %) perceived the sound generated from Rössler*, Rössler and UD systems to be "Slightly" annoying, however, some differences were found for the "Moderately" values being 34.3 %, 28.1 % and 25.0 %, respectively.

On the other hand, 56.2 % of participants perceived the sound generated from Chen system as "Slightly" bothering, but 28.1 % as "Not at all" annoying. Given these results, we could fairly say that this system was the one obtaining higher percentage scores for low annoyance perception. However, a more robust analysis will be explained in next subsections to provide more accurate results.

Table 5.1: Percentages of answers obtained for QV

Sound	Not at all	Slightly	Moderately	Very	Extremely
Chen system	28.1%	56.2%	15.6%	0.0%	0.0%
Rössler* system	12.5%	46.8%	34.3%	3.1%	3.1%
Rössler system	15.6%	46.8%	28.1%	6.2%	3.1%
UD system	18.7%	46.8%	25.0%	9.3%	0.0%
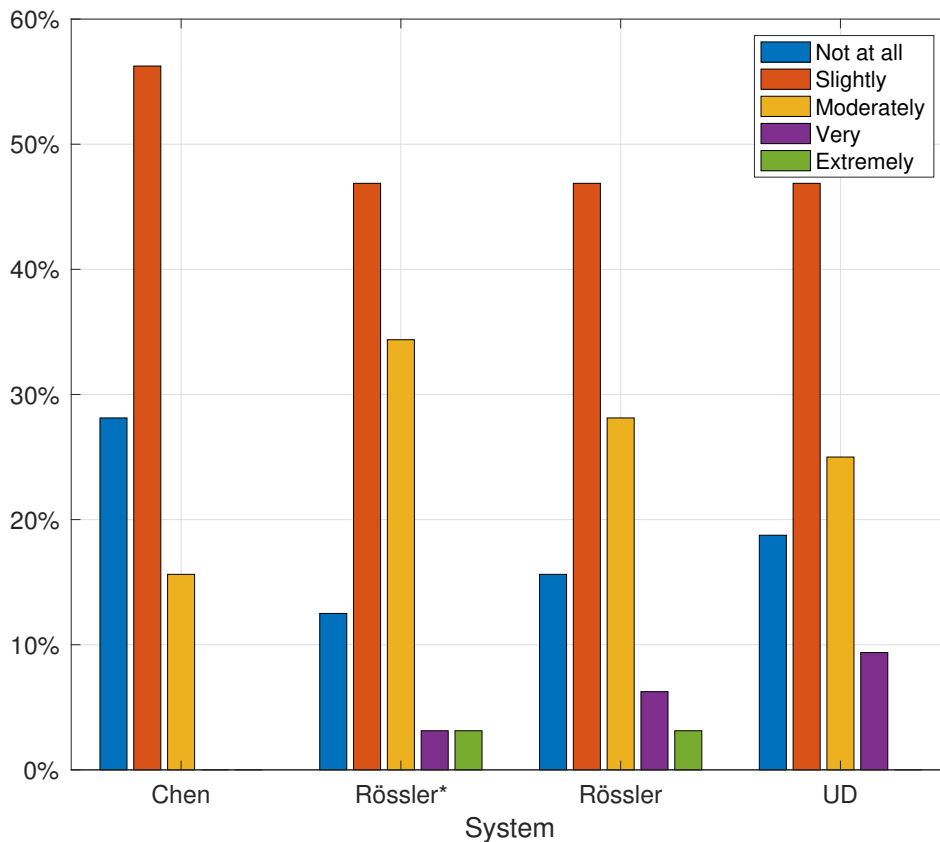
Figure 5.1: Bar graph of answers obtained for QV

5.1.2 Numerical QV and QN Analysis

As mentioned before, a numerical assignation (Table 4.2) was made to the verbal scale answers in order to analyze results from both questions using the same level for perceived nuisance. This value for annoyance is defined in a unit-less numerical scale from 0 to 100, corresponding to the minimum and maximum levels for perceived nuisance.

It's important to note that results from these pair of questions is supposed to represent a related level of perception, therefore, it is expected that results present similar values. Next follows a description of the numerical values obtained.

Chen System

Figure 5.2A shows the results obtained for the sound derived from Chen system. The median results for both questions resulted very similar, being 21.93 for QV and 20 for QN, corresponding to the red line in the box plot figure. Despite this similarity, we can see from the quartile values that a higher percentage of the population is represented by lower values of perception on QV. In other words, the median and the 0.75 quartile correspond to the same value.

Figure 5.2A also shows that for QV, the 0.25 quartile correspond to the minimum
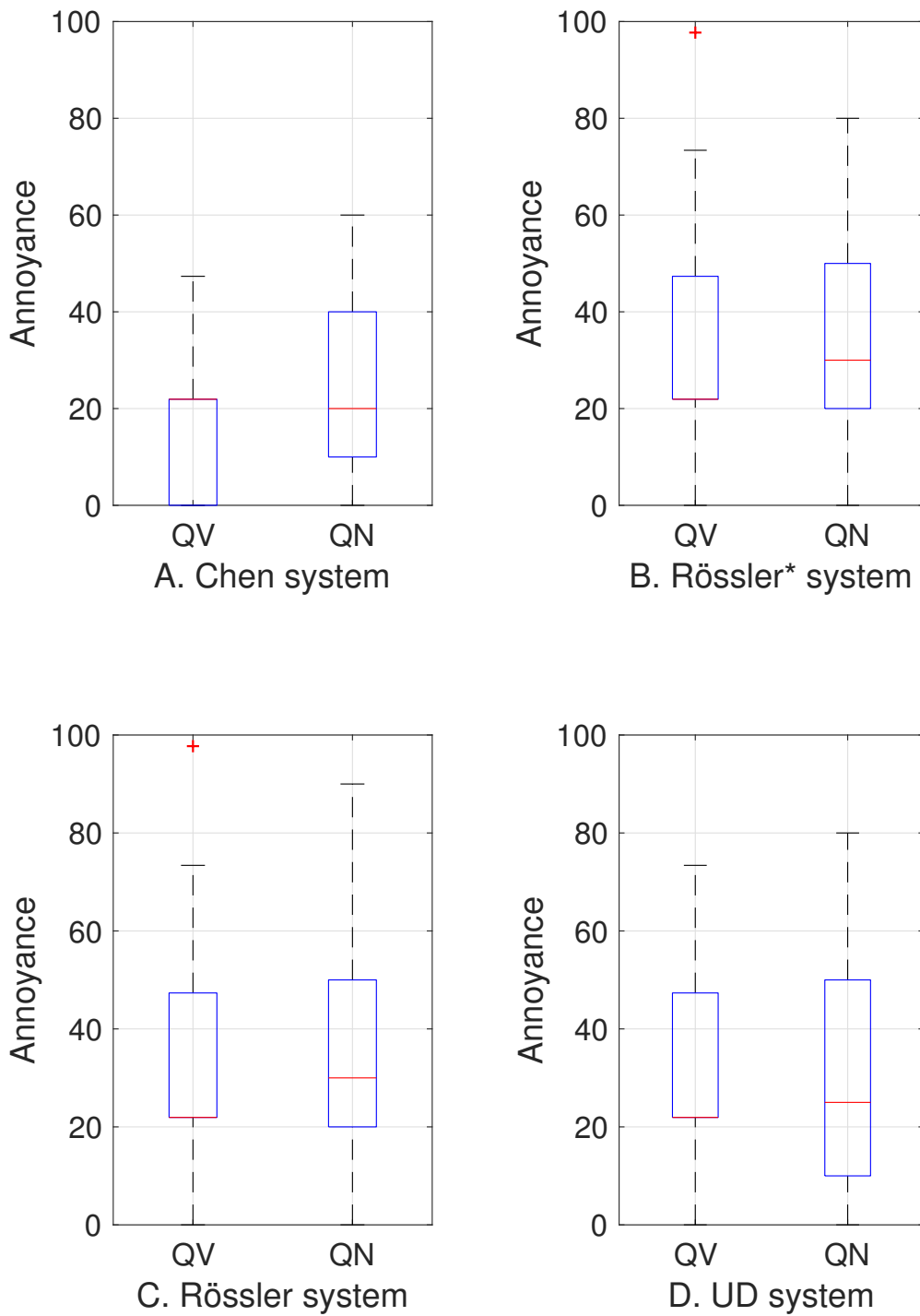
Figure 5.2: Annoyance values obtained for chaotic systems sound

value of 0. As for the most upper extreme data points, QV was slightly higher than QN, being 60 and 47.3, respectively.

Rössler* System

Results from Rössler system with periodic dynamic are shown in Figure 5.2B. The median value for QV and QN was 21.93 and 30, respectively. It's worth mentioning that the obtained numerical mean value was the one assigned for the "Slightly" verbal scale. This result seems to go along with the percentages of verbal scale values described above, given the 46.8% of responses for this verbal scale shown in Figure 5.1.

The most extreme values for QV was 0 and 73.9 of annoyance. It's clear that, in contrast with the Chen system, the median and 0.75 quartile correspond to the same value. As for the numerical question QN, we can see that Rössler* received a median of 30, a minimum extreme of 0 and a maximum value of 80. We can also note an outlier for QV answers situated at 97, which represents the numerical value for the "Extremely" verbal scale.

Rössler System

Results for Rössler system with chaotic parameters of bifurcation are shown in Figure 5.2C. As expected, these results are almost identical with the Rössler* system, with only difference in a most extreme data point of 90 given to QN. Even the outlier mentioned on Figure 5.2B still appears in QV for the chaotic Rössler, noting that it came from the same participant. From a perspective point of view, the sound from both Rössler systems; chaotic and limit cycle, were same for many participants, as themselves reported after having finished the survey. However, these similarities in the perception analysis does not hold onto further EEG experiments, as will be described in the next section.

UD System

Figure 5.2D shows the numerical values of perceived annoyance from the sound derived from UD system. The median and 0.25 quartile of QV correspond to the same value of 21.93, and most extreme data points are 0 and 73.9, respectively. QN received a general nuisance of 25(10 to 50).

Table 5.2: Wilcoxon test for values obtained from QV and QN

System	QV	QN	p
Chen	21.93 (0 to 21.93)	20 (10 to 40)	0.82
Rössler*	21.93 (21.93 to 47.34)	30 (20 to 50)	0.43
Rössler	21.93 (21.93 to 47.34)	30 (20 to 50)	0.60
UD	21.93 (21.93 to 47.34)	25 (10 to 50)	0.96
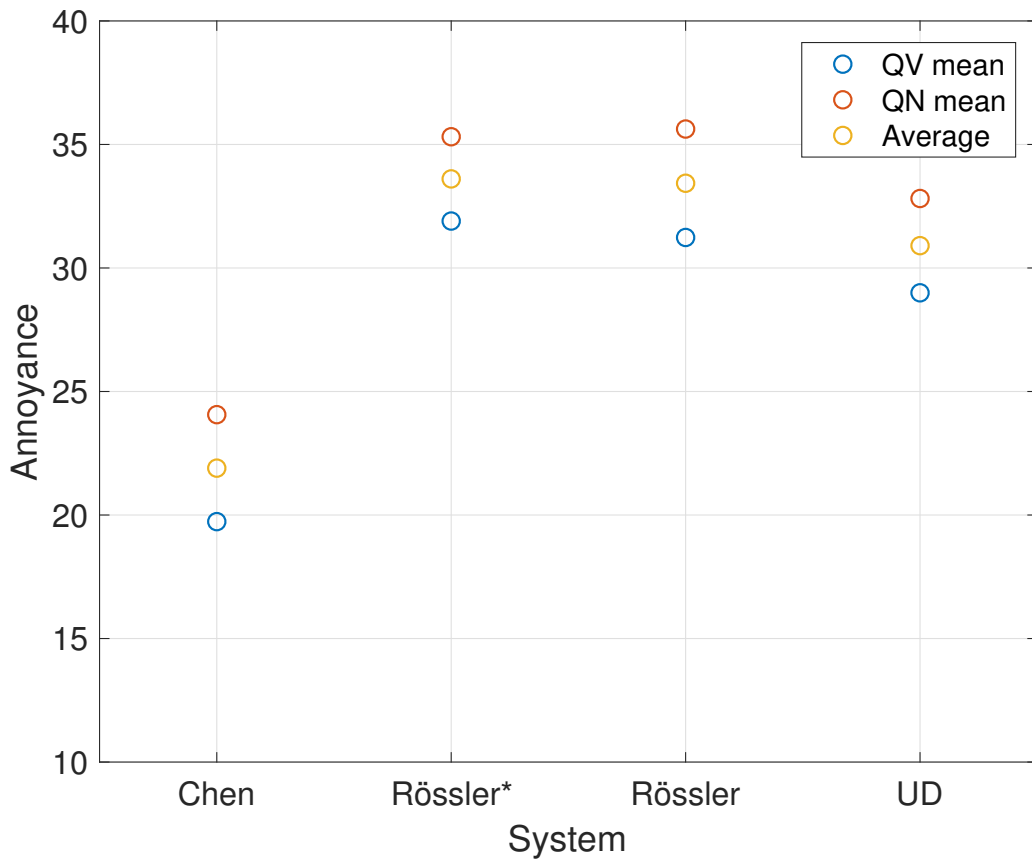
Figure 5.3: Comparison between QV and QN means

5.1.3 Relation between QV and QN

In order to determine if results obtained from both answers were statistically different, an analysis of variance was assessed. All data from QV did not passed the Kolmogorov-Smirnov normality test, therefore, a non parametric Wilcoxon signed-rank test, was used to compare the median values of the distributions.

Table 5.2 shows the ANOVA results for the null hypothesis of equal medians, where small values of p cast doubt of the hypothesis. As expected from the box plots analyzed in previous subsection, none of the sounds presented statistical difference since they were all far superior than our significance level placed at $p = 0.05$. Table 5.2 indicates that the sound from UD system obtained the highest p value from all sounds, receiving

Table 5.3: Nuisance assignation according to QV and QN means average

System	QV mean	QN mean	Average	Verbal score
Chen	19.73	24.06	21.89	Slightly
Rössler*	31.90	35.31	33.60	Moderately
Rössler	31.23	35.62	33.42	Moderately
UD	28.99	32.81	30.90	Moderately

$p = 0.96$ for the variance between 21.93 and 25 median value from QV and QN. Result for Rössler* analysis correspond to the lowest p value of 0.43, meaning the least similar medians.

This lack of difference between the questions results suggest strong correlation between the two scales. We can then calculate a general numerical nuisance value from the average of means from both questions. In this way, it will be assigned a verbal score obtained from numerical average of scales using the reaction tables (Table 4.3) provided by ICBEN.

Table 5.3 shows the means and average for both questions. The highlighted column correspond to the general value scored for perceived nuisance from the sounds. We can now clearly see that Chen was the sound that produced lower annoyance and both Rössler system sounds received fair closely the higher values of nuisance. These results are showed graphically in Figure 5.3, where the blue line represents the QV mean, red line corresponds to QN mean and yellow line to the average from aforementioned blue and red line.

5.2 EEG Experiment

As mentioned before, the main objective of this investigation was to asses differences in power band features. In order to achieve this, the results from each particular sound stimuli are presented in the next subsections, featuring specific brain zone analysis (as it was depicted in the arrangement of Figure 4.6 in Chapter 4) along with a wider spatial analysis consideration of the band powers [24].

Next, the measurements and analysis of each system stimulus will be reported and analyzed.

5.2.1 Chen System Stimulation

Table 3.4 shows the mean powers of the Rest and Stimulus windows obtained from all participants. The table is organized as follows. The first column correspond to the 16 electrode localizations registered for the experiment (see Figure 2.3), the following columns are divided according the each one of the 5 frequency bands (δ, θ, α, β, γ, respectively).

Each frequency band depicts three columns in which the first two correspond to the Power Band Area $\overline{PBA^{\varepsilon}\varphi}$ as described in Equation 4.5 for the Rest and Stimulus classes, respectively. The third column shows the results from statistical tests for mean differences between powers from the Rest and Stimulus signals using the p-value obtained from the t-test. This implies that the powers from $P = 31$ participants utilized in Equation 4.5 were also used to perform an equal-means test between the two classes. Here, values of $p < 0.05$ indicate rejection of the null hypothesis of equal-means. In other words, values of $p < 0.05$ represent significant change relative to basal state.

Last row of the table corresponds to the mean value from the 16 electrode-rows above, this value will be addressed and utilized also in Table 5.5. The rest of Table 5.4 is divided into results obtained for theta, alpha, beta, and gamma bands using the exact same procedure described above for delta band.

We can see from Table 5.4 that Chen stimulus had greater influence over channels in delta band. It was obtained $p < 0.05$ in most of the brain channels recorded for this band, with the exceptions of F4, T8, F8 and Fpz. These values are highlighted on the table (fourth column) and correspond to changes induced by the stimulus in delta band powers relative to the silence class (Rest). Following analyses will make easier to determine whether if these changes correspond to an increment or a decrement of the feature power.

To have a wider perspective of the behaviour of each power band in all brain localizations, we consider the following. If we take the mean values of the 16 electrodes in each class we can again analyze the difference, now considering all power of the electrodes as a sample. This would asses difference considering our total EEG spatial resolution of the brain, corresponding to values showed in the last row of Table 5.4 for each power band.

Table 5.5 shows the result of this analysis, data reported using mean $\pm$ standard deviation. The first column indicates the brain rhythms denoted as their $\overline{PBA}$ value, given that we are referring to the powers from all participants. Second and third columns correspond to the Rest and Stimulus power obtained from all the brain localizations, as depicted in the last row of Table 5.4. The fourth column shows the p-value from the statistical analysis of means from these pair of aforementioned columns.

In Table 5.5 we can see that the Chen system produced decrements in the stimulus class relative to the basal state over all the brain rhythms. However, only highlighted rows correspond to effects that resulted in p-value inferior to 0.05. This implies that there were statistical differences for delta and theta bands between the Rest and Stimulus classes.

It's worth to emphasize that this result involves the 16 electrodes recorded for the experiment—which suggest a widespread and significant decrease in the bands. These

Table 5.4: Test for mean differences of Rest versus Stimulus classes in EEG power areas for all participants using Chen system

| | $\overline{PBA^\varepsilon\varphi}$ (mW) | | | | | | | | | | | | | | |
| | δ | | | θ | | | α | | | β | | | γ | | |
	Rest	Stim	p	Rest	Stim	p	Rest	Stim	p	Rest	Stim	p	Rest	Stim	p
Pz	518	314	0.001	75	55	0.048	123	120	0.827	48	44	0.009	15	14	0.332
F4	600	558	0.289	65	59	0.147	50	46	0.211	32	30	0.088	13	11	0.040
Cz	529	407	0.002	96	78	0.134	109	107	0.848	64	61	0.414	22	21	0.613
T8	390	288	0.113	44	40	0.499	53	47	0.136	90	74	0.010	56	41	0.006
P8	454	316	0.022	65	52	0.094	87	76	0.191	56	48	0.00º	23	19	0.001
F8	660	479	0.068	74	45	0.008	41	31	0.054	33	27	0.016	16	12	0.001
C4	540	459	0.013	72	65	0.069	108	100	0.433	64	55	0.010	27	22	0.022
P4	489	330	0.003	78	68	0.306	134	136	0.917	59	64	0.630	20	21	0.682
P7	361	266	0.010	56	50	0.249	81	81	0.979	57	52	0.350	23	18	0.055
F7	603	402	0.004	63	46	0.005	40	40	0.957	38	35	0.533	20	17	0.135
F3	600	476	0.025	74	65	0.283	56	59	0.793	36	41	0.556	14	14	0.782
C3	520	401	0.002	77	72	0.406	112	119	0.592	71	70	0.942	30	26	0.304
T7	477	286	0.014	48	36	0.003	49	45	0.200	63	49	0.009	34	25	0.004
Fz	617	484	0.003	81	70	0.104	68	68	0.986	41	46	0.620	14	15	0.675
P3	492	326	0.005	88	65	0.173	130	132	0.922	58	60	0.828	19	19	0.992
Fpz	692	546	0.105	80	52	0.003	27	22	0.029	14	12	0.019	6	5	0.030
Mean	**534**	**396**		**71**	**57**		**79**	**77**		**52**	**48**		**22**	**19**	

results go along with the analysis showed on Table 5.4, given the intra-electrode statistical differences found between the classes.

Table 5.6 shows the RD and SD obtained from the data reported on Tables 5.4 & 5.5 determined by the Equations 4.5 & 4.6 defined in Chapter 4.4, page 35.

The first column of Table 5.6 indicates the corresponding brain wave, while the second column shows values for RD of the bands. As explained in the previous chapter, this value represents the ratio of power before/during stimulation. Results are presented using the *topoplot* function of EEGLAB toolbox for MATLAB®. The output graph from the topoplot represents sensors viewed from above the head, and nose corresponds to the top—as mentioned in Section 4.4 of the previous chapter.

For the topoplots corresponding to RD, colors closer to the blue spectrum in the topoplots correspond to negative values, it indicates a decrement of the power Stimulus class relative to Rest class. Colors closer to the red spectrum correspond to positive values, and it indicates an increment of the Stimulation/Rest power ratio of the classes. Meaning that, positive values imply that EEG power under experimental stimulation are greater than EEG power before stimulation.

In order to have a better perspective of the RD, the color maps for all bands were standardized into (-0.4 to 0.4) map limits. The minimum value of -0.4 implies a negative power band ratio (unit-less), which also could be expressed as a percentage of change if multiplied by 100. This would correspond to a 40% reduction of Stimulus relative to the Rest power. Likewise, the maximum value of 0.4 corresponds to a increment of 40% produced on the band power during stimulation. Green colors correspond to a ratio of zero, indicating a lack of change between classes. The color assigned for inter-electrode space is interpolated by the topoplot function.

The null hypothesis value h for the t-test presented on Table 5.4 is shown on the third column of Table 5.6. Values of $h = 1$ indicate rejection of the null hypothesis of equal means, suggesting the presence of statistical effects induced by the stimulus (SD = 1). On the other hand, values of $h = 0$ indicate that the test fails to reject the hypothesis, meaning equal means and SD = 0.

Results for SD are also reported using topoplots, where dark blue color correspond to $h = 0$ and lighter blue represents $h = 1$. Unlike the topoplots described above for the power ratio, results for the null hypothesis are binary (0 and 1), this implies no middle tones here. Map color corresponding to intermediate values are faded to white, which makes a fine white line that separates both color poles for the hypothesis result in the topoplots.

Table 5.5: Analysis of variance for Rest and Stimulus power area means obtained from all electrodes using Chen system

Band	Rest (mW)	Stimulus (mW)	p
$\overline{\delta}$	534 ± 92	396 ±96	0.001
$\overline{\theta}$	71 ± 14	57 ±12	0.006
$\overline{\alpha}$	79 ±36	77 ±38	0.848
$\overline{\beta}$	52 ± 18	48 ± 17	0.585
$\overline{\gamma}$	22 ±11	19 ± 8	0.388

Table 5.6: EEG power differences of Rest versus Stimulus classes using Chen system

Band	Relative difference	Significant difference
Delta		
Theta		
Alpha		
Beta		
Gamma		
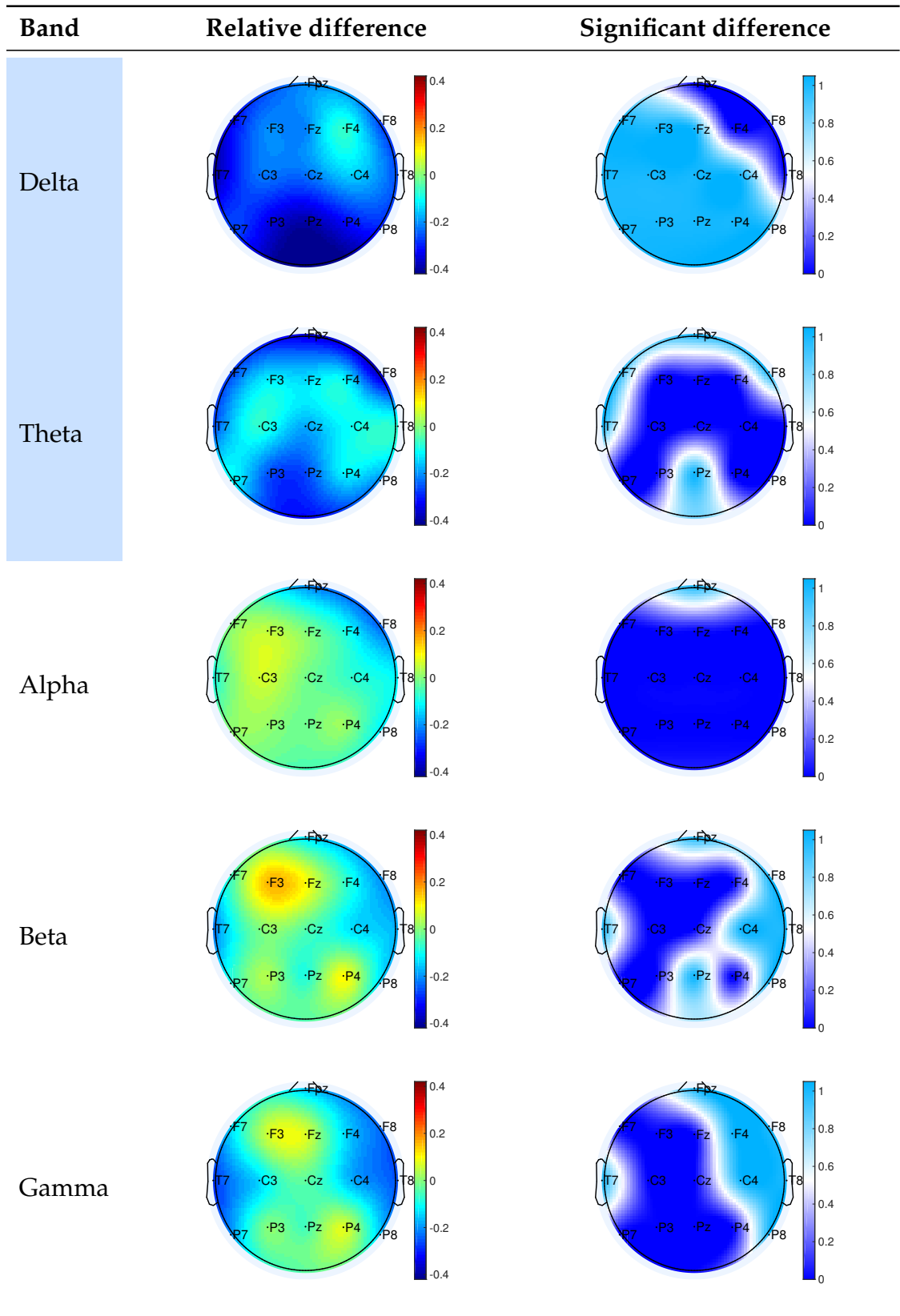
In Table 5.6 we can note that effects on delta mentioned in Table 5.4, correspond all to decrements in the band relative to rest class, given by the blue color on the relative difference figure. We can also see from the plot that these decrements were stronger for the temporal left side T7 and smoothly spread on the parietal Pz, P3 and P4 channels. The right-frontal near region showed the smaller decrements, which also received no significance, represented by the dark blue region of the significant change plot.

Theta changes corresponded also to a negative EEG power ratio of Stimulus / Rest classes. Table 5.6 shows significant decrements for this band in Fpz, F7, T7, F8 and Pz, where the tonality of blue color on relative difference indicates a power ratio of 0.2 to 0.3, which implies a reduction of (20 to 30) % on Stimulus power band relative to basal state power.

Highlighted cells Delta and Theta on Table 5.6 allude at results presented on Table 5.5, where it was found a widespread and significant decrease for the bands using all EEG channels. The remaining bands alpha, beta and gamma didn't show this uniformity on the effects produced by the Chen stimulus. Meaning that for these bands, some of the channels presented positive EEG relative ratio while others showed negative ratios, which is clear to neutralize the overall sum of differences between the classes.

Alpha band, for instance, presented slight increments, more visible around the left-localized C3, P3 and F3. Whereas the right hemisphere seems to be more negative—in terms of the relative ratio. However, none of these results presented statistical significance, with the exception of Fpz. Both beta and gamma band presented significant decreases during stimulation on T7, C4, F8, T8, P8 and Fpz localizations. While regions around F3 and P4 show an increment of relative difference but with no statistical significance.

Table 5.7: Test for mean differences of Rest versus Stimulus classes in EEG power areas for all participants using Rössler* system

| | $\overline{PBA^{\varepsilon}\varphi}$ (mW) | | | | | | | | | | | | | | | | | |
| | δ | | | θ | | | α | | | β | | | γ | | |
	Rest	Stim	p	Rest	Stim	p	Rest	Stim	p	Rest	Stim	p	Rest	Stim	p
Pz	456	382	0.060	72	67	0.322	116	139	0.199	84	48	0.312	17	14	0.069
F4	619	536	0.065	78	62	0.010	49	51	0.443	30	28	0.010	12	9	0.040
Cz	525	467	0.069	92	85	0.059	101	117	0.139	59	56	0.127	18	16	0.124
T8	416	318	0.037	53	46	0.068	55	57	0.630	98	92	0.105	60	50	0.028
P8	399	388	0.790	60	58	0.635	83	88	0.288	68	58	0.378	27	26	0.889
F8	609	485	0.095	73	55	0.014	30	30	0.644	23	21	0.001	10	9	0.008
C4	517	481	0.281	81	70	0.006	92	108	0.011	60	58	0.294	25	20	0.113
P4	439	372	0.060	74	70	0.276	116	133	0.186	63	56	0.262	21	19	0.083
P7	356	305	0.310	57	52	0.135	75	86	0.100	71	67	0.570	29	29	0.939
F7	592	463	0.037	75	54	0.007	35	34	0.582	30	28	0.119	13	12	0.136
F3	622	532	0.074	80	65	0.005	50	52	0.466	34	31	0.023	12	10	0.034
C3	509	455	0.094	84	75	0.009	108	120	0.114	75	63	0.058	33	23	0.049
T7	363	300	0.144	46	43	0.368	45	47	0.682	65	62	0.343	39	36	0.199
Fz	631	525	0.050	81	69	0.017	61	62	0.729	34	32	0.038	10	9	0.036
P3	462	385	0.121	72	69	0.493	116	146	0.097	76	55	0.297	22	18	0.018
Fpz	654	591	0.445	93	76	0.160	34	34	0.904	16	14	0.012	5	5	0.044
Mean	**511**	**437**		**73**	**63**		**73**	**81**		**55**	**48**		**22**	**19**	

5.2.2 Rössler* System Stimulation

Now regarding results derived from the stimulation performed with sound generated from Rössler* system. We will continue with the same structure, starting as explained before for Table 5.4, where we present the obtained mean powers of Rest and Stimulus windows from all participants according to Equation 4.5 on page 41. As noted for Table 5.4, the first column correspond to the respective brain wave and the groups of following three columns represent the powers from our two experimental classes with its respective p-value for equal means.

In Table 5.7 we highlight that, in contrast with the delta, beta, theta and gamma bands—the alpha inter-electrode mean (last row) shows an increment of (73 to 81) mW power during stimulation relative to basal class. This was also the case with intra-electrode analysis of the band, where it was obtained a power raise from silent state for 13 from the 16 EEG channels (highlighted cells in Table 5.7).

In Table 5.8, however, we will see that this increment on the power (Stim/Rest) for alpha band did not received significance, given $p > 0.05$. This table shows the inter-electrode analysis of mean variance for the brain rhythms $\bar{\delta}$, $\bar{\theta}$, $\bar{\alpha}$, $\bar{\beta}$ and $\bar{\gamma}$, which correspond to values shown on last row of Table 5.7.

As mentioned above, the analysis of variance test for alpha resulted on a p-value of 0.51, which suggests that these changes were not spatially uniform or strong enough. On the other hand, mean power differences for delta and theta bands were found with p-values of 0.036 and 0.037, respectively. These changes correspond to the highlighted rows of Table 5.8.

Table 5.9 shows the results obtained from Equation 4.6 and t-test described in Section 4.4 of the previous chapter. Values obtained from relative difference correspond to second column of the table and null hypothesis value to the third column.

Obtained significant differences for delta wave show that only F7 and T8 channels resulted in rejection of the hypothesis $h = 1$, this implies that only these localizations presented statistical effects. However, referring to the RD values, we can see a uniformly spatial reduction of (10 to 20) % in the power ratio. This explains why, even though there was found only a pair of localized significant differences, the band showed statistical difference in analysis of Table 5.8; the sum of small decrements inter electrode gave way to a significant wide-spatial reduction of the band during stimulation.

The butterfly-shaped light-blue form depicted on significant difference results for

Table 5.8: Analysis of variance for Rest and Stimulus power area means obtained from all electrodes using Rössler* system

Band	Rest (mW)	Stimulus (mW)	p
$\bar{\delta}$	511 ± 101	437 ± 89	0.036
$\bar{\theta}$	73 ± 13	63 ± 12	0.037
$\bar{\alpha}$	73 ± 32	81 ± 42	0.514
$\bar{\beta}$	55 ± 24	48 ± 21	0.368
$\bar{\gamma}$	22 ± 14	19 ± 12	0.494

Table 5.9: EEG power differences of Rest versus Stimulus classes using Rössler* system

Band	Relative difference	Significant difference
Delta		
Theta		
Alpha		
Beta		
Gamma		
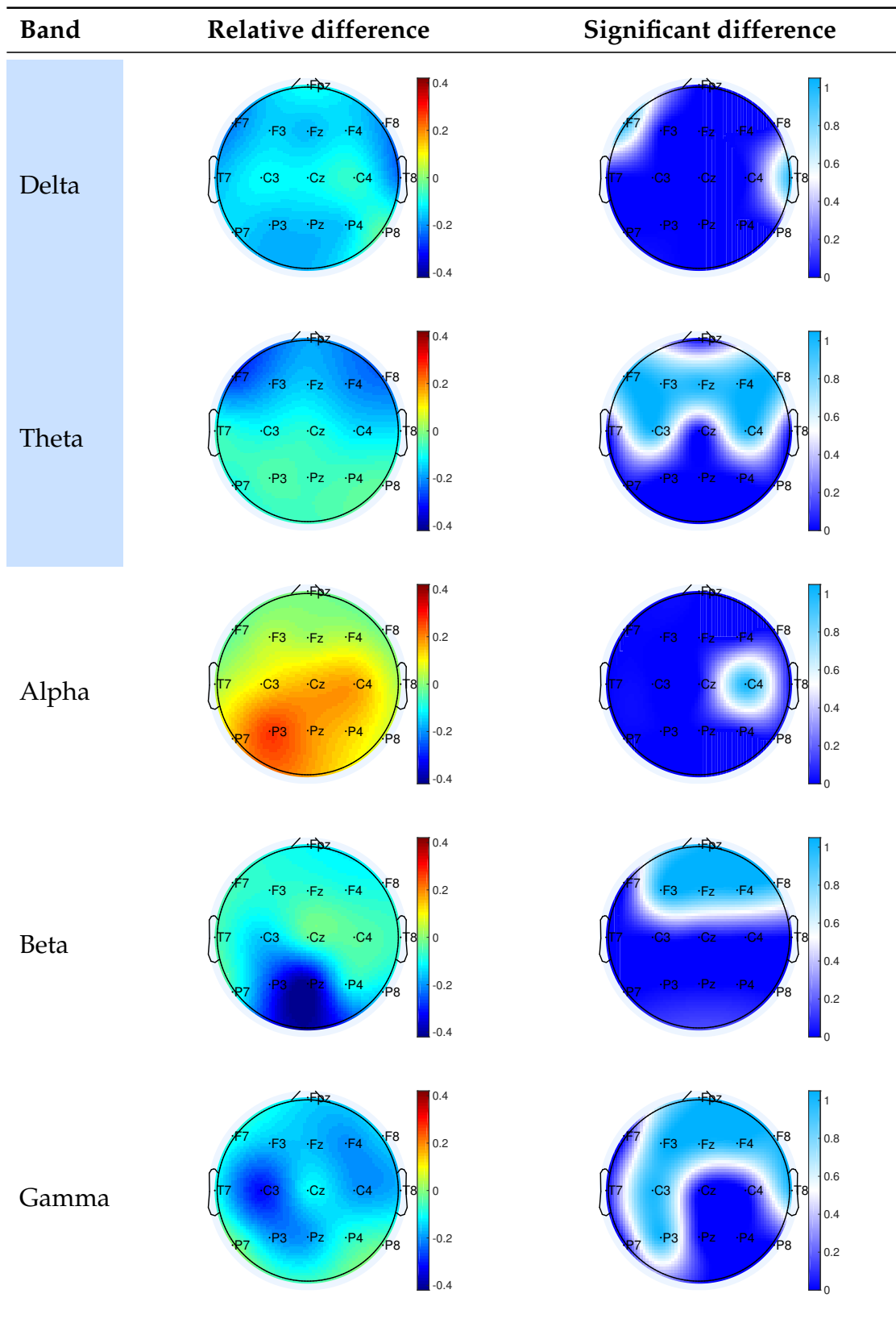
theta band indicates that all electrodes corresponding to frontal lobe region (F label) presented statistical changes, along with C3 and C4 channels. RD topoplot shows that these changes correspond to negative EEG power ratios of 0.15 to 0.25, according to the map color scale.

Cells corresponding to Delta and Theta features are highlighted alluding to significance obtained in Table 5.8. It's worth mentioning that RD results for alpha band also suggest a uniform (10 to 20) % increase of power during stimulation but only considering back central and parietal regions (C & F). We hypothesize that the inert effects from frontal and temporal regions (as seen from the greenish color on RD) disfavored the inter-electrode analysis for this band. Future analyses for this band could be performed considering mostly parietal and occipital regions.

Both beta and gamma bands showed statistical differences on electrodes Fpz, Fz, F3, F4 and F8 according to last rows of Figure 5.9. Relative difference indicates that changes correspond mostly to negative ratios of EEG power, going down to -(0.3 to 0.4) % on electrodes Pz and P3. Oddly enough, these channels did not present statistical significance, given $h = 0$. These decrements could have been then caused by very strong outliers.

5.2.3   Rössler System Stimulation

Next, results obtained using the sound generated from the chaotic Rössler as auditory stimulus will be presented. First, the inter-participant PBA means were calculated for both classes according to Equation 4.5 in Chapter 4.4. Results are reported in Table 5.10, presenting the $\overline{PBA}$ value for δ, θ, α, β, and γ power brain features, as commented before for Table 5.4.

In Table 5.10 we can note that there were found several EEG channels presenting

Table 5.10: Test for mean differences of Rest versus Stimulus classes in EEG power areas for all participants using Rössler system

	$\overline{PBA^{\varepsilon}\varphi}$ (mW)														
	δ			θ			α			β			γ		
	Rest	Stim	p	Rest	Stim	p	Rest	Stim	p	Rest	Stim	p	Rest	Stim	p
Pz	456	325	0.007	63	58	0.275	118	132	0.258	48	47	0.642	17	16	0.734
F4	634	490	0.001	59	49	0.033	40	41	0.747	25	24	0.479	10	8	0.314
Cz	499	356	0.002	77	67	0.070	100	103	0.744	61	54	0.036	22	19	0.146
T8	533	259	0.001	45	30	0.003	40	36	0.104	66	56	0.114	39	31	0.145
P8	504	325	0.044	62	44	0.052	82	79	0.724	56	53	0.268	25	23	0.264
F8	668	435	0.010	60	43	0.002	32	30	0.519	23	23	0.745	11	10	0.238
C4	563	412	0.008	66	56	0.025	89	89	0.981	54	47	0.188	25	19	0.315
P4	512	354	0.039	66	57	0.078	122	120	0.841	51	50	0.471	19	19	0.602
P7	344	242	0.016	56	48	0.128	90	93	0.609	67	62	0.163	29	23	0.060
F7	636	399	0.002	55	43	0.037	33	35	0.497	29	28	0.675	15	14	0.281
F3	604	438	0.001	67	53	0.003	52	54	0.670	34	33	0.345	12	11	0.319
C3	492	381	0.011	70	62	0.021	108	110	0.844	65	58	0.084	30	22	0.053
T7	459	246	0.006	37	29	0.035	36	32	0.146	49	44	0.188	29	26	0.139
Fz	617	475	0.002	74	62	0.009	63	59	0.363	37	33	0.027	13	11	0.051
P3	454	346	0.003	67	60	0.059	122	133	0.321	56	55	0.712	21	19	0.269
Fpz	652	535	0.118	69	53	0.059	33	33	0.910	15	15	0.951	6	6	0.969
Mean	**539**	**376**		**62**	**51**		**73**	**74**		**46**	**43**		**20**	**17**	

rejection of null hypothesis for the t-test of equal means in delta band. This implies $p < 0.05$, which correspond to powers and analysis results highlighted on the second, third and fourth column. From means showed on the last row of the table we could anticipate that most of effects for each electrode correspond to a decrement of power during stimulation. However, this will be easier to visualize in the following analysis.

In Table 5.11 are presented the results from analysis of mean variance considering 16 EEG channels (as depicted in last row of Table 5.10). The results are reported as mean and standard deviation corresponding to the averaged powers for Rest and Stimuli classes, respectively. Along with p-value obtained from the ANOVA.

As expected, given the results noted in the previous table, on Table 5.11 is confirmed that mean variance inter-electrode resulted significant for delta power band. It was obtained a p-value of 0.001 from the test, corresponding to a decrement from (539 to 376) mW of power for this band.

As seen from highlighted columns on Table 5.12, significant changes were also found for theta band, receiving $p = 0.006$ for a difference of mean powers from (62 to 51) mW. In order to summarize these reported results, next are addressed the obtained values for relative and significant differences of the feature powers. These are presented in Table 5.12, which consist of results obtained from the equations and methods described in Subsection 4.4 of Chapter 4 now using the auditory stimulus generated from Rössler system.

Power bands that resulted on effects-significance $p < 0.05$ of inter-electrode mean differences (delta and theta) are highlighted on the first column of Table 5.12. For delta band, we can see from third column that almost all of the EEG channels obtained $h = 1$ values according to the light blue tone, with the only exception of Fpz. Relative difference shows that changes of delta power during stimulation correspond to decrements in all the channels, being the temporal electrodes T7 and T8 the most notable reductions (around 30 % to 40 %).

These results from Rössler system sound contrast with the ones obtained from the Rössler* stimulation. Even though there were also found general decrements in delta band for Rössler* system, only F7 and T8 presented statistical significance (Table 5.9). Hence, the stimulation from Rössler system seemed to yield stronger reduction effects on the delta power, which also agrees with the -0.3 to -0.4 received values of relative difference for Rössler versus the -0.1 to -0.2 results for Rössler* system.

On the other hand, theta band effects during both Rössler stimulations seemed to hold. The significant difference in second row of Table 5.12 shows closely the same

Table 5.11: Analysis of variance for Rest and Stimulus power area means obtained from all electrodes using Rössler system

Band	Rest (mW)	Stimulus (mW)	p
$\overline{\delta}$	539 ± 91	376 ± 87	0.001
$\overline{\theta}$	62 ± 10	51 ± 11	0.006
$\overline{\alpha}$	73 ± 35	74 ± 38	0.927
$\overline{\beta}$	46 ± 17	43 ± 15	0.543
$\overline{\gamma}$	20 ± 9	17 ± 7	0.287

Table 5.12: EEG power differences of Rest versus Stimulus classes using Rössler system

Band	Relative difference	Significant difference
Delta		
Theta		
Alpha		
Beta		
Gamma		
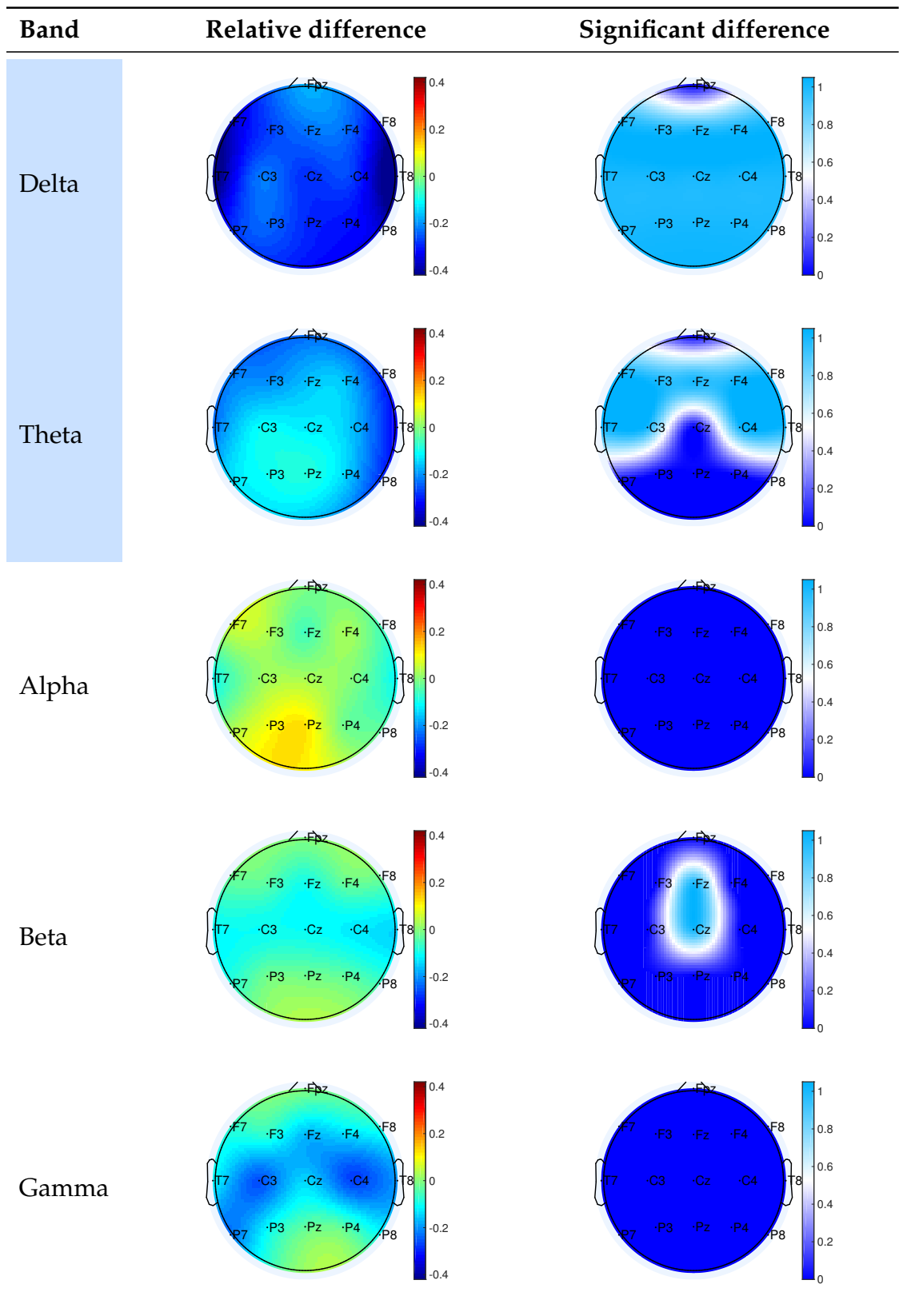
form presented back on Table 5.9 for the same analysis, but with the additional T7 and T8 channels with $h = 1$ values on the temporal region. Relative difference in theta also shows similar results for Rössler* and Rössler system sounds, both obtaining around (10 to 20) % decrease of band power during stimulation.

Results in Table 5.12 show a lack of effects on alpha, beta, and gamma. For these bands, the only statistical differences found correspond to Cz and Fz electrodes for beta wave, corresponding to the $h = 1$ values of the fourth row of the table. As shown in relative difference for beta, these significant changes correspond to a (5 to 10) % decrease on Stimulus relative to Rest class.

Given the values presented above, we could fairly state that in general, results of the limit cycle Rössler* and the chaotic-dynamic Rössler system sounds seemed to digress, with the exception of theta band. The Rössler system showed greater influence over the low-frequency bands delta and theta, while proving inert over alpha, beta, and gamma waves. This also contrasts with results obtained from the analysis of perception from Section 5.1, where participants gave both sounds the same score and reported no perceived difference between them.

Moreover, these results will be discussed in depth on the following final chapter of the investigation.

5.2.4 UD System Stimulation

Moving on to results obtained from the auditory stimulation with sound generated from UD system. Table 5.13 presents the intra-electrode power means from all participants, as described in the Materials and Methods Chapter. In order to accomplish this, the PSD from Stimulus and Rest windows was calculated for each participant as mentioned for Table 5.4.

Table 5.13: Test for mean differences of Rest versus Stimulus classes in EEG power areas for all participants using UD system

| | $\overline{PBA^\varepsilon\varphi}$ (mW) | | | | | | | | | | | | | | | | | |
| | δ | | | θ | | | α | | | β | | | γ | | |
	Rest	Stim	p	Rest	Stim	p	Rest	Stim	p	Rest	Stim	p	Rest	Stim	p
Pz	449	335	0.007	64	60	0.245	108	151	0.049	42	44	0.417	13	13	0.630
F4	632	532	0.031	69	55	0.001	47	46	0.896	26	26	0.718	9	8	0.022
Cz	484	389	0.005	81	76	0.123	101	127	0.119	53	57	0.438	18	18	0.815
T8	448	332	0.025	53	41	0.001	56	51	0.247	84	68	0.016	49	35	0.005
P8	460	331	0.003	61	55	0.082	93	96	0.691	60	54	0.053	28	23	0.034
F8	586	538	0.503	65	50	0.002	35	32	0.292	24	22	0.069	10	9	0.034
C4	494	441	0.161	68	63	0.101	94	107	0.289	53	54	0.754	21	20	0.437
P4	444	347	0.024	72	60	0.022	115	143	0.149	58	49	0.312	18	15	0.046
P7	372	254	0.007	56	48	0.020	80	81	0.893	64	52	0.088	28	20	0.015
F7	550	449	0.018	63	48	0.000	39	37	0.674	37	31	0.157	16	14	0.025
F3	607	480	0.001	73	61	0.003	52	57	0.278	33	32	0.714	11	10	0.072
C3	513	397	0.001	78	70	0.019	100	110	0.262	60	53	0.144	27	19	0.095
T7	463	275	0.024	50	40	0.004	42	43	0.655	54	49	0.033	30	25	0.020
Fz	598	484	0.007	81	72	0.045	64	69	0.368	32	31	0.633	10	9	0.060
P3	481	344	0.004	78	68	0.036	117	147	0.134	56	49	0.376	19	15	0.054
Fpz	702	527	0.001	83	59	0.001	29	28	0.676	14	14	0.651	5	5	0.156
Mean	**518**	**403**		**68**	**58**		**73**	**83**		**47**	**43**		**19**	**16**	

Highlighted columns show that several of the EEG channels corresponding to alpha band presented increases in the Stimulus class compared to Rest class. Moreover, results from the *t*-test of the band indicate that statistical difference was found for Pz location, receiving a p value below the significance level of the test.

Table 5.14 shows the analysis of variance taking into consideration the EEG band powers that correspond to means showed in last row of 5.13. Values of $p = 0.001$ and $p = 0.006$ were obtained for delta and theta bands, respectively. These results correspond to rows highlighted in Table 5.14. Not unlike effects from Chen and both Rösser systems, these statistic significance correspond to decrements in the EEG bands during Stimulus class.

Results from Table 5.13 & 5.14 are summarized into Table 5.15, where the highlighted cells allude to the statistical differences found on Table 5.14, just described above. We can see that delta band obtained $h = 1$ values for the significant difference for almost all of the EEG localizations, with the exceptions of C4 and F8. Blue color on the relative difference panel indicates that these statistical differences correspond to negative values of the power ratio Stimulus/Rest. This could be foreseen from the full-spatial means of 5.14 for delta, which showed a general decrement from (518 to 403) mW.

Theta band also presented high statistical effects according to the light blue color on the significant difference panel. Negative (blue) values on relative difference confirm that changes are derived from a decrease of power during the auditory stimulation from UD system. We can also see that the sound influence resulted stronger for the frontal and temporal regions (F & T labels), going down to 20 % reductions of the theta power.

RD values for alpha band seem to indicate that the UD system sound provoked some robust effects over some parietal and central EEG regions, mostly Pz, P4, P3, C3, C4, and Cz. The strong red color indicates a (30 to 40) % increase of power during stimulation. Influence over Pz was particularly greater, where the null hypothesis value of equal means was rejected according to the light blue tone on the significant difference panel.

These alpha effects seem worth noting, even more given the nature of alpha waves, which are known to manifest mostly on occipital lobe and with eyes closed. We empathize that, if occipital regions were considered for future analyses, these reported results suggest that significant differences might be provoked.

Table 5.14: Analysis of variance for Rest and Stimulus power area means obtained from all electrodes using UD system

Band	Rest (mW)	Stimulus (mW)	p
$\overline{\delta}$	518 ± 87	403 ± 92	0.001
$\overline{\theta}$	68 ± 10	58 ± 11	0.007
$\overline{\alpha}$	73 ± 31	83 ± 43	0.477
$\overline{\beta}$	47 ± 18	43 ± 15	0.484
$\overline{\gamma}$	19 ± 11	16 ± 8	0.323

Table 5.15: EEG power differences of Rest versus Stimulus classes using UD system

Band	Relative difference	Significant difference
Delta		
Theta		
Alpha		
Beta		
Gamma		
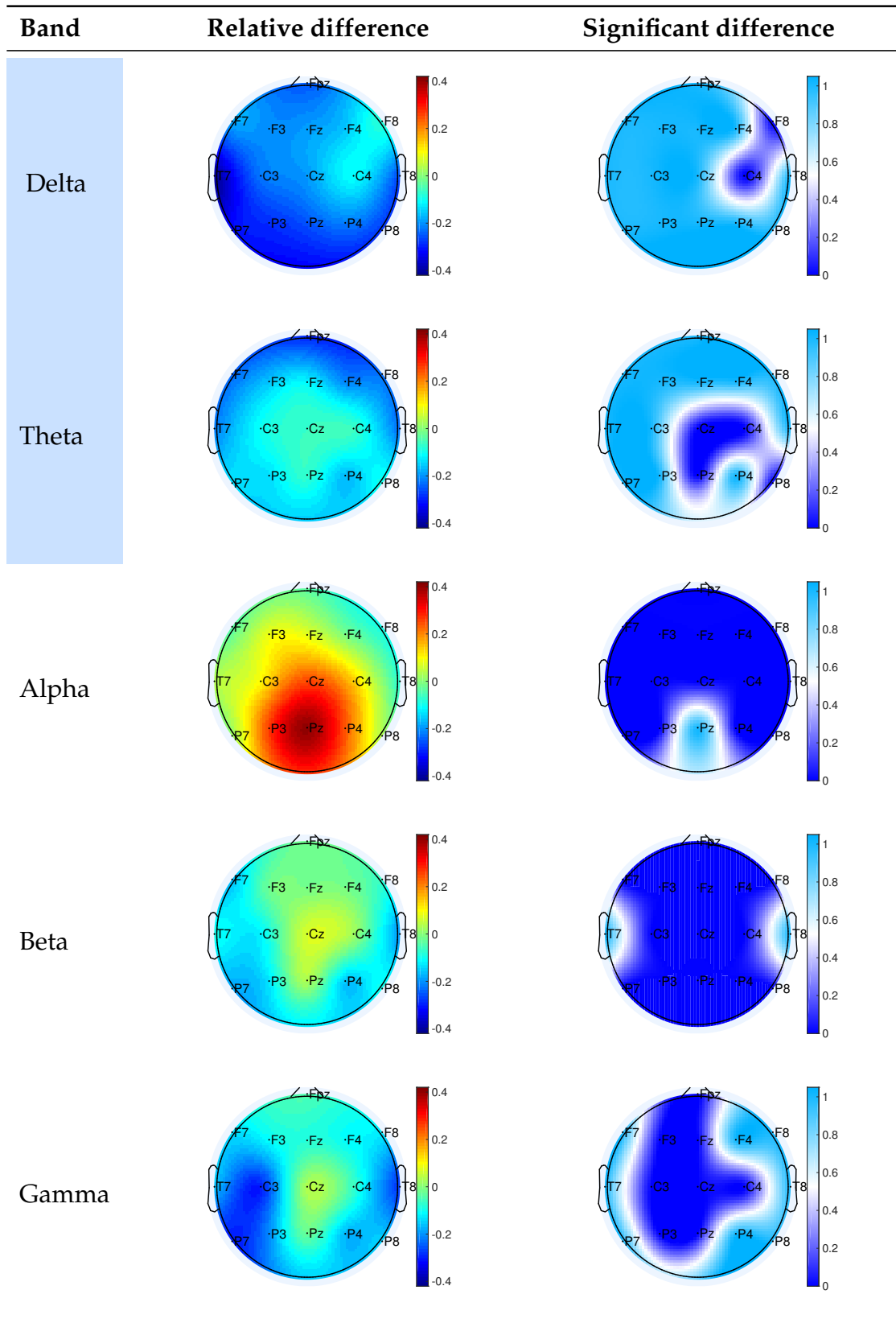
5.2.5 Pink Noise Stimulation

As expected from the literature [24], power bands using Pink Noise as stimulus did not show differences between Rest vs Stimuli classes. The presented results confirm the standard assumption for the Pink Noise as being "Neutral" and the paradigm for control signal in stimulation studies.

There is really not much to note from the results derived from the pink noise stimulation. Power mean for Stimulus and Rest windows are presented on Table 5.16, hardly showing any changes between the classes. Some significant effects were found on the temporal lobes, mostly in beta band, as shown in Table 5.18. However, the analysis of variance from Table 5.17 proved no general differences in any band, having any p-value under 0.05.

Given these inert effects, future analyses can be performed now comparing the power ratios (EEG power during stimulation/EEG power before stimulation) for the different dynamic stimuli proposed in this study. However, this and other perspectives of the results will be addressed in depth on the following concluding chapter.

Table 5.16: Test for mean differences of Rest versus Stimulus classes in EEG power areas for all participants using Pink noise

| | $\overline{PBA^\varepsilon\varphi}$ (mW) | | | | | | | | | | | | | | |
| | δ | | | θ | | | α | | | β | | | γ | | |
	Rest	Stim	p	Rest	Stim	p	Rest	Stim	p	Rest	Stim	p	Rest	Stim	p
Pz	446	383	0.077	76	70	0.397	140	158	0.060	55	54	0.722	17	18	0.390
F4	585	578	0.898	63	58	0.438	50	48	0.505	29	30	0.633	10	11	0.415
Cz	481	463 0	.611	89	88	0.824	117	129	0.347	65	66	0.845	23	25	0.403
T8	440	323	0.058	54	43	0.029	60	59	0.891	81	71	0.003	43	38	0.097
P8	389	359	0.484	61	59	0.675	96	103	0.394	61	56	0.157	26	23	0.156
F8	570	554	0.840	65	59	0.441	41	41	0.935	29	29	0.777	13	12	0.612
C4	486	487	0.991	71	70	0.874	110	115	0.561	61	59	0.423	25	24	0.913
P4	462	385	0.110	76	75	0.794	138	154	0.287	61	58	0.156	21	21	0.744
P7	385	355	0.580	64	60	0.460	93	88	0.293	69	62	0.073	27	23	0.186
F7	553	506	0.547	57	53	0.490	42	42	0.955	33	32	0.710	16	16	0.899
F3	574	512	0.185	72	63	0.096	59	57	0.411	35	34	0.786	12	13	0.359
C3	466	432	0.355	84	78	0.304	120	128	0.425	73	70	0.415	28	29	0.718
T7	403	326	0.271	57	49	0.158	57	53	0.206	72	64	0.025	41	35	0.023
Fz	571	544	0.632	78	73	0.367	69	65	0.306	37	36	0.449	12	12	0.739
P3	449	386	0.268	91	82	0.216	131	138	0.682	60	57	0.280	19	19	0.945
Fpz	661	591	0.415	71	65	0.576	29	31	0.530	13	14	0.369	4	5	0.308
Mean	**495**	**449**		**70**	**65**		**84**	**88**		**52**	**49**		**21**	**20**	

Table 5.17: Analysis of variance for Rest and Stimulus power area means obtained from all electrodes using Pink noise

Band	Rest (mW)	Stimulus (mW)	p
$\overline{\delta}$	495 ± 81	449 ± 92	0.143
$\overline{\theta}$	70 ± 11	65 ± 12	0.231
$\overline{\alpha}$	84 ± 38	88 ± 44	0.805
$\overline{\beta}$	52 ± 20	49 ± 17	0.688
$\overline{\gamma}$	21 ± 11	20 ± 9	0.854

Table 5.18: EEG power differences of Rest versus Stimulus classes using Pink noise

Band	Relative difference	Significant difference
Delta		
Theta		
Alpha		
Beta		
Gamma		
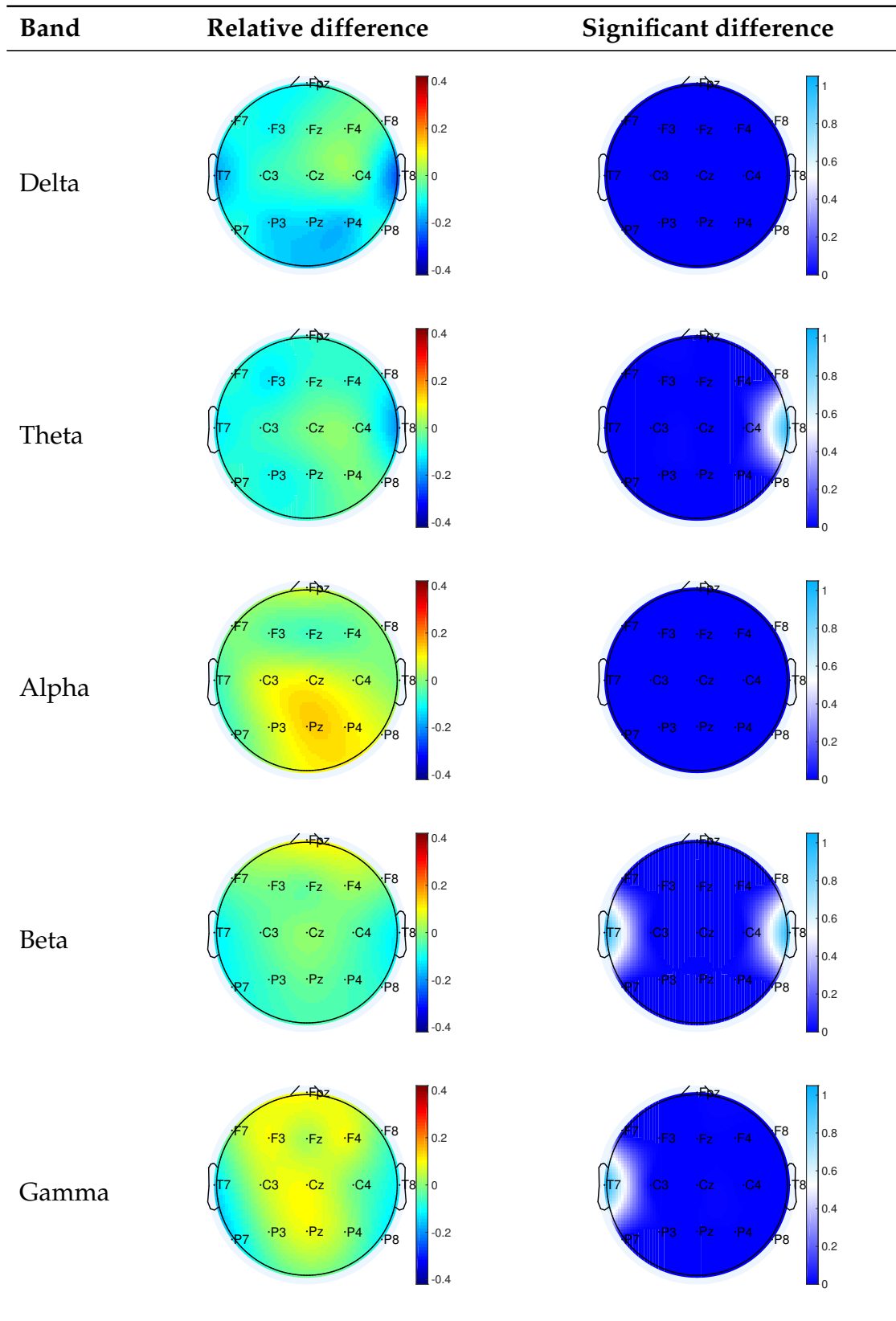
Chapter 6

CONCLUSIONS

In this investigation we acquired acoustic signals from one aleatory and four deterministic processes. Among the later, three of them constituted signals derived from strange attractors and one from a limit cycle behavior. The aim was to study the different effects that these random and deterministic processes could provoke in the human brain, specially those derived from chaotic dynamics. In spite of the presented results, we conclude that random, periodic and chaotic based stimulation were possible to characterize using brain power features in EEG signals.

The present work confirmed that the three auditory stimulation processes derived from chaotic systems presented stronger relative and statistical differences from basal state compared to the aleatory and periodic stimulations. Specifically, up to negative (30 and 40) % relative differences in delta and theta power were found in localized EEG channels, mainly around frontal regions of the brain, using these chaotic stimulations. It's worth to mention that these found decreases in theta band were similar to those reported by Gálvez *et al*. [24] in the pursuit to normalize theta power in Parkinson's disease patients using binaural rhythms.

The rise on alpha power band using the UD system and Rossler* system stimulations is also important to remark, noting that statistical significance of the increment was found on Pz localization for the chaotic stimulation from UD system. We can not overemphasize the perspective of new analyses from chaotic stimulus using occipital localizations in the EEG channels.

Moreover, the comparisons from the limit cycle and strange attractor from the Rössler system seem to indicate that subjective perception from the sounds is not necessarily related to dynamics or induced effects on electrophysiology, as we hypothesized at the beginning of this investigation. Participants characterized both deterministic systems Rössler* and Rössler as essentially the same. But even so, the EEG experiments showed that the brain features from these two dynamical attractors was effectively different.

As closing thoughts, we emphasize the relationship between chaotic processes and theoretical models, mathematical tools and experimental techniques to analyze brain dynamics, which is not novel in neuroscience. On the contrary, there is an emerging boom referring to new sophisticated methods for chaos detection or quantification in brain paradigms, extending to high dimensional systems. Even so, to our knowledge, finding investigations that study any kind of stimulation derived from signals of these

chaotic dynamics is not an easy task, as there is not much research investigated around this topic. In the present study we aimed to provide a new perspective from where acoustic waves can be analyzed and understand.

As Lorenz writes: "Systems that presumably qualify as examples of chaos can very often be seen and appreciated without telescopes or microscopes, and they can be recorded without time-lapse or high-speed cameras. Phenomena that are supposedly chaotic include everyday occurrences, like falling of a leaf or the flapping of a flag . . ." According to chaos theory, sounds that are listened in every-day life, as well as more involved processes, like the turbulence of sea waves or a waterfall, could be classified as chaotic. As such, this investigation tried to answer the question of how do they influence the human mind, through the specific applications in mathematical models and analog circuits.

It is our future hope, however, that further analyses can find relationships between the chaotic sounds of the kind that we developed and the ones that occur naturally in everyday occurrences. After all, the evolving interest in chaos theory can be complemented by the interaction of the chaotic processes in the environment, the controversy of chaos-existence in the mind, and the nonlinear-chaotic methods to quantify them.

Appendix A

PRELIMINARY EXPERIMENTS

For this experiments we utilized the sound generated from the following chaotic systems:

- Chen system

- Chua system

- Lorenz system

- Lu system

- Rössler system

- Delgado system

We performed sound assessment questionnaires of perceived annoyance using the exact same methodology and data analysis described in Chapter 4, Section 4.3 on page 33.

The experiments were performed at Instituto de Investigación en Comunicación Óptica (IICO). Table A.1 shows the characteristics of the participants for the investigation, who were bachelor, master, and doctorate students from the same institute. In total, we had a fair number of 40 volunteers, 26 males and 14 female students.

From these results of pilot studies, we decided to utilize the sound from Chen and Rössler systems for further experiments. Both chaotic systems were the ones that received the lowest levels of annoyance according to the results shown in Figures A.1 & A.2, and Table A.2.

Table A.1: Characteristics of participants

Sex	N	Age	Degree	N
Masculine	26	18-50	Bachelor	21
Female	14	18-47	Master	15
Total	40		PhD	4
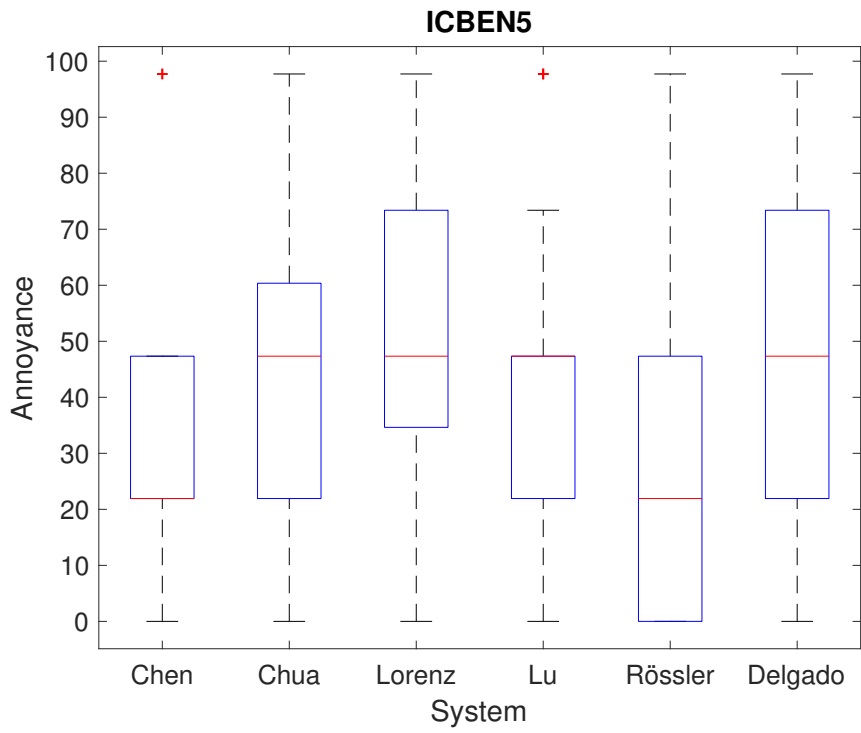
Figure A.1: QV numerical results
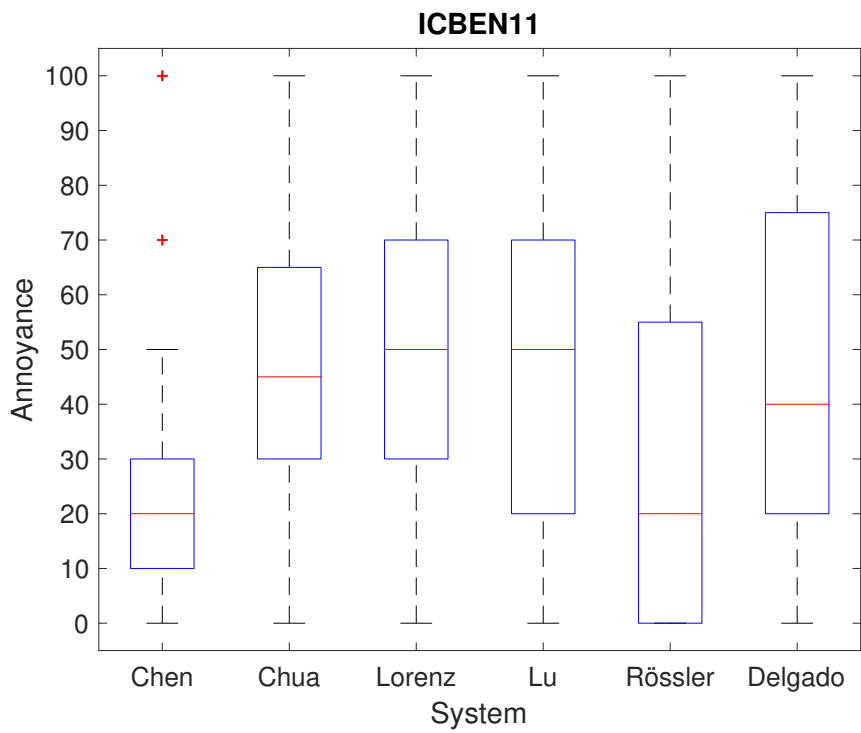
Figure A.2: QN results

Table A.2: Preliminary results

System	QV average	QN average	Mean	Verbal score
Chen	28.15	27.25	27.70	Moderately
Chua	45.08	46.25	45.66	Moderately
Lorenz	50.04	50.75	50.39	Moderately
Lu	41.45	46.00	43.72	Moderately
Rössler	29.27	30.50	29.88	Moderately
Delgado	43.94	45.25	44.59	Moderately

Appendix B

MATERIAL IN PORTUGUESE

Here is presented the precise information responded by participants of the experiment. As described in Sections 4.2 & 4.3, both were written in Portuguese.

Perception Questionnaire

QV

Pensando nos últimos 10 segundos, quanto o som dessa gravação te incomodou, estressou ou irritou?

<div align="center">

a) Nada
b) Algo
c) Medianamente
d) Muito
e) Extremamente

</div>

QN

Em seguida é dada uma escala de zero a dez para a sua opinião sobre o quanto o som dessa gravação te incomodou, estressou ou irritou. Se você se irritou nada escolha zero, se você ficou extremamente irritadou, escolha dez, se você ficou em algum lugar entre as opções, escolha um número entre zero e dez.

Nada | 0 | 1 | 2 | 3 | 4 | 5 | 6 | 7 | 8 | 9 | 10 | Extremamente

Consent Letter

Begins on the next page.

Termo de Consentimento Livre e Esclarecido

O Sr(a)_____

RG n^o _____, nascido em_____,

do sexo _____, residente à_____

_____

na cidade de _____, está sendo convidado a participar do estudo "Estudo da dinâmica cerebral a partir de sinais de EEG mediante estímulos acústicos". O objetivo deste estudo é determinar e caracterizar as mudanças produzidas por estímulos acústicos específicos na atividade elétrica cerebral medida a partir da eletroencefalografia de superfície.

Para tanto, podem participar deste experimento, o voluntário de qualquer sexo ou raça, saudável, com idade entre 18 e 60 anos. Será realizada uma avaliação da potencial perda auditiva por meio da audiometria baseada em aplicativo, os participantes que apresentarem ou excedam perda auditiva de 20 dB na faixa de frequência de 125 Hz a 8 kHz serão excluídos do estudo. Para prosseguir com o experimento:

- Os participantes devem ler, concordar e assinar este termo de consentimento livre e esclarecido, entendendo que eles podem desistir a qualquer momento do mesmo;
- É vedada a participação de voluntário que tenham bebido ou usado substâncias ou bebida estimulante ou intoxicante antes da sessão;
- Os participantes devem ter dormido pelo menos oito horas na noite anterior e não possuir histórico médico de enxaqueca e transtornos de ansiedade;
- Os participantes devem informar ao responsável qualquer histórico de doenças psiquiátricas;

Preparação experimental: a touca de EEG deverá ser vestida pelo usuário. Nenhum procedimento deste experimento é invasivo ou causa qualquer lesão. Os níveis sonoros empregados não são lesivos e qualquer desconforto em relação a este aspecto deve ser informado ao experimentador. Os eletrodos podem causar algum desconforto no primeiro momento, mas não devem causar qualquer lesão. Informe caso considere que

_____   _____
Rubrica do participante/representante legal   Rubrica do pesquisador Responsável

a touca está justa demais. O contato dos eletrodos com a pele é direto e não emprega qualquer outra substância que possa provocar alergias ou irritações na pele;

Realização do experimento: o voluntário deve estar confortavelmente sentado com fone de ouvido confortável. Estímulos sonoros em intensidade adequada (não lesiva – inferior a 60 dB) serão apresentados. Um primeiro estímulo de curta duração, conforme demonstrado pelo experimentador, será apresentado, seguido por 30 s de silêncio e 30 s de um estímulo acústico. Ao final deste registro tem-se uma pausa para descanso. O processo será repetido 25 vezes levando a um total de tempo de aproximadamente de 40 minutos. Ao final do experimento serão apresentadas instruções para preenchimento de um questionário em relação às sensações associadas a cada estímulo (agradável ou desagradável).

Não há benefício direto para o participante. Trata-se de um estudo experimental que busca melhor entender a atividade cerebral mediante diferentes estímulos acústicos.

Em qualquer etapa do estudo, você terá acesso aos profissionais responsáveis pela pesquisa para esclarecimento de eventuais dúvidas. O principal investigador é o Prof. Dr. Diogo Coutinho Soriano que pode ser encontrado no endereço Rua Arcturus, n. 3, Jardim Antares, São Bernardo do Campo, bloco Delta, sala 335, Telefone(s) (11) 23206166 ou (11) 976459591. Se você tiver alguma consideração ou dúvida sobre a ética da pesquisa, entre em contato com o Comitê de Ética em Pesquisa da UFABC, localizado na Avenida dos Estados, 5001, Bloco A, Torre 1, 1° andar, Santo André, SP - telefone: (11) 3356-7632, email: cep@ufabc.edu.br

É garantida a liberdade da retirada de consentimento a qualquer momento e deixar de participar do estudo, sem qualquer prejuízo à continuidade de seu tratamento na Instituição.

As informações obtidas serão analisadas em conjunto com as de outros voluntários, não sendo divulgado a identificação de nenhum participante.

Você tem direito de ser mantido atualizado sobre os resultados parciais das pesquisas, quando em estudos abertos, ou de resultados que sejam do conhecimento dos pesquisadores

Não há despesas pessoais para o participante em qualquer fase do estudo, incluindo, quando existirem, exames e consultas. Também não há compensação financeira

relacionada à sua participação. Se existir qualquer despesa adicional, ela será absorvida pelo orçamento da pesquisa.

Em caso de dano pessoal comprovadamente causado pelos procedimentos deste estudo, você tem direito de solicitar indenizações legalmente estabelecidas.

Os dados e os materiais coletados serão utilizados somente para esta pesquisa.

Acredito ter sido suficientemente esclarecido a respeito das informações que li ou que foram lidas para mim, descrevendo o estudo "Estudo da dinâmica cerebral a partir de sinais de EEG mediante estímulos acústicos". Eu ME INFORMEI com o Prof. Dr. Diogo Soriano. Sobre a minha decisão em participar nesse estudo. Ficaram claros para mim quais são os propósitos, os procedimentos a serem realizados, seus desconfortos e riscos, as garantias de confidencialidade e de esclarecimentos permanentes. Ficou claro também que minha participação é isenta de despesas e que tenho garantia do acesso a tratamento hospitalar quando necessário. Concordo voluntariamente em participar deste estudo e poderei retirar o meu consentimento a qualquer momento, antes ou durante o mesmo, sem penalidades, prejuízo ou perda de qualquer benefício que eu possa ter adquirido, ou no atendimento que recebo nesta instituição.

Assinatura do participante/representante legal Data____/____/____

Assinatura da testemunha*   Data____/____/____

*OBS (Para casos de voluntários analfabetos, semianalfabetos ou portadores de deficiência auditiva ou visual.)

Declaro que obtive de forma apropriada e voluntária o Consentimento Livre e Esclarecido deste paciente ou representante legal para a participação neste estudo. Sendo que uma via deste documento deve ficar com o participante e outra em posse do pesquisador.

_____   _____
Rubrica do participante/representante legal   Rubrica do pesquisador Responsável

Appendix C

AUDIOGRAM

This page shows the graph obtained from the hearing test described in Chapter 4.2. It indicates hearing loss levels in dB for 250 Hz to 8 kHz octave bands, where positive values (below 0 dB) correspond to hearing attenuation. This graph represents an audiogram of a given apt participant, having no value under 20 dB in any band.
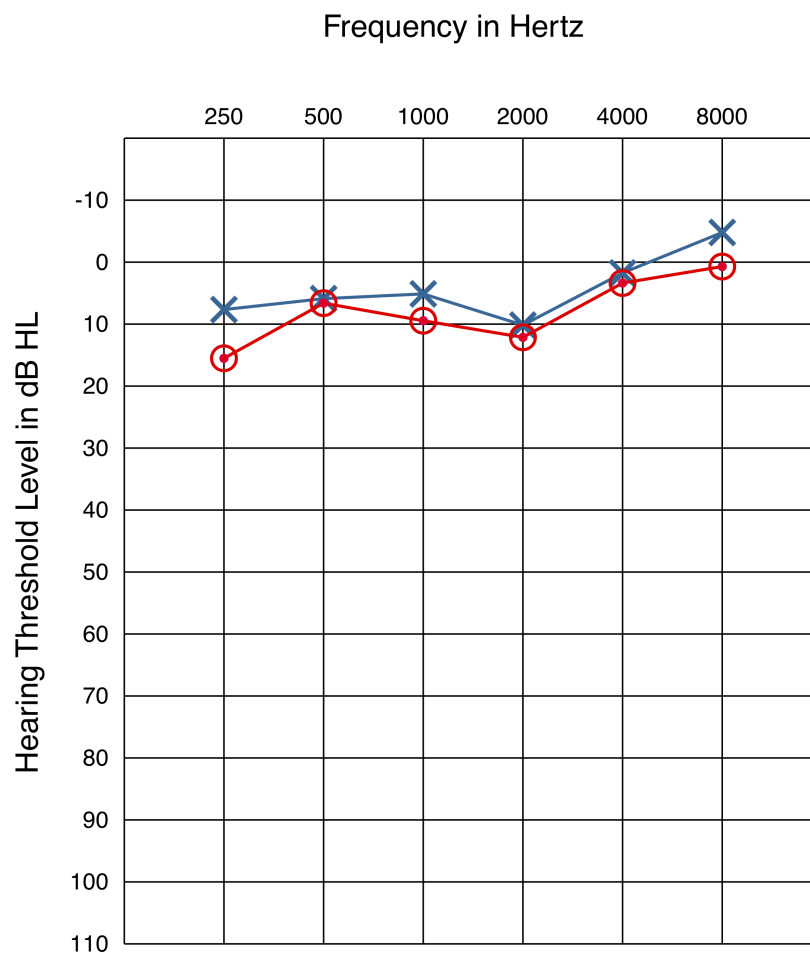

Figure C.1: Hearing results from an experimental participant

Appendix D

CERTIFICATE FOR PARTICIPATION IN NSC-2018

The Organizing Committee

awards this

Certificate

to **G. Acosta-Martínez, E. Tritán-Hernández, D. C. Soriano, L. J. Ontañón-García**

For their Poster participation:

"PERCEPTION ANALYSIS OF CHAOTIC SYSTEM SOUND AND LOUD-NESS PSYCHOACUSTIC PARAMETER"
in the 7th International Conference on Nonlinear Science and Complexity (NSC-2018), held the 14th - 17 of August of 2018 in San Luis Potosi, Mexico.

August, 2018
San Luis Potosi, Mexico.

Albert Luo
Chair

Appendix E

CERTIFICATE AND PUBLICATION IN 6-TH BRAINN

Certificate for Participation

Certificamos que o trabalho intitulado **"EEG classification using acoustic stimuli from chaotic system circuits"**, de autoria de

G. Acosta, P. G. Rodrigues, D. C. Soriano, L. J. Ontañón-García,

foi apresentado na modalidade pôster, categoria "Master degree student",

durante o **6th BRAINN Congress**, realizado de 01 a 03 de Abril de 2019,

no Auditórioda Faculdade de Ciências Médicas da UNICAMP.

Prof. Dr. Li Li Min	**Prof. Dr. Fernando Cendes**	**Profa. Dra. Gabriela Castellano**
Coordenador de Educação e Difusão do Conhecimento	Coordenador Geral do Programa CEPID BRAINN	Coordenadora do Comitê Científico do 6th BRAINN Congress

Abstract

Begins on next page

EEG classification using acoustic stimuli from chaotic system circuits

G. Acosta[1], P. G. Rodrigues[2], D. C. Soriano[2], L. J. Ontañón-García[1]

[1]IICO, UASLP, [2]Engineering, Modeling and Applied Social Sciences, UFABC

Introduction: The use of Electroencephalography (EEG) to assess the influence of sound, consisting mainly of music and random distributions, over brain activity is not novel [1]. The nonlinear EEG methods of characterization [2] aroused the question of how would the brain respond to exposure to this kind of dynamic. This study aimed to use voltage derived from chaotic systems as acoustic stimuli and compare the obtained accuracy of classification between stimuli and rest classes in EEG recordings.

Materials and Methods: 32 healthy volunteers (23.6 ± 4.77) participated following the presented experimental protocol of sound exposure (Table 1). The implemented circuits were Chen, Unstable dissipative (UDS), two attractors of Rössler System: chaos and limit cycle (Rossler*), along with pink noise, which is commonly used as the reference for neutral sound. EEGs were recorded using g.USBamp with 16 Sahara dry electrodes positioned according to Figure 1, stimulation was presented through Sennheiser CX 300-II Earbuds. Experiments were approved by the local ethics committee.
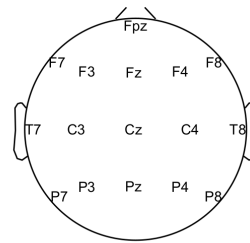

Figure 1. Electrode configuration

Table 1. Timeline of the experiment

EEG recording			EEG recording			EEG recording			EEG recording			EEG recording	
30 sec Rest	30 sec Rössler	10 sec Pause	30 sec Rest	30 sec Chen	10 sec Pause	30 sec Rest	30 sec UDS	10 sec Pause	30 sec Rest	30 sec Rössler*	10 sec Pause	30 sec Rest	30 sec Pink Noise
Block (Performed 5 times using an aleatory pattern of stimuli distribution)													

Results: Figure 2 shows a box plot for the classification accuracy distribution using a least square classifier and a *Leave M Out* cross-validation scheme (70% of trials for training and 30% for test) with 100 repetitions. The mean spectral powers in classical EEG rhythms (Delta, Theta, Alpha, Beta and Gamma) were used as attributes for classification (5 power features by 16 electrodes) of the stimulus vs. rest condition.

Discussion: It was found high inter-subject variability, ranging from 82% of accuracy in the best case overall (Participants number 1&3 using Rössler Chaotic System stimulus) to 51% (Participant 30, using Pink Noise stimulus).

Conclusion: The present work confirmed that both deterministic and random audio stimuli can be discriminated from rest state based on EEG behavior. However, a further statistical comparison is still required for determining the significance on the generative model and dynamics on such process, which outlines a natural perspective of this work.
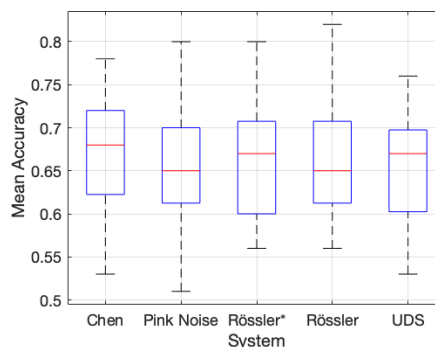

Figure 2. Classification Accuracy obtained for the 32 volunteers.

References: [1] Galvés G et al., doi: 10.1142/S0129065717500551; [2] Faure P et al., doi: 10.1016/S0764-4469(01)01377-4.

Table E.1: Experimental results of classification

Participant	Chen	Pink	Rossler*	Rossler	UD
1	0.70 ± 0.094	0.75 ± 0.158	0.74 ± 0.097	0.82 ± 0.079	0.74 ± 0.135
2	0.71 ± 0.160	0.70 ± 0.125	0.65 ± 0.118	0.82 ± 0.140	0.62 ± 0.042
3	0.73 ± 0.134	0.63 ± 0.116	0.63 ± 0.095	0.73 ± 0.116	0.76 ± 0.070
4	0.65 ± 0.085	0.62 ± 0.123	0.64 ± 0.135	0.72 ± 0.204	0.68 ± 0.103
5	0.65 ± 0.118	0.66 ± 0.165	0.71 ± 0.129	0.65 ± 0.143	0.74 ± 0.165
6	0.68 ± 0.123	0.72 ± 0.199	0.68 ± 0.155	0.72 ± 0.204	0.67 ± 0.200
7	0.62 ± 0.193	0.66 ± 0.107	0.62 ± 0.193	0.62 ± 0.155	0.53 ± 0.106
8	0.63 ± 0.106	0.59 ± 0.099	0.60 ± 0.149	0.57 ± 0.095	0.57 ± 0.116
9	0.63 ± 0.164	0.75 ± 0.108	0.68 ± 0.155	0.71 ± 0.137	0.69 ± 0.160
10	0.73 ± 0.149	0.62 ± 0.123	0.67 ± 0.183	0.67 ± 0.116	0.75 ± 0.118
11	0.53 ± 0.164	0.59 ± 0.137	0.59 ± 0.179	0.63 ± 0.116	0.56 ± 0.143
12	0.73 ± 0.134	0.70 ± 0.115	0.67 ± 0.157	0.56 ± 0.117	0.67 ± 0.082
13	0.61 ± 0.120	0.61 ± 0.185	0.59 ± 0.074	0.65 ± 0.118	0.70 ± 0.105
14	0.72 ± 0.103	0.58 ± 0.193	0.67 ± 0.082	0.67 ± 0.157	0.70 ± 0.115
15	0.69 ± 0.120	0.75 ± 0.151	0.70 ± 0.170	0.80 ± 0.094	0.70 ± 0.141
16	0.53 ± 0.211	0.70 ± 0.141	0.63 ± 0.157	0.57 ± 0.125	0.54 ± 0.143
17	0.58 ± 0.155	0.65 ± 0.097	0.60 ± 0.105	0.60 ± 0.141	0.66 ± 0.126
18	0.56 ± 0.178	0.63 ± 0.106	0.56 ± 0.184	0.66 ± 0.107	0.60 ± 0.133
19	0.74 ± 0.158	0.63 ± 0.157	0.80 ± 0.094	0.62 ± 0.123	0.68 ± 0.148
20	0.77 ± 0.116	0.80 ± 0.163	0.71 ± 0.145	0.70 ± 0.105	0.67 ± 0.189
21	0.72 ± 0.132	0.66 ± 0.151	0.58 ± 0.187	0.63 ± 0.134	0.54 ± 0.052
22	0.75 ± 0.118	0.65 ± 0.108	0.72 ± 0.132	0.56 ± 0.143	0.68 ± 0.103
23	0.68 ± 0.132	0.68 ± 0.123	0.74 ± 0.184	0.68 ± 0.123	0.69 ± 0.208
24	0.65 ± 0.178	0.65 ± 0.151	0.69 ± 0.129	0.62 ± 0.193	0.64 ± 0.135
25	0.78 ± 0.079	0.69 ± 0.152	0.60 ± 0.115	0.67 ± 0.149	0.70 ± 0.125
26	0.56 ± 0.107	0.60 ± 0.141	0.57 ± 0.095	0.61 ± 0.179	0.61 ± 0.152
27	0.72 ± 0.140	0.65 ± 0.135	0.71 ± 0.074	0.65 ± 0.085	0.61 ± 0.110
28	0.69 ± 0.129	0.59 ± 0.166	0.58 ± 0.123	0.73 ± 0.116	0.65 ± 0.071
29	0.67 ± 0.134	0.70 ± 0.105	0.74 ± 0.117	0.65 ± 0.108	0.60 ± 0.170
30	0.55 ± 0.165	0.54 ± 0.084	0.67 ± 0.149	0.57 ± 0.149	0.60 ± 0.105
31	0.63 ± 0.142	0.51 ± 0.099	0.62 ± 0.103	0.61 ± 0.099	0.63 ± 0.106
Mean	**0.66 ± 0.071**	**0.65 ± 0.064**	**0.66 ± 0.061**	**0.66 ± 0.071**	**0.65 ± 0.063**

Bibliography

[1] Faure, P., & Korn, H. (2001). Is there chaos in the brain? I. Concepts of nonlinear dynamics and methods of investigation. Comptes Rendus de l'Académie des Sciences-Series III-Sciences de la Vie, 324(9), 773-793.

[2] Glass, L., & Mackey, M. C. (1988). From clocks to chaos: The rhythms of life. Princeton University Press.

[3] Buzsaki, G. (2006). Rhythms of the Brain. Oxford University Press.

[4] Devaney, R. (1986). An Introduction to Chaotic Dynamical Systems. Benjamin/Cummings.

[5] Poincaré, H. (1881). Mémoire sur les courbes définies par une équation différentielle (I). Journal de mathématiques pures et appliquées, 7, 375-422.

[6] Lorenz, E. N. (1963). Deterministic nonperiodic flow. Journal of the atmospheric sciences, 20(2), 130-141.

[7] Bergé, P., Pomeau, Y., & Vidal, C. (1988). L'ordre dans le chaos: vers une approche déterministe de la turbulence. Hermann.

[8] Busse, F. H. (1978). Non-linear properties of thermal convection. Reports on Progress in Physics, 41(12), 1929.

[9] Scott, S. K. (1993). Chemical chaos (No. 24). Oxford University Press.

[10] Ontanon-Garcia, L. J., & Lozoya-Ponce, R. E. (2017). Analog Electronic Implementation of Unstable Dissipative Systems of Type I with Multi-Scrolls Displaced Along Space. International Journal of Bifurcation and Chaos, 27(06), 1750093.

[11] Hindmarsh, J. L., & Rose, R. M. (1984). A model of neuronal bursting using three coupled first order differential equations. Proceedings of the Royal society of London. Series B. Biological sciences, 221(1222), 87-102.

[12] Niedermeyer, E., & da Silva, F. L. (Eds.). (2005). Electroencephalography: basic principles, clinical applications, and related fields. Lippincott Williams & Wilkins.

[13] Rapp, P. E. (1993). Chaos in the neurosciences: cautionary tales from the frontier. Biologist, 40(2), 89-94.

[14] Aur, D., & Jog, M. S. (2010). Neuroelectrodynamics: Understanding the brain language (Vol. 74). IOS Press.

[15] Korn, H., & Faure, P. (2003). Is there chaos in the brain? II. Experimental evidence and related models. Comptes rendus biologies, 326(9), 787-840.

[16] Fries, P. (2005). A mechanism for cognitive dynamics: neuronal communication through neuronal coherence. Trends in cognitive sciences, 9(10), 474-480.

[17] Sarbadhikari, S. N., & Chakrabarty, K. (2001). Chaos in the brain: a short review alluding to epilepsy, depression, exercise and lateralization. Medical Engineering and Physics, 23(7), 447-457.

[18] Tristán-Hernández, E., Pavón-García, I., Campos-Cantón, I., Ontañón-García, L. J., & Kolosovas-Machuca, E. S. (2017). Influence of Background Noise Produced in University Facilities on the Brain Waves Associated With Attention of Students and Employees. Perception, 46(9), 1105-1117.

[19] Pamuła, H., Kasprzak, C., & Kłaczyński, M. (2016). Nuisance assessment of different annoying sounds based on psychoacoustic metrics and electroencephalography. Diagnostyka, 17.

[20] Başar, E., Başar-Eroglu, C., Karakaş, S., & Schürmann, M. (2001). Gamma, alpha, delta, and theta oscillations govern cognitive processes. International journal of psychophysiology, 39(2-3), 241-248.

[21] Voss, U., Holzmann, R., Hobson, A., Paulus, W., Koppehele-Gossel, J., Klimke, A., & Nitsche, M. A. (2014). Induction of self awareness in dreams through frontal low current stimulation of gamma activity. Nature neuroscience, 17(6), 810.

[22] Larsson, P. G., & Kostov, H. (2005). Lower frequency variability in the alpha activity in EEG among patients with epilepsy. Clinical Neurophysiology, 116(11), 2701-2706.

[23] Lane, J. D., Kasian, S. J., Owens, J. E., & Marsh, G. R. (1998). Binaural auditory beats affect vigilance performance and mood. Physiology & behavior, 63(2), 249-252.

[24] Gálvez, G., Recuero, M., Canuet, L., & Del-Pozo, F. (2018). Short-Term Effects of Binaural Beats on EEG Power, Functional Connectivity, Cognition, Gait and Anxiety in Parkinson's Disease. International journal of neural systems, 28(05), 1750055.

[25] Bear, M. F., Connors, B. W., & Paradiso, M. A. (Eds.). (2007). Neuroscience (Vol. 2). Lippincott Williams & Wilkins.

[26] Clark, D. L., Boutros, N. N., & Mendez, M. F. (2010). The brain and behavior: an introduction to behavioral neuroanatomy. Cambridge university press.

[27] Gray, H. (1878). Anatomy of the human body (Vol. 8). Lea & Febiger.

[28] Nicholls, J. G., Martin, A. R., Wallace, B. G., & Fuchs, P. A. (2001). From neuron to brain (Vol. 271). Sunderland, MA: Sinauer Associates.

[29] Hodgkin, A. L., & Huxley, A. F. (1952). A quantitative description of membrane current and its application to conduction and excitation in nerve. The Journal of physiology, 117(4), 500-544.

[30] Miller, C. (1992). Ionic channels of excitable membranes.: By Bertil Hille. Sunderland, Massachusetts: Sinauer.(1991). 607 pp. 46.95.

[31] Aidley, D. J., & Ashley, D. J. (1998). The physiology of excitable cells (Vol. 4). Cambridge: Cambridge University Press.

[32] Barnett, M. W., & Larkman, P. M. (2007). The action potential. Practical neurology, 7(3), 192-197.

[33] Molecular Devices (1983). What is an action potential?. http://moleculardevices.com.

[34] Huxley, A. F., & Stämpfli, R. (1951). Direct determination of membrane resting potential and action potential in single myelinated nerve fibres. The Journal of physiology, 112(3-4), 476-495.

[35] Purves, D., Augustine, G. J., Fitzpatrick, D., Hall, W. C., LaMantia, A. S., McNamara, J. O., & White, L. E. (2001). Neuroscience. Sunderland. MA: Sinauer Associates.

[36] Singh, S. P. (2014). Magnetoencephalography: basic principles. Annals of Indian Academy of Neurology, 17(Suppl 1), S107.

[37] Marks Jr, W. J., & Laxer, K. D. (2005). Invasive clinical neurophysiology in epilepsy and movement disorders. In Electrodiagnosis in Clinical Neurology (pp. 163-184). Churchill Livingstone.

[38] Glover, G. H. (2011). Overview of functional magnetic resonance imaging. Neurosurgery Clinics, 22(2), 133-139.

[39] Berger, H. (1929). Uber das elektrenkephalogramm des menschen. European archives of psychiatry and clinical neuroscience, 87(1), 527-570.

[40] Wolpaw, J. R., Birbaumer, N., McFarland, D. J., Pfurtscheller, G., & Vaughan, T. M. (2002). Brain-computer interfaces for communication and control. Clinical neurophysiology, 113(6), 767-791.

[41] Niedermeyer, E., & da Silva, F. L. (Eds.). (2005). Electroencephalography: basic principles, clinical applications, and related fields. Lippincott Williams & Wilkins.

[42] Morley, A., Hill, L. & Kaditis A.G. (2016). 10-20 system EEG Placement. E-Learning Resources.

[43] Klem, G. H., Lüders, H. O., Jasper, H. H., & Elger, C. (1999). The ten-twenty electrode system of the International Federation. Electroencephalogr Clin Neurophysiol, 52(3), 3-6.

[44] Pinegger, A., Wriessnegger, S. C., Faller, J., & Müller-Putz, G. R. (2016). Evaluation of different EEG acquisition systems concerning their suitability for building a brain–computer interface: case studies. Frontiers in neuroscience, 10, 441.

[45] Schnupp, J., Nelken, I., & King, A. (2011). Auditory neuroscience: Making sense of sound. MIT press.

[46] Mayo foundation for medical education and research. (2019). How you hear: parts of the ear. http://mayoclinic.org.

[47] Kern, A., Heid, C., Steeb, W. H., Stoop, N., & Stoop, R. (2008). Biophysical parameters modification could overcome essential hearing gaps. PLoS computational biology, 4(8), e1000161.

[48] Hudspeth, A. J. (2014). Integrating the active process of hair cells with cochlear function. Nature Reviews Neuroscience, 15(9), 600.

[49] Department of Biochemistry and Molecular Biophysics Thomas Jessell, Siegelbaum, S., & Hudspeth, A. J. (2000). Principles of neural science (Vol. 4, pp. 1227-1246). E. R. Kandel, J. H. Schwartz, & T. M. Jessell (Eds.). New York: McGraw-hill.

[50] Strogatz, S. H. (2001). Nonlinear Dynamics and Chaos: with Applications to Physics, Biology and Chemistry. Perseus Books.

[51] Perko, L. (2013). Differential equations and dynamical systems (Vol. 7). Springer Science & Business Media.

[52] Ruelle, D., & Takens, F. (1971). On the nature of turbulence. Les rencontres physiciens-mathématiciens de Strasbourg-RCP25, 12, 1-44.

[53] Takens, F. (1981). Detecting strange attractors in turbulence. In Dynamical systems and turbulence, Warwick 1980 (pp. 366-381). Springer, Berlin, Heidelberg.

[54] Orponen, P. (1997). A survey of continuous-time computation theory. Advances in Algorithms, Languages, and Complexity (Springer, US). (pp. 209–224).

[55] Salas P. (2018). Análisis y diseño de sistemas caóticos clásicos con base en filtros pasa-bajas. Doctoral Dissertation.

[56] Chen, G., & Ueta, T. (1999). Yet another chaotic attractor. International Journal of Bifurcation and chaos, 9(07), 1465-1466.

[57] Ontanon-Garcia, L. J., Jiménez-López, E., Campos-Cantón, E., & Basin, M. (2014). A family of hyperchaotic multi-scroll attractors in Rn. Applied Mathematics and Computation, 233, 522-533.

[58] Rössler, O. E. (1976). An equation for continuous chaos. Physics Letters A, 57(5), 397-398.

[59] Ontañón L. J. (2010). Estudio del fenómeno de sincronización en sistemas alineales. Master Dissertation.

[60] Li, T. Y., & Yorke, J. A. (1975). Period three implies chaos. The American Mathematical Monthly, 82(10), 985-992.

[61] Kardous, C. A., & Shaw, P. B. (2014). Evaluation of smartphone sound measurement applications. The Journal of the Acoustical Society of America, 135(4), EL186-EL192.

[62] Fields, J. M., De Jong, R. G., Gjestland, T., Flindell, I. H., Job, R. F. S., Kurra, S., ... & Guski, R. (2001). Standardized general-purpose noise reaction questions for community noise surveys: Research and a recommendation. Journal of sound and vibration, 242(4), 641-679.

[63] Gjestland, T. (2017). Standardized general-purpose noise reaction questions. 12th ICBEN Congress on Noise as a Public Health Problem.

[64] Günther, H., Iglesias, F., & de Sousa, J. M. (2007). Note on the development of a Brazilian version of a noise annoyance scale. Journal of Sound and Vibration, 308(1-2), 343-347.

[65] Marsaglia G., Tsang W. W., Wang J. (2003). Evaluating Kolmogorov's Distribution. Journal of Statistical Software. 8 (18): 1–4.

[66] Kruskal W. (1952). Use of ranks in one-criterion variance analysis. Journal of the American Statistical Association. 47 (260): 583–621.

[67] Fisher, R. A. (1992). Statistical methods for research workers. In Breakthroughs in statistics (pp. 66-70). Springer, New York, NY.

[68] Kleiner, M., Brainard, D., Pelli, D., Ingling, A., Murray, R., & Broussard, C. (2007). What's new in Psychtoolbox-3. Perception, 36(14), 1.

[69] Rodrigues, P. G. (2018). Extração de características em Interfaces cérebro-máquina utilizando métricas de redes complexas. Dissertation for Master in Biomedical Engineering.

[70] Welch, P. D. (1967), The use of Fast Fourier Transform for the estimation of power spectra: A method based on time averaging over short, modified periodograms (PDF), IEEE Transactions on Audio and Electroacoustics, AU-15 (2) 70–73,

[71] Anton, H. (1999). Calculus: A New Horizon, 6th ed. New York: Wiley, 324-327.

[72] Delorme, A., & Makeig, S. (2004). EEGLAB: an open source toolbox for analysis of single-trial EEG dynamics including independent component analysis. Journal of neuroscience methods, 134(1), 9-21.

Acknowledgments

A man . . . is not born to be left to himself, but to devote himself to art [science] and good masters who will make something of him.

—Johann Wolfgang von Goethe

First, I want to express my deep gratitude to my director Dr. Luis Javier Ontañón, and co-director Dr. Edgar Tristán for all their orientation throughout this investigation. I want to particularly thank Edgar for luring me to pursue this master's degree, and Ontañón for the financial support given by the project FAI-287760059 and for his patient and insightful comments on the redaction of this document.

I also want to thank Dr. Diogo Soriano for everything; accepting our invitation to be part of this project, his invaluable contributions to the investigation, all his support with the requirements for the stay, the EEG equipment, and the amazing academic experience in Brazil. Obrigado, prof. Diogo!

I owe special gratitude to Dr. Joel Uriel Cisneros Parra. Getting this far into my professional path would have never happened without his knowledge to inspire me not to give up and help me through during the early stages of my career. I am very grateful to him for introducing me to the marvelous world of sound physics and acoustics.

I would like to thank the Universidad Autónoma de San Luis Potosí and Instituto de Investigación en Comunicación Óptica. Thanks to all personnel and friends at the institute, particularly to Finees and Pablo for their help with chaos. Many thanks to the synodal committee as well, and of course, to my professors at the university.

I also want to thank the Universidade Federal do ABC and all the amazing people I met along the way: Paula (thanks for all the help with the EEG setup!), Piethra, Ju, Miriam, Vitor, my Portuguese-teacher Rebeca, my Jiu-Jitsu senzei Pedro, Jimena, Victor, Anna, Heitor, Samila, and all the patient participants of my experiments.

I cannot forget to thank the Consejo Nacional de Ciencia y Tecnología for the support with a scholarship for mixed master's studies and the international stay.

I would need to thank artists: Layne Staley, James Keenan Maynard, Daniel Tompkins, Louise Phelan (thanks for all the lovely lessons!), Jerry Cantrell, Billy Howerdel, Acle Kahney, Glenn Tipton, Amos Williams, Anup Sastry, Danny Carey, Scott Travis, Jay Postones, to name a few; whose work was essential for me to endure the endless writing process. Your music and spirit are suffused throughout this work.

Last but not least, I must thank my parents, Sonia and Miguel. My greatest masters who taught me how to think and always question everything.